Doctoral Dissertation

# Development of conducting polymer based organic thermoelectric materials and their applications

## (導電性高分子系有機熱電材料の開発と応用)

**ZHANG   LU**

Department of Applied Chemistry

Graduate School of Engineering, Hiroshima University

(広島大学大学院工学研究科 応用化学専攻)

September, 2017

# Table of Contents

# Chapter 1  General Introduction

## 1.1 Background

1.1.1 Significance of thermoelectric materials

Energy is an indispensable material basis for human survival and development and also an essential guarantee for social progress and economic development. However, the rapid development of the economy makes the traditional energy (oil, coal and natural gas) facing depletion, the resulting energy crisis and the environmental problems brought about (toxic emission and greenhouse gas) has become an international key words in the world. The grim situation prompted us to search for an effective way to solve these problems. How to obtain and effective use of efficient and green clean energy will be a difficult but significant project. At present, people try to solve the energy problem from two aspects. One is the development of green renewable energy such as solar energy, water energy and wind energy. Another way is to improve the efficiency via the recycling of the waste heat from the use of mineral energy. According to statistics, the utilization efficiency of the conventional energy source is extremely low (20% ~30%), and most of them is wasted in the way in the form of heat emissions. Obviously, if we can effectively reuse this part of heat, then the energy conversion efficiency will be substantial increase. It is not difficult to imagine that an increasingly serious energy crisis will be effectively mitigated. [1-3] However, implementing effective waste heat recovery requires the relevant energy conversion technologies.

Thermoelectric (TE) materials, based on thermoelectricity, is known to be able to convert thermal power into electrical power. [4-6] By converting waste heat into electricity, engine performance, efficiency, reliability, and environmental protection could be improved significantly. Moreover, thermoelectric generators are solid-state devices that contain no moving parts and thus can operate over a long period of time without significant maintenance. Small heat sources and limited temperature differences are sufficient to drive thermoelectric generators, which makes these devices interesting for applications where traditional dynamic heat engines cannot be employed. Namely, if the

TE devices can be popularized, the efficiency of the use of mineral energy will be undoubtedly greatly improved. Imagining that if the thermoelectric devices can be integrated into the car to recover the waste heat generated during the operation of the car, the fuel efficiency must be greatly increased, which will be considerable effect.

1.1.2 Thermoelectric effect

The research of thermoelectric materials begins with the discovery of thermoelectric phenomena. In 1821, Thomas J. Seebeck discovered that electricity would be generated by a closed loop formed by two different conductors joined in two places, with a temperature difference between the joints, which is called Seebeck effect. Physical principles of the effect can be explained by the change of carrier distribution (holes for p-type and electrons for n-type) within the conductors via temperature gradient, simply schematized by Figure 1-1A. When the temperature gradient reaches the inside of the conductor, the carrier at hot end diffuses and accumulates to the cold end due to its large kinetic energy, so that the number of carriers at cold end will exceed that at hot end, establishing a self-built electric field to prevent the continued diffusion of carriers. The two effects will eventually maintain a certain potential difference at both ends of the conductor, resulting in a current flow through the circuit. Nowadays, thermoelectric power generation gets increasing application in advanced scientific fields, and the thermal source could be fuels, waste-heat, geothermal energy, solar energy and radioisotope. [2, 7]

A few years later, Jean Peltier found the inverse effect of the Seebeck effect accidentally in 1834, named Peltier effect: when the current flow through the junctions between two conductors, heat may be generated or removed at the junctions. The Peltier effect is originated from the potential energy difference of carriers in the different conductors that make up the loop. When the carrier flows into the conductor from the other through the junctions, thermal energy must be exchanged to eliminate potential energy differences of the two conductors, resulting in endothermic and exothermic phenomena, schematized in Figure 1-1B. Accordingly, Peltier effect is commonly used to

convert electrical energy to thermal energy, which is of interest for spot cooling or heating applications.

Subsequently, after systematical analysis of Seebeck and Peltier effect, William Thomson revealed the relationship between the two and further found a third effect named Thomson effect: when current is driven through the conductor with a temperature gradient, except the production of irreversible resistance-related Joule heat, a continuous version of the endothermic and exothermic phenomena will also occur. It seems that the physical principle of Thomson effect is similar to that of Peltier effect, however, in Peltier effect, the potential difference of carriers is derived at the junctions of two different conductors, while in Thomson effect, the difference comes from the temperature gradient in the conductor.

When the contact temperature at the joints of the circuit consisted by two conductors is different, the three thermoelectric effects mentioned above will be generated at the same time. With temperature gradient, Seebeek effect will produce thermal potentials and thermal currents, when the thermal current flows through the joints, Peltier effect would occur, when flow through the conductor, Thomson effect is produced, which is the interrelations of the three effects. Based on the three effects, conversion between electric and thermal energy can be achieved.
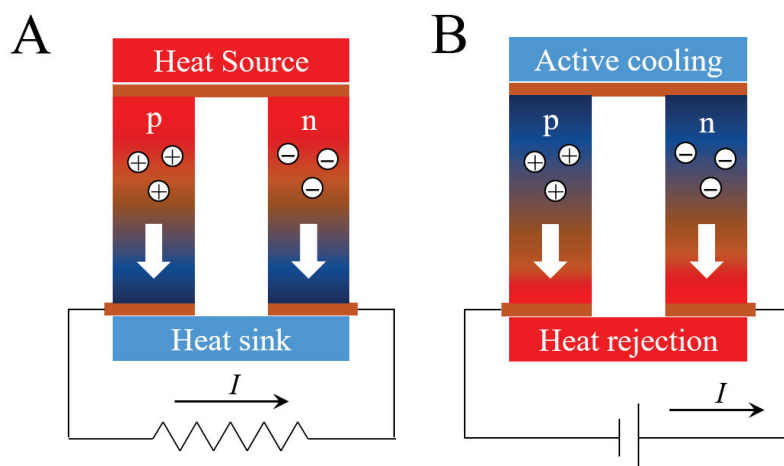


Figure 1-1 Schematic diagrams of working principle of TE devices. (A) Seebeck effect; (B) Peltier effect.

1.1.3 Thermoelectric conversion efficiency

Up to now, thermoelectrometry has been studied for hundreds of years, and several thermoelectric conversion devices upon thermoelectric effect have been successfully developed in power generation. In a thermoelectric device, the charge carriers are transported by the formation of p–n junctions by p- and n-type materials, with holes/electrons acting as a working "fluid" (Figure 1-1). The applied temperature gradient generates gradients of charge carriers, which diffuse from the hot side to the cold side, in turn producing an electrostatic potential. As a TE generator, the evaluation index: thermoelectric conversion efficiency $\eta$ is defined as follows [7]:

$$\eta = \frac{T_h - T_c}{T_h}\left[\frac{\sqrt{1 + ZT} - 1}{\sqrt{1 + ZT} + T_c/T_h}\right]$$

where $T_h$ (K) is the hot end temperature, $T_c$ (K) is the cold end temperature, and $ZT$ is the dimensionless figure of merit which is used to assess the thermoelectric transport properties of a material.

Accordingly, a high $ZT$ value, as well as a large temperature difference ($\Delta T = T_h - T_c$) is conducive to a high conversion efficiency $\eta$. Details are described in the plot of different effects of $ZT$ on thermoelectric conversion efficiency with varying $T_h$. [8] (Figure 1-2) As shown, when $\Delta T \sim 500$ K, $\eta$ could reach 20% at $ZT$ around 2, while 27% at $ZT$ around 4, which is comparable to that of traditional heat engines. [2, 7]
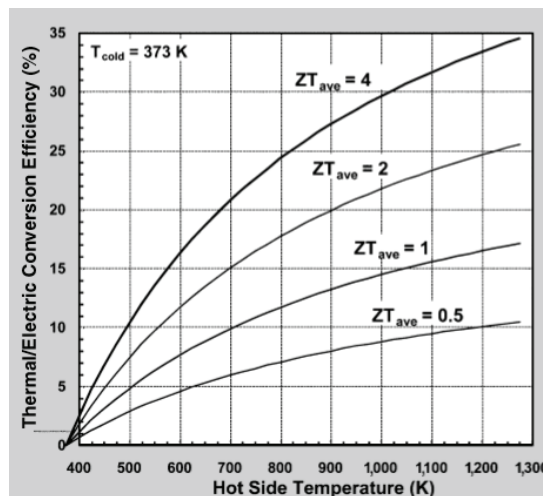


Figure 1-2 Plot shows the thermoelectric conversion efficiency as a function of differential operating temperature and ZT. [8]

4

1.1.4 Comparison of inorganic and organic materials

Nowadays, ZT values above unity are well established based on inorganic TE materials. [9-14] Several typical inorganic TE materials with *ZT* value higher than 2 are list in Table 1-1. It seems that we have already successfully obtained the promising TE materials. However, the wide application for TE devices are still under anticipation. For inorganic TE materials, firstly, the composing elements such as Sn, Te, Sb and Pb are toxic and rare. Second, laboratory processing of inorganic materials, including melt-spinning, ball milling, hot pressing, etc., is costly in terms of energy and instruments, and hence requires a long payback time. Lastly, most inorganic materials are too heavy and brittle to be of use in everyday life. [15]

Table 1-1. Thermoelectric parameters of several typical inorganic TE materials (ZT > 2).

| Material | $\sigma$ / S cm$^{-1}$ | $S$ / $\mu$V K$^{-1}$ | $\kappa$ / W m$^{-1}$ K$^{-1}$ | *ZT* | |
|---|---|---|---|---|---|
| SnSe single crystals [11] | ~60 | ~330 | 0.23 | 2.62 | at 923 K |
| $Cu_{1.94}Al_{0.02}Se$ [9] | 261 | ~250 | 0.611 | 2.62 | at 1000 K |
| $Na_{0.025}Eu_{0.03}Pb_{0.945}Te$ [12] | - | - | ~ 0.4 | 2.2 | at 900 K |
| PbTe [10] | ~300 | ~284 | 0.96 | 2.2 | at 915K |
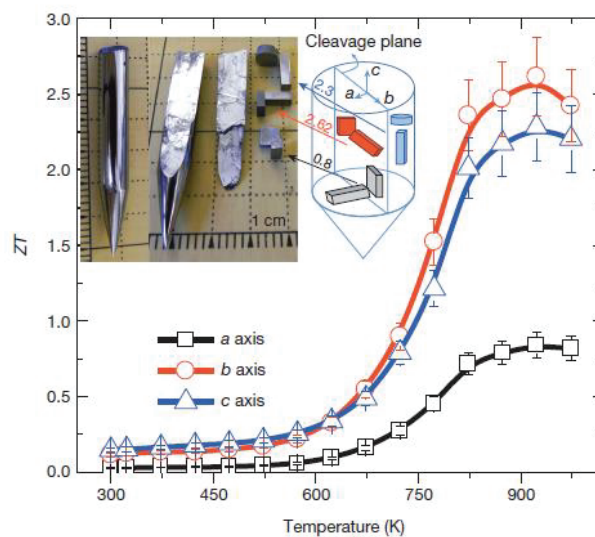


Figure 1-3 Relationship between ZT value of the inorganic TE material and temperature T. [11]

Moreover, inorganic materials exhibit excellent TE performance for medium-grade (500–750 K) and high-grade (above 750 K) heat sources. A common relationship of current inorganic materials between *ZT* value and *T* is given in Figure 1-3. As observed,

for low-grade (300–500K) heat sources, however, they don't show outstanding performance. Since low-grade (300–500K) heat sources which generated from industry, transportation, appliances and housing are more common, it is necessary to further develop promising TE materials at low-grade temperature. [1]

Given the aforementioned obstacles met by current inorganic thermoelectric materials, organic candidates are attracting more and more attention. Compared to inorganic materials, organic materials have low thermal conductivity and rich electronic band structure, as well as the advantages like potentially abundant, light-weight, flexible, solution-processable and low-cost. Specifically, the advantage of organic materials are as follows: (1) They have lower negative environmental impact due to their chemical composition, lower manufacturing and processing costs, potentially abundant resources and recycling ability; (2) They possess excellent material processibility and may be formed in a variety of shapes, which is important from the application point of view; (3) They are easy to make thin film, the additional weight is light, which is suitable in the special occasions such as spacecraft and computer chips; (4) Conducting polymers are thermoelectrically active even at an ambient temperature which could cover the shortage of inorganic materials at low-grade sources. This is still a relatively new group of materials not fully investigated. Thus, even a small change in their properties may cause a fundamental step forward for their wider application for direct heat recovery and conversion.

## 1.2 Conductive Mechanism of Conductive Polymers

### 1.2.1 Development of Conductive Polymers
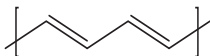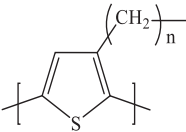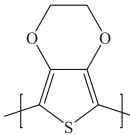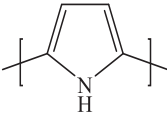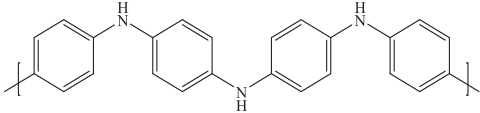
Long time ago, we are used to polymers - that is, plastics - being somehow the opposite of metals, which are insulating and do not conduct electricity. However, since Shirakawa *et al.* [16, 17] discovered that oxidation with chlorine, bromine or iodine vapor could make polyacetylene films $10^9$ times more conductive than they were originally in 1977, the concept that organic polymer was not conductive has been completely changed. Such treatment with halogen was called "doping" by analogy with the doping of

semiconductors. The "doped" polyacetylene exhibited metal conductance properties of $10^3$ S cm$^{-1}$, which was higher than that of any previously known polymer. As a comparison, teflon has a conductivity of $10^{-18}$ S cm$^{-1}$ and silver $10^5$ S cm$^{-1}$. This research not only opens up a new field for the application of organic polymer materials, but also makes important contributions to the establishment and improvement of low-dimensional organic solid electronics which has important scientific significance.

1.2.2 Structural Characteristics of Conductive Polymers

According to the conductive mechanism, the conductive polymer can be divided into two types: composite type and structural type. The former relies on the combination of polymers with certain amount of conductive material (such as black carbon, graphite, carbon fiber, metal, metal oxides), while the latter refers to the conductive carriers generated by the polymer itself via doping process. Generally, conductive polymer refers to the structural conductive polymer, including polyacetylene (PA), polypyrrole (PPY), polythiophene (PTH), polyaniline (PAn) and poly(3,4-ethylenedioxythiophene) (PEDOT). This is mainly because the raw materials of their monomer is easy to be obtained and the synthesis process is simple. There are several typical conductive polymers.

Table 1-2. Molecular structures of typical conductive polymers.

| Polymer | Structure | Polymer | Structure |
|---|---|---|---|
| Polyacetylene | | Polyalkyl thiophene | |
| PEDOT | | Polypyrrole | |
| Polyaniline | | | |

1.2.3 Conductive Mechanism of Conductive Polymers

A key property of a conductive polymer is the presence of conjugated double bonds

along the backbone of the polymer. In conjugation, the bonds between the carbon atoms are alternately single and double. Single and double bonds both contain a chemically strong, localized σ-bond, while the double bonds also contain a less strongly localized π-bond. The p-orbitals in the series of π-bonds overlap with each other, allowing the electrons to be more easily delocalized (i.e. they do not belong to a single atom, but to a group of atoms). [18, 19] However, due to the energy gap Eg (around 1.4 - 4.0 eV) between valence band (formed by π-π bond in the molecular) and conduct band (formed by π*-π* bond), such conjugation system is not enough to make the polymer material conductive at room temperature. In addition - and this is what the dopant does - charge carriers in the form of extra electrons or "holes" have to be injected into the material. A hole is a position where an electron is missing. When such a hole is filled by an electron jumping in from a neighboring position, a new hole is created and so on, allowing charge to migrate a long distance along the conjugated chains and then achieve the conductivity. After proper doping, the conductivity of the "insulating" conjugated polymer can be dramatically increased by several orders of magnitude, which almost close to the conductivity of the semiconductor, or even metal. However, the doping mechanism of conjugated polymer and semiconductor is completely different. The doping mechanism of conjugated polymer can be summarized as the following:

(1) Redox Doping [20]: This kind of doping is the charge transfer via redox reaction that occurs on the polymer chain of the conjugated structure. The π electrons in the conjugated polymer chains could have a high degree of delocalization, exhibiting sufficient electron affinity as well as low electron dissociation energy, thus the polymer chain itself may be oxidized (loss or partial loss of electrons, p-type doping), or be reduced (obtained or partially obtained electrons, n-type doping). The p-type doping process is schematically explained using poly(acetylene) as examples in Figure 1-4A. First, the abstraction of an electron from the π-system of poly(acetylene) chain results in the formation of a radical cation. Removal of a second electron gives rise to a second radical cation. Then two radicals recombine to give a spinless dication.

8

Further oxidation occurring in the same manner leads to spinless charge carriers called positive solitons. Note that each soliton constitutes a boundary which separates domains differing in the phase of their π-bonds. Figure 1-4B shows schematically the n-type doping process of poly(acetylene) similarly.
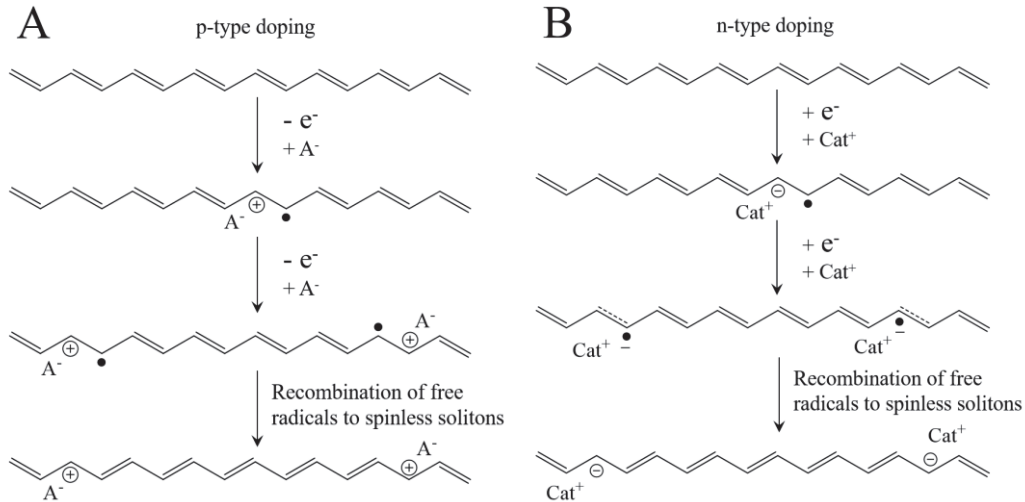


Figure 1-4 (A) p-type doping and (B) n-type doping of polyacetylene. [20]

(2) Proton acid doping: when a proton is introduced into the conjugated polymer chain, the charge distribution on the polymer chain changes, the positive charge of the proton would transfer and disperse to the molecular chain, in equivalent to the oxidation of the polymer chain via the loss of electron (p-type doping). However, different from the oxidation doping, the total number of electrons on the polymer chain via proton acid doping did not change and the charge transfer is just accompanied by the protonation process. This doping form is most typical of polyaniline doping due to the strong basic centers in their backbone. [20]

(3) Ion implantation doping [21-23]: Ion implantation is a materials engineering process by which selective ions are accelerated in an electrical field and then impacted into the target. Through the control of ions, ion energy, current density and dosage, polymer conductivity can be regulated expectably. The select of implanted ions will result in different types of doping. For instance, when $K^+$ was injected into polyaniline, n-type doping was observed. [24] Moreover, as known, implantation process would

damage the original structure of the materials, however, for polymer, the main result of damage-induced structural changes is carbonization, which could lead to highly fused graphite-like sheet structures, further facilitating the electrical conductivity. [25]

Although the concept of "doping" is used in the field of conductive polymers, it is completely different from the "doping" concept of inorganic semiconductors. The difference is mainly: (1) the doping of inorganic semiconductor means the atomic substitution, while in conductive polymer, doping is the charge transfer via redox process; (2) the doping level of inorganic semiconductor is very low (ten thousandths), while for conductive polymer, it may be up to 50%; (3) In inorganic semiconductor, there is no de-doping process, while in conductive polymer, it existed, and moreover, the doping and de-doping process can be completely reversible; (4) In order to maintain the neutral nature of the molecular, in addition of the conductive carriers, the negative or positive ions must be present, which may have a certain impact on the properties of conductive polymers.

According to the theory of energy band, it is known that when the polymer wants to have conductivity, it must satisfy the following two requirements: (1) the orbital of macromolecule can be strongly delocalized; (2) the orbital of macromolecule chains can overlap each other. The polymers that meet the above two conditions are: (1) conjugated polymers, electrons on the conjugate bond can be delimited on the whole molecule, resulting in the production and transport of carriers (electrons or holes); (2) Non-conjugated polymer with overlapped $\pi$ intermolecular orbital; (3) with electron donor and acceptor system. Generally, the conductivity of polymers is always lower than semiconductor, which may be due to the small carrier concentration (only about $10^{-1} \sim 10^{-2}$ of the semiconductor) as well as the orders of magnitude different carrier mobility.

Moreover, aside from the intramolecular charge transport, which mainly determined by the chain structure and the degree of delocalization of $\pi$ electrons, the phonon-assisted hopping between the molecular chains would also occur. [26] Explained by the small polaron transport model [27], the strong electron- phonon interaction causes lattice distortion around the electron which moves along the chain but is also trapped by the

polarized field formed itself. (Figure 1-5) Each monomer unit of the conducting polymer can be viewed as a site. Electrical transport arises from the polarons hopping from one site to another caused by overlap of the electron wave functions on adjacent sites, where the intersite coupling is essential for TE properties.
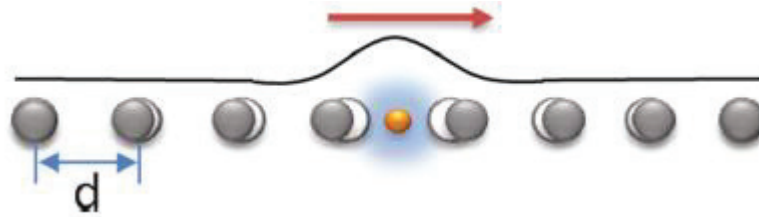


Figure 1-5 Schematic of small-polaron transport model to describe the thermoelectric transport in organic materials. The strong electron-phonon interaction in these organic materials causes lattice distortions around the electron. The electron is trapped by the polarized field formed itself. [27]

## 1.3 Thermoelectric parameters

As explained above, $ZT$ is the determinant of thermoelectric materials which is indispensably defined by the thermoelectric parameters. The definition is described below:

$$ZT = \frac{S^2 \sigma}{\kappa} T$$

where $S$, $\sigma$, $\kappa$, and $T$ are Seebeck coefficient, electric conductivity, thermal conductivity, and absolute temperature, respectively. Since, in particular, the thermal conductivity $\kappa$ can be challenging to measure, the power factor $PF$ ($\sigma^2 S$) is often used instead of $ZT$ for the purpose of comparing the thermoelectric performance of different materials.

Accordingly, to obtain an expectable $ZT$ value, the following criteria should be achieved: (1) a higher electrical conductivity $\sigma$ which required for larger short-circuit current; (2) a higher Seebeck coefficient $S$ is preferred to achieve higher Seebeck voltages and (3) the thermal conductivity $\kappa$ need to be as low as possible to maintain larger temperature difference. However, the parameters $S$, $\sigma$, $\kappa$ are intimately linked and can vary with temperature, which complicates optimization and typically requires a compromise.

1.3.1 Electrical conductivity

Electrical conductivity $\sigma$ related to electronic charge e ($1.6* 10^{-19}$ C), charge carrier concentration $n$ ($cm^{-3}$) and carrier mobility $\mu$ ($cm^2$ $V^{-1}$ $s^{-1}$) is defined as:

$$\sigma = en\mu$$

Typically, for organic semiconductors $\sigma$ is $\sim10^{-2}$ S $cm^{-1}$, $n$ is $\sim10^{16}$ $cm^{-3}$, and $\mu$ is $\sim10^{-4}$ $cm^2$ $V^{-1}$ $s^{-1}$. Explained by Liang [28], doping (the process of adding charge carriers to the semiconducting material either chemical or electrochemical treatments) is directly related to the variation of $n$. Upon doping, $n$ would be increased, which facilitates the $\sigma$ in a certain degree. Note that instead of specified values of carrier concentration, it is doping levels (the number of counterions per repeat unit of the polymer) that are mostly cited in the description of conjugated polymers because accurate measurement of carrier concentration in polymers is nontrivial. On the other hand, tunable molecular structures of organic semiconductors which can be acquired through synthetic chemistry, has a great impact on intrinsic $\mu$. Moreover, the doping level also has influence on the $\mu$ in $\pi$-$\pi$ conjugated polymers over a wide range. [29, 30] For a typical conducting polymer PMT (Figure 1-6), the carrier mobility strikingly increases by several orders of magnitude at high doping level. Accordingly, in highly doped organic semiconductors, $\sigma$ is able to reach the values of $10^1$ to more than $10^3$ S $cm^{-1}$. [31]
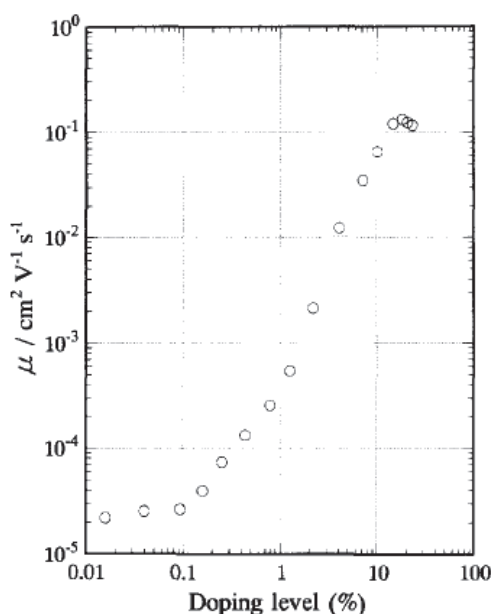


Figure 1-6 Mobilities of positive charge carriers in the PMT film of different doping levels. [29]

1.3.2 Seebeck Coefficient

The temperature-dependent Seebeck coefficient $S(T)$, which can be considered as the entropy per charge carrier, describes the potential difference that arises per unit temperature difference. For small changes in temperature, $S(T)$ is almost constant and thus we obtain: [32]

$$S = -\frac{\Delta V}{\Delta T}$$

By convention, the sign of $S$ is given by the potential of the cold side with respect to the hot side and thus indicates the type of majority charge carriers, i.e. electrons or holes, with $S < 0$ for n-type and $S > 0$ for p-type semiconductors.

In the framework of energy band theory and Boltzmann distribution, Seebeck coefficient expressed from the weighted average of the difference between the Fermi level ($E_F$) and the carrier energy of the localized states contributing to the conductivity ($E$) can also be defined as: [28]

$$S = \frac{k_B}{e}\left[\frac{E - E_F}{k_B T} + A\right]$$

where $k_B$ is the Boltzmann constant ($1.38 * 10^{-23}$ J K$^{-1}$), $E_F$ is Fermi energy level (eV), $E$ is the energy level occupied by the carrier (eV), and A is the heat of transport constant for motion.

Accordingly, the Seebeck coefficient, is related to the energy difference between $E$ and $E_F$. Normally, in conducting polymers, highly conductive materials tend to exhibit the conductivity from carriers close to the $E_F$. Moreover, high doping levels will push $E_F$ into the conduction band for n-type semiconductor while into valence band for p-type due to the increased carrier concentration. This subsequently causes the number of electronic states above and below $E_F$ to be more equivalent, negatively reducing $S$. Typical values for a range from $10^3$ $\mu$V K$^{-1}$ for intrinsic semiconductors (e.g., undoped conjugated polymers) to $10^2$ to $10^1$ $\mu$V K$^{-1}$ for moderately to heavily doped (extrinsic) semiconductors, and $S < 10^1$ $\mu$V K$^{-1}$ for good conductors, including metals. [32]

Thus, it is necessary to take all these factors into consideration to make tradeoff and

reach remarkable TE performances. A common relationship between the electrical properties of a thermoelectric material as a function of carrier concentration is given by Kar. [5] It can be observed that with the increase of carrier concentration, the electrical conductivity increases, while Seebeck coefficient decreases, inducing an optimization of power factor. (Figure 1-7A) As the carrier concentration $n$ is directly dominated by the doping level, Bubnova [31] also gave the specific experimental explanation for the trade-off relationship of oxidation level between $\sigma$ and $S$: with the increase of oxidation level of the PEDOT:Tos film, $\sigma$ increased, while $S$ decreased, inducing an optimized $PF$ with the oxidation level of 22%. (Figure 1-7B)
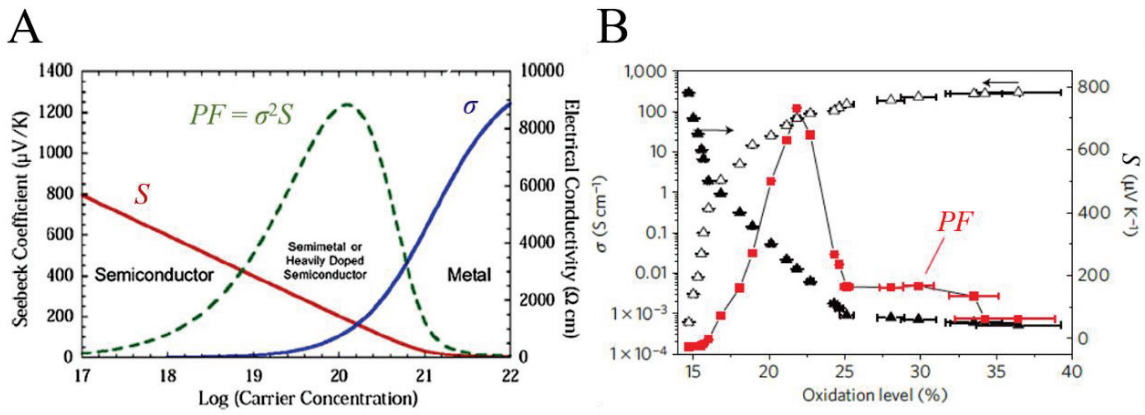


Figure 1-7 (A) Relationship between the electrical properties of a thermoelectric material as a function of carrier concentration[5]; (B) Seebeck coefficient (filled triangles), electrical conductivity (open triangles) and corresponding power factor (red squares) of PEDOT:Tos film versus oxidation level. [31]

## 1.3.3 Thermal conductivity

To estimate the figure of merit, a careful determination of the thermal conductivity $\kappa$ is required. As for organic TE materials, the thermal conductivity value is typically below 1 W m$^{-1}$ K$^{-1}$, approaching the lowest limit of $\kappa$ of inorganic ones, which is a non-negligible advantage for promising TE materials. The thermal conductivity is defined by the relationship of $\kappa = \rho \alpha C_p$ (W m$^{-1}$ K$^{-1}$) where $C_p$ is the specific heat capacity (J g$^{-1}$ K$^{-1}$), $\rho$ is the density (g cm$^{-3}$) and $\alpha$ is the thermal diffusivity (m$^2$ s$^{-1}$). The thermal conductivity is also described by

$$\kappa = \kappa_L + \kappa_e$$

14

where $\kappa_L$ corresponds to lattice or phonon contribution and $\kappa_e$ relates to electron contribution.

For organic polymers, $\kappa_L$ is low and often exits in the range of 0.1~ 1.0 W m$^{-1}$ K$^{-1}$, and more importantly, $\kappa_L$ is independent of the doping level. Enormous studies have shown that rich hetero-interfaces, grain boundaries and nanoinclusions originating from doping [33], nanostructuring [5], and heterostructures [6] can cause phonon scattering, thus decreasing $\kappa_L$. Moreover, for typical organic polymers, the electrical conductivity reaches ~10$^{-2}$ S cm$^{-1}$, making $\kappa_e$ several orders of magnitude lower than $\kappa_L$, which can be ignored compared to $\kappa_L$. [28] As a consequence, thermal conductivity in organic TE materials is most likely independent of the doping level and is mainly dominated by phonons. However, when the electrical conductivity of polymer become a few orders of magnitude higher, the electron contribution should be taken into account.

## 1.4 Optimization Strategies for Thermoelectric properties of organic materials

As mentioned above, thermoelectric performance is strongly dependent on the material doping level, chemical structures, electronic structures which is intimately related. Generally, there is a trade-off relationship between the electrical conductivity $\sigma$ and the Seebeck coefficient $S$. For this reason, an optimal compromise should be reach to obtain the maximum thermoelectric efficiency. In the past years, many works dealing with the improved TE properties in organic polymers have been published. Since this topic is of special interest for designing devices, several methods will be analyzed in the next subsections.

1.4.1 Optimization of polymerization conditions

Basically, most conductive polymers are prepared by oxidative coupling of monocyclic precursors, which entail dehydrogenation:

$$n\ H–[X]–H \rightarrow H–[X]_n–H + 2(n–1)\ H^+ + 2(n–1)\ e^-$$
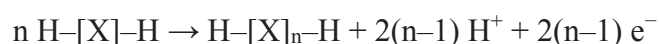
Common methods for polymerization mainly include chemical and electrochemical polymerization. [34] Thermoelectric properties of the conducting polymers are strongly

affected by the synthesis and/or processing conditions.

*1.4.1.1 Chemical polymerization*

The oxidative chemical polymerization is the most usual method to synthesize conductive polymers. [31, 35, 36] Basically, this method consists of the reaction between the monomer and an oxidizing agent. Typically, polymers synthesized by this method are p-type semiconductors, exhibiting an electron deficiency along its backbone. The polymerization mechanism of the chemical synthesis is normally described as below: as the first step, monomer is oxidized to give a radical cation. The radical cation then reacts with a neutral monomer, followed by oxidation and deprotonation, giving a dimer (an oligomer of two monomers). The dimer is continuously oxidized, yielding the dimeric radical cation. After combination with a new neutral monomer, a trimer (an oligomer of three monomers) was obtained. This reaction continues and the chain grows monomer by monomer to achieve high degree of polymerization. [19]

As accepted, polymerization process is highly sensitive to the choice and purity of the solvent, oxidant, reagent concentration, reaction time, pH, temperature, stirring rate and so on. The classical oxidizing agents used for monomer polymerization is always described as (1) transition metal halides with oxidizing properties, such as $FeCl_3$ [37]; (2) transition metal oxidants, such as manganese dioxide ($MnO_2$) [38]; (3) persulfate compounds, such as ammonium persulfate (APS) [35]; (4) strongly or mildly peroxide system, such as Benzoyl peroxide (BPO) [39] and so on. Moreover, besides the oxidation level [40], the choice of the oxidants is also important for the polymer structure.

For instance, Farrokhi et al. successfully synthesized the flower-like polypyrrole (PPy) using $MnO_2$ as the oxidizing agent. [38] During the polymerization, the flower-like $MnO_2$ was served as the oxidative polymerization initiator as well as physical template, inducing the in situ oxidation of pyrrole monomer on the surface of the $MnO_2$ and finally result in a flowerlike structure PPy. (Figure 1-8)

In the case of PANI, the doping level can be controlled with the molar ratio of the acid used in its synthesis, as previously reported. [41] The electrical conductivity could be

16

controlled in the range from 1 to 6 S cm$^{-1}$, depending on the concentration of HCl in the solution. The electrical conductivity increases as the HCl concentration increases. However, the Seebeck coefficient shows an opposite trend: at low HCl concentration it increases up to 35 $\mu$V K$^{-1}$.
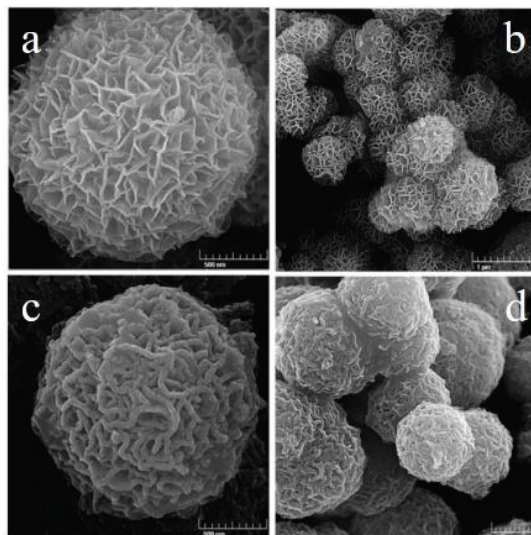


Figure 1-8 SEM images of (a) and (b) the flower-like MnO$_2$, (c) and (d) PPy microspheres consisted of interweaved PPy nanostructures. [38]

Chemical polymerization not only provides the possibilities to synthesize all the conducting polymers, but also permits the scale-up production of these materials. However, as mentioned above, properties of the created polymer is highly sensitive to synthesis condition, making it difficult to be carried out reliably and repeatably. Moreover, the conductivity of the polymers via chemical synthesis is known to be lower than their electrochemically synthesized counterparts. [42]

*1.4.1.2 Electrochemical polymerization*

Electrochemical polymerization is usually carried out using the electrode configuration in a solutions containing the monomer of the polymer, the solvent and the electrolyte. During the polymerization, the monomer is being oxidized at the anode and in the same time the dopant anions such as such as ClO$_4^-$, BF$_4^-$, PF$_6^-$, originating from the electrolyte, are inserted to the polymer matrix, hence forming insoluble polymer chains on the electrode surface. [43] The polymerization can be performed using the galvanostatic [44],

17

potentiostatic [45] and potentiodynamic [46] methods. By precise control of the polymerization techniques, deposition time, electrolytes, solvent, and the electrode system, properties of the synthesized polymers such as the film morphology, mechanics, and conductivity could be well defined. [47, 48]

For example, Culebras *et al.* reported the different TE performances of PEDOT synthesized in the presence of three different counter-ions: $ClO_4^-$, $PF_6^-$ and bis(trifluoromethylsulfonyl)imide (BTFMSI). [49] Depending on the sizes of different counter-ions, a change from a typical coil conformation to a linear or expanded-coil conformation takes place in the PEDOT chains. As seen in Figure 1-9A, a more extended PEDOT chain is obtained by the BTFMSI anions, leading to an increase of the electrical conductivity than that by $ClO_4^-$ and $PF_6^-$ (Figure 1-9B).
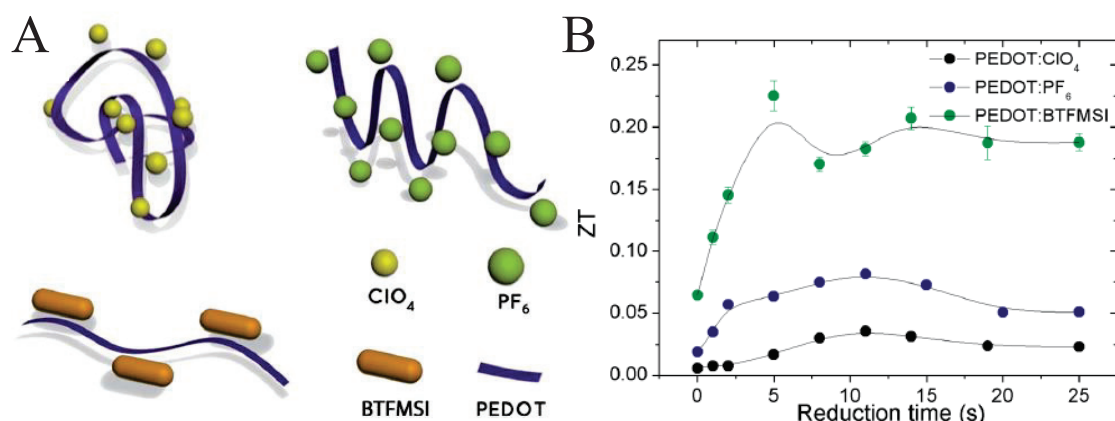


Figure 1-9 (A) PEDOT conformation in the presence of different counterions; (B) ZT values of PEDOT:$ClO_4$, PEDOT:$PF_6$ and PEDOT:BTFMSI as a function of chemical reduction time at 25 °C. [49]

Namely, electrochemical polymerization enables the precise control and rapid deposition of conductive polymers on the electrode. In addition, the oxidation level is also possible to be precisely defined via coulometric measurements of the current passed through. Despite of the advantages, it is worth noting that, different from the chemical synthesis, electrochemical polymerization only allows the synthesis of the polymer which its monomer can undergo oxidation in the presence of an electrical potential which may be not suitable for all the polymers. [48] Moreover, with the restriction of the geometry

and surface area of the working electrode, it becomes difficult for the large-scale production of the polymers via electrochemical polymerization.

Except the commonly used synthetic methods mentioned above (chemical/ electrochemical polymerization), photochemical polymerization is also applied to polymer synthesis. [50] In general, the photochemical polymerization reaction occurs in three distinct stages: initiation, propagation and termination. In the initiation step, reactive species are efficiently generated by the photo-induced fragmentation of photo-initiators. [51] These reactive species will then react with the monomer to generate chain-starting species (radical photopolymerization) or ion pairs (ionic photopolymerization) responsible for the propagation step. The last step corresponding to termination of polymeric chain may occur by disproportionation or combination of active species or by the transfer of chains. [52] Compared with the chemical and electrochemical polymerization, photochemical polymerization exhibits the advantages such as low costs required for its implementation, the fast processing speed of the reactions, the low energy cost required and less pollution.

1.4.2 Chemical/ Electrochemical doping

Another route to improve the electrical conductivity in polymers is chemical or electrochemical doping to introduce extra charge carriers, such as polarons and dipolarons, and favor charge transfer along the polymer chains over hopping.

As mentioned, the first semiconducting polymer synthesized was the polyacetylene (PA), in the decade of the seventies. In its natural state, PA is almost insulating. When exposing the film to the vapor of iodine in room temperature, the conductivity dramatically increased. At highly doped state (iodine concentration was 30% per CH unit), the conductivity enhanced up to $2 * 10^4$ S cm$^{-1}$, which is comparable to that of common metals. However, such high conductivity is not stable and rapidly decreased, making it difficult for further study. [53] Anyway, it provides an effective path to change the properties of the materials.

Even so, it is difficult to precisely control the chemical doping processes, partly

because the measurement of the exact oxidation level is not straightforward, and also the choice of dopants is limited. Therefore, an electrochemical doping process was demonstrated by the Crispin team as a versatile tool to optimize the TE power factor of conducting polymers. [54] In their work, the TE properties of PEDOT doped with PSS were controlled electrically by varying the gate voltage of the organic electrochemical transistor (OECT). An increase in gate voltage to +1.4 V led to a decrease in electrical conductivity from more than 224 to 0.3 S cm$^{-1}$, which was accompanied by an increase in the Seebeck coefficient to 400 μV K$^{-1}$. At an intermediate gate voltage of +0.8 V (corresponding to an oxidation level of 14.5%), an optimal compromise between $\sigma$ and $S$ was obtained, resulting in the highest measured power factor of 23.5 μW m$^{-1}$ K$^{-2}$. (Figure 1-10)

Electrochemical doping facilitates the control and measurement of the oxidation level via tuning of the electrode potential while enabling the measurement of the charging currents. Moreover, many counterions are available to balance the doping charges along the polymer chains simply by adding different salts in the electrolyte.
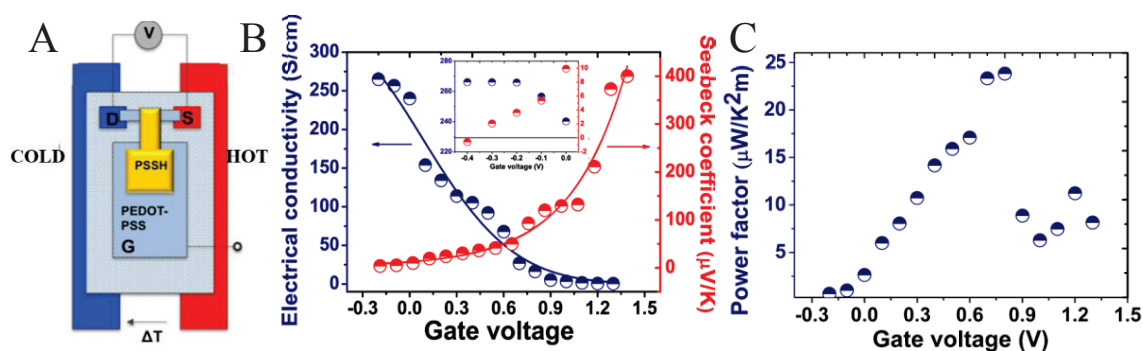


Figure 1-10 (A) Schematic view of the setup for thermoelectric characterization of PEDOT−PSS between the source (S) and drain (D) in a three-terminal OECT; (B) electrical conductivity (blue symbols) and Seebeck coefficient (red symbols) as functions of gate voltage; (C) calculated power factor as functions of gate voltage. [54]

A few months later, similarly, Kim *et al.* exhibited a very large power factor of PEDOT films of 1,270 μW m$^{-1}$ K$^{-2}$ at the doping potential of 0.1 V vs Ag/Ag$^{+}$, operated on a three-electrode system. Such high performance TE material could be processed as flexible and cuttable thermoelectric films to generate electricity by fingertips. [55] Sometimes, the

electrochemical doping could also be named as electrochemical dedoping, when the applied potential results in a dedoping process of the polymers.

1.4.3 Secondary doping

Phenomenologically, a primary dopant for a conducting polymer drastically changes the electronic, optical, magnetic and/or structural properties of the polymer and is accompanied by a large increase in conductivity. De-doping of the dopants would result in a reversal of the newly induced properties. Defined by MacDiarmid and Epstein, a secondary dopant is an apparently 'inert' substance which, when applied to a primary-doped polymer, induces still further changes in the above properties including a further increase in conductivity. It differs from a primary dopant in that the newly enhanced properties may persist even upon complete removal of the secondary dopant. It is shown that the effects of secondary doping are based primarily on a change in molecular conformation of the polymers. [56]
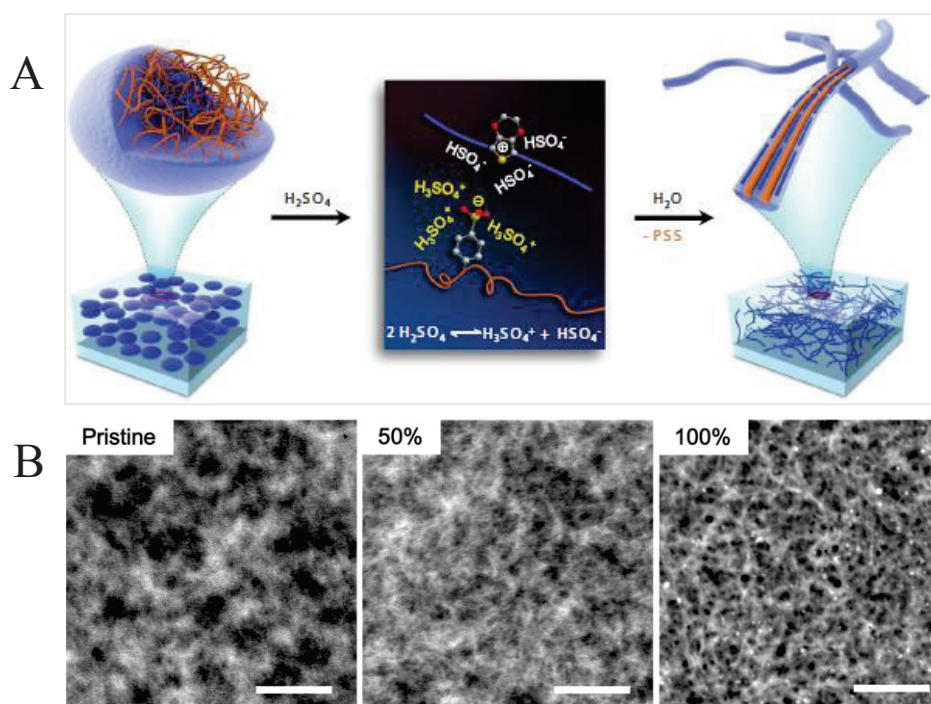


Figure 1-11 (A) Diagram of the structural rearrangement of PEDOT:PSS. The amorphous PEDOT:PSS grains (left) are reformed into crystalline PEDOT:PSS nanofibrils (right) via a charge-separated transition mechanism (middle) via a concentrated $H_2SO_4$ treatment; (B) HAADF-STEM images of PEDOT:PSS films treated with various concentrations of $H_2SO_4$. Scale bars, 200 nm. [57]

Recently, Kim et al. reported the solution-processed crystalline formation of PEDOT:PSS via $H_2SO_4$ treatment, and the conditions were rigorously controlled (i.e., the $H_2SO_4$ concentration, treatment $T$, and processing details). When PEDOT:PSS is treated with highly concentrated $H_2SO_4$ that can undergo autoprotolysis ($2H_2SO_4 \leftrightarrow H_3SO_4^+ + HSO_4^-$), the two ions could stabilize the segregated states of the positively charged PEDOT and negatively charged PSS and then induce a significant structural rearrangement in the PEDOT:PSS with the removal of PSS and lead to the formation of crystallized nanofibrils, as shown in Figure 1-11. Due to the highly ordered and densely packed PEDOT:PSS nanofibrils via structural rearrangement, the corresponding conductivity increased up to 4380 S cm$^{-1}$. [57]

Another typical case is the use of polar organic solvent treatments such as dimethyl sulfoxide (DMSO), ethylene glycol (EG), N,N-dimethylformamide (DMF) and tetrahydrofuran (THF) for the improvement of PEDOT:PSS. [58, 59] Generally, the corresponding electrical conductivity would increase from 0.1 ~ 1 S cm$^{-1}$ to over 1,000 S cm$^{-1}$. Such remarkable increase is primarily ascribed to the improvement in mobility as a result of more extended conformation of polymer chains, thinning of insulating PSS shells, improved orientation and coherence of conductive PEDOT grains, etc. Very recently, Pipe et al. observed the simultaneous increase of both electrical conductivity and Seebeck coefficient by immersing the PEDOT:PSS film in EG or DMSO bath for a certain time in inert atmosphere. [60] Different from the common observed trade-off relationship for $\sigma$ and $S$, the simultaneous increase indicates the mobility enhancement due to the chain rearrangement overwhelms the reduction in carrier concentration via the removal of PSS. (Figure 1-12) Moreover, as PSS molecules are much larger than PEDOT molecules and contain a much greater number of covalent bonds, the removal of PSS and consequent increase in the average van der Waals character of bonds within the polymers makes a decrease in the cross-plane thermal conductivity $\kappa$. As it is challenging to measure the thermal conductivity in plane for films less than 100nm thick, the authors used an approximation of $\kappa$, and finally derived a maximum ZT value of 0.42 at room temperature,

which is still the highest value yet reported among conducting polymers.
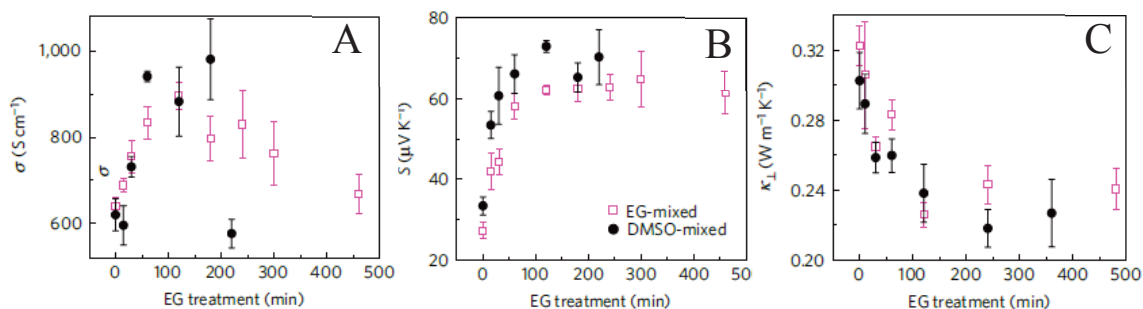


Figure 1-12 (A) electrical conductivities $\sigma$; (B) Seebeck coefficients $S$ and (C) vertical (cross-plane) thermal conductivities $\kappa$ of the PEDOT:PSS films at different treating times. [60]

1.4.4 Stretching treatment

Highly oriented polymer chains allow the carrier to move easily because of the increased carrier mobility via the overlap of π-π bonds in conjugated polymer chains. In particular, stretching the polymers could yield highly oriented films which are expected to show high electrical conductivity. [61-63] As reported [61], Hiroshige et al. evaluated uniaxial stretching effect on thermoelectric properties of a series of copolymers consisting of both unsubstituted and 2,5-dialkoxy-substituted phenylenevinylenes (P(ROPV-co-PV); RO = MeO, EtO (ethoxy) and BuO (butoxy)). It is found that electrical conductivities of the polymers were increased largely with the increase in stretching ratio. Moreover, the change of $S$ via stretching treatment is associated with the properties of the substituent in polymers. For P(MeOPV-co-PV) and P(EtOPV-co-PV), $S$ remained stable at the almost same level irrespective of stretching ratio, indicating the unchanged carrier concentration in the stretching alignment. While for P(BuOPV-co-PV), $S$ varied inversely with $\sigma$. Possibly, incorporation of a highly electron-donating butoxy group, having high affinity to an acceptor dopant, affected the domination of the carrier concentration over thermoelectric properties. In addition, due to the rearranged molecular structure via stretching, stretched poly(p-phenylene vinylene) (PPV) exhibited a higher doping level in FeCl$_3$ solution than the unstretched one. [63] In general, stretching treatment is proved to be an effective way to optimize the thermoelectric properties of the polymers.

## 1.5 Polymer blends: Polymer nanocomposites

Recently, in addition to the modification of polymer itself, organic-based nanocomposites have also become the central focus of developing the next generation TE materials in that it is possible to enhance the electrical conductivity while reducing the thermal conductivity significantly in such nanocomposites. [64, 65] Besides the dramatically increased electrical conductivity via the combination with highly conductive materials such as carbon nanotube, graphene, inorganic materials, another two main physical mechanisms are accounted for the TE performance enhancements of nanocomposites: (1) the nanoscale grain size or inclusion which enhances phonon boundary scattering even at elevated temperatures, and (2) the energy filtering effect of charge carriers at the boundary and/or via enhanced ionized impurity scattering at the organic/inorganic interfaces, both of which strongly scatter the heat phonons and thus largely decrease the lattice thermal conductivity of nanocomposites and increase the ZT value. As a result, recent advances in organic TE nanocomposites exhibited remarkable performances and also showed great promise of printing large-area, flexible TE modules.

### 1.5.1 Carbon materials

In general, carbon-based materials are abundant, non-toxic, easy to scale-up, and compatible with solution-based processes for large-scale production. They are also lightweight and mechanically flexible, which provide a new form factor to produce flexible and portable TE devices. In addition, their large $\pi-\pi$ conjugated systems (formed through fused aromatic rings) and the large specific surface areas greatly promote effective interfacial contacts between carbon particles and conducting polymers, thereby leading to a synergistic effect of property enhancements.

### 1.5.1.1 Carbon nanotubes

Being a typical example of 1D nanoparticles, carbon nanotubes (CNTs) have been extensively studied in both fundamental and technological researches due to their extremely high mechanical, electrical and thermal conductive properties (intrinsic values:

$\sigma > 10^4$ S cm$^{-1}$, $\kappa \sim 10^3$ W m$^{-1}$ K$^{-1}$). It is generally accepted that CNTs cannot be directly used as TE materials due to their high thermal conductivity, however, when effectively combining with polymer materials with intrinsic low conductivities, conducting polymer/CNT composites have become one main class of the promising TE materials.

Yu et al. found that the electrical conductivity of the PEDOT:PSS/CNTs composites dramatically enhanced up to $\sim 10^5$ S cm$^{-1}$, while the corresponding $S$ almost keeps constant, inducing an optimized power factor of $\sim 160$ μW m$^{-1}$ K$^{-2}$ at room temperature. [66] Due to the π−π interaction between CNT and polymers, the nanotubes establish intermolecular connections (the junctions shown in Figure 1-13) which facilitates electrical conduction. Additionally, the highly orientated CNT can also enhance the degree of ordering of the polymer chains around the aligned CNT, thereby enhancing the $\sigma$. [67] On the other hand, as mentioned, the thermal conductivity in organic TE materials is probably dominated by the phonons of varying frequencies. [28] Although the junctions could promote electron conduction, it can reversely lead to phonon scattering, making the CNT/polymer composites to exhibit a polymer-like thermal conductivity, ranging from 0.2 to 0.7 W m$^{-1}$ K$^{-1}$, which is much smaller than that of pure CNT. [3, 68, 69]
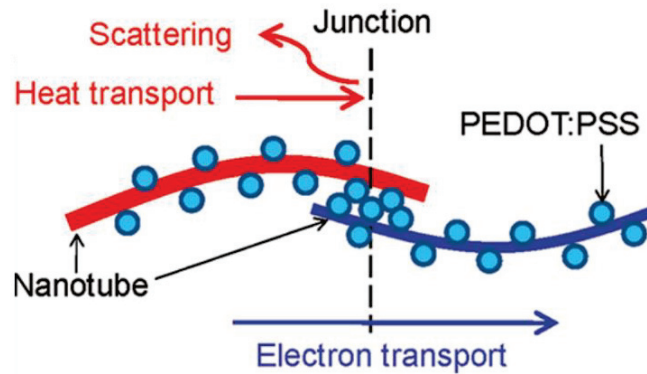


Figure 1-13 Nanotubes are coated by PEDOT:PSS particles, making nanotube-PEDOT:PSS-nanotube junctions in the composites. The presence of the junction is believed to give rise to exceptional thermoelectric transport properties (i.e., deterring heat transport as opposed to favorable pathways for electrons). [66]

It is worth mentioning that processing condition including the coating method, the type of carbon nanotubes, mixing ratio, solvent, stabilizer, temperature and so on could

strongly affect the properties of the polymer/CNT composites. [70, 71] For example, compared to the drop-casting method, spray-printed CNT/poly(3-hexylthiophene) composites with 50 wt% CNT exhibits a much higher power factor of 325 $\mu$W m$^{-1}$ K$^{-2}$ under the same conditions. [65]

*1.5.1.2 Graphene*

Graphene, an atomically thin sheet of hexagonally arranged carbon atoms, with its unique properties such as high specific surface area (~2630m$^2$ g$^{-1}$ in theory), good mechanical and electrical properties, and the possibility of functionalizing the graphene surface, has aroused much attention in the flexible TE application. [28, 72] It is also reported that graphene remains stable over a vast range of temperatures that is essential for reliability in the energy related applications. In addition, the large specific surface areas offered by atomically thin sheet structure is considered to strengthen the $\pi-\pi$ conjugation interactions between the polymers and graphene which can induce the formation of an ordered polymer chain.

PANI/graphene nanocomposite films with three types of graphenes with different structure characteristics were prepared through a solution-assistant dispersing method. It was found that structural defects and oxygen content in the graphene were closely related to the TE performance of the resulting composites. Higher TE properties were obtained in the composite film using graphene with lower levels of structural defects and oxygen impurities. This could be explained by the weakening of the $\pi-\pi$ conjugation interactions between polymer and graphene as well as the worsening of electrical transport of graphene itself, resulting from the impurity and defects in the graphene. The conformation of PANI molecules was first changed from a compacted coil to an expended coil by the chemical interactions between PANI and m-cresol solvent and then was further expanded by the strong $\pi$-$\pi$ stacking between PANI and graphene. (Illustration in Figure 1-14) The highly expanded molecular conformation of PANI facilitated the chain ordering during solvent evaporation while decreasing the structural defects along the backbone, thus leading to the increase in carrier mobility. Ultimately, the maximum electrical

conductivity and power factor of the composite films reached 856 S cm$^{-1}$ and 19 μW m$^{-1}$ K$^{-2}$, respectively. [73]
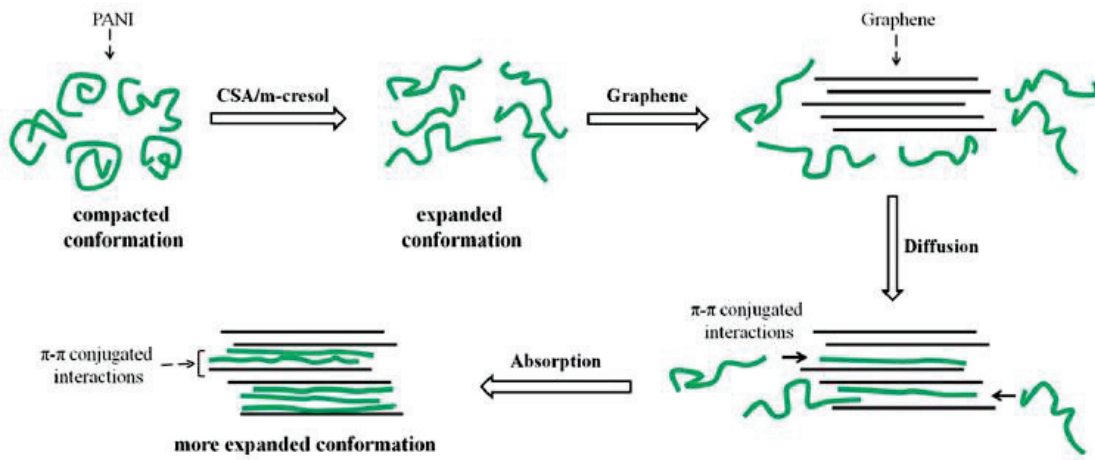


Figure 1-14 Schematic illustration of the synthesis procedure of PANI/graphene composite film by a simple solution-assistant dispersing process. [73]

### 1.5.1.3 Co-polymer

Despite the carbon tubes and graphene, there are still works on co-polymers for thermoelectric applications. On one hand, the co-polymerization is a strong tool to incorporate molecular segments of different nature in a polymer chain. This method allows to synthesize co-polymers with better thermoelectric efficiency than the corresponding homo-polymers. On the other hand, the co-polymerization of two monomers could lead to a multilayer structured co-polymer films, which may yield exciting results.
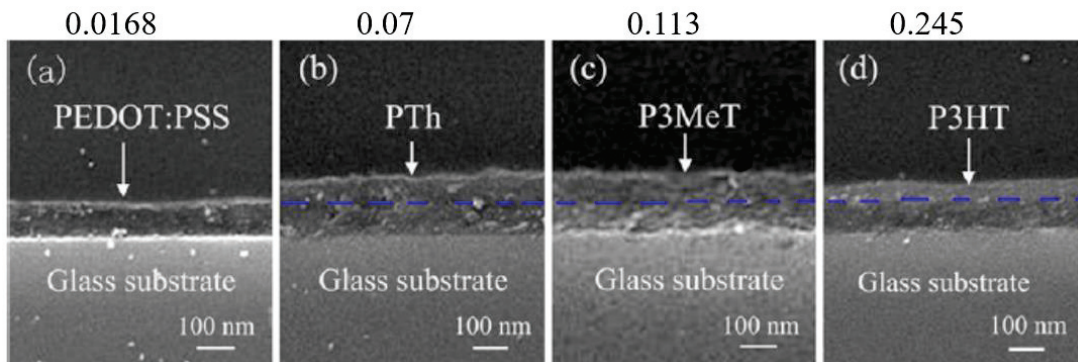


Figure 1-15 Cross-section SEM images of the nanofilms: (a) PEDOT:PSS, (b) PEDOT:PSS/PTh, (c) PEDOT:PSS/P3MeT, (d) PEDOT:PSS/P3HT. The values given above the SEM images are the carrier mobility (cm$^2$ V$^{-1}$ s$^{-1}$)) corresponding to the co-polymers. [74]

As shown in Figure 1-15, compared to the pristine PEDOT:PSS, carrier mobility of the co-polymers with the layered structure was largely enhanced, providing a facile and general method for synthesizing materials with better TE performance for a wider array of applications. [74]

1.5.2 Inorganic Nanoparticles

Although the combination of carbon material with polymers intriguingly results in high electrical conductivities and low thermal conductivities, the Seebeck coefficient almost keeps constant during the processing. On such basis, inorganic materials with high Seebeck coefficient is considered to be another promising filler for the improvement of organic polymers. Similarly, such nanocomposites would also exhibit low thermal conductivity due to the phonon scattering or energy filtering effect at the junctions. Moreover, these nanoparticles could also react as the templates for rearrangement of the polymer chains, further improving the properties of the polymer/inorganic material composites.

Through a facile synthesis, PEDOT:PSS/ tellurium nanocomposites with a power factor of 71 $\mu$W m$^{-1}$ K$^{-2}$ was obtained. [75] Interestingly, the $\sigma$ of the composite was found to be higher than values obtained for both neat PEDOT:PSS and tellurium nanowires. The authors ascribed the increase to the fact that the PEDOT:PSS protects the Te nanorods from oxidation and improves interparticle contact. Moreover, Te nanorods can also react as the template which impacts the nanostructure of the polymer complex, and then further enhance the $\sigma$. [32] Moreover, the thermal conductivity of the composites was calculated around 0.3 W m$^{-1}$ K$^{-1}$, which is much lower than the bulk $\kappa$ of tellurium of 2 W m$^{-1}$ K$^{-1}$. The high interfacial area between tellurium nanowires and PEDOT:PSS was thought to lead to phonon scattering, which reduces the thermal conductivity. Overall, a figure of merit ZT ~ 0.1 was achieved.

Consequently, the polymer blends is proved to be an effective strategy towards high-performance thermoelectric materials. Moreover, the modification method such as chemical/electrochemical doping, secondary treatment we mentioned above for the

polymer itself could also be applied to the further improvement of the obtained polymer blends. Nowadays, organic TE materials with high ZT value can be easily obtained. Here, several typical organic materials with expectable properties at room temperature are summarized in Table 1-3.

Table 1-3 Typical values of the main thermoelectric parameters in conducting polymers, carbon materials and inorganic nanoparticles based polymer composites at room temperature.

| Material | $\sigma$ (S cm$^{-1}$) | $S$ ($\mu$V K$^{-1}$) | $\kappa$ (W m$^{-1}$ K$^{-1}$) | $PF$ ($\mu$W m$^{-1}$ K$^{-2}$) | $ZT$ | Ref |
|---|---|---|---|---|---|---|
| Conducting polymers | | | | | | |
| EC-PP-PEDOT | ~1200 | ~100 | | 1270 | | [55] |
| heavily I-doped PA | 11110 | 28.4 | | ~900 | | [76] |
| DMSO-mixed PEDOT:PSS+EG | ~900 | ~75 | ~0.32 | 469 | 0.42 | [60] |
| EG-mixed PEDOT:PSS+EG | ~900 | ~62 | ~0.37 | ~350 | 0.28 | [60] |
| EC-PEDOS-C6 | 335 | ~100 | | 354.7 | | [77] |
| DMSO-mixed PEDOT:PSS+HZ | 1310 | 49.3 | 0.3 | 318.4 | 0.31 | [78] |
| PEDOT:Tos +TDEA | ~80 | ~200 | 0.37 | 324 | 0.25 | [31] |
| PEDOT:BTFMSI+HZ | ~1080 | ~37 | 0.19 | 147 | 0.22 | [49] |
| EC-PEDOT:PSS | ~23 | ~100 | 0.17 | 23.5 | 0.04 | [54] |
| Carbon materials based polymer composites | | | | | | |
| PANi/rGO/PEDOT /CNT | ~1900 | ~120 | | ~2710 | | [79] |
| DWNT/(PEDOT:PSS)/TCPP | 960 | ~70 | | ~500 | | [70] |
| Polystyrene/SSWCNT | ~1250 | ~58 | ~0.3 | 413 | 0.41 | [80] |
| Spray-printed CNT/P3HT | ~345 | ~97 | | ~325 | | [65] |
| SWNT/PANI hybrid | 769 | ~48 | 0.43 | 176 | 0.12 | [64] |
| PEDOT:PSS/CNT+EG | ~750 | ~45 | | ~151 | | [81] |
| PEDOT:PSS/SWNT | ~4000 | ~18 | ~0.53 | ~140 | | [69] |
| Inorganic nanoparticles based polymer composites | | | | | | |
| PEDOT:PSS/PAA/Bi$_2$Te$_3$ | 380 | 79 | 0.36 | ~240 | 0.2 | [82] |
| PEDOT:PSS/Bi$_2$Te$_3$ | ~250 | ~150 | 0.558 | 131 | 0.08 | [83] |
| DMSO-PEDOT:PSS/ Te | ~15 | 260 | | 100 | | [84] |
| PEDOT:PSS/ Te | 19.3 | 163 | 0.2~0.3 | 71 | ~0.1 | [75] |
| PEDOT:PSS/ Gold Nanorod | ~2000 | ~12 | | ~30 | | [85] |

## 1.6 Outlines

As one kind of "green" energy conversion materials, organic TE materials have caused more and more concerns. In order to practical application, researchers are strived to improve the thermoelectric properties. Experimentally, it is important to control the structure and surface morphology of organic materials, and optimize the doping level, thereby collectively leading to the balanced TE properties while simultaneously engineering an electronic structure. As known, high doping level results in a high electrical conductivity $\sigma$. However, excessive doping would generate detrimental defects and traps, which reduces carrier mobility $\mu$ and then $\sigma$. Generally, when a low doping level is maintained, a small $\sigma$ is achieved because of the comparatively low carrier concentration $n$. The reduced $\sigma$ can be reversely compensated by significantly improved $S$ due to the low level of doping, giving rise to the maximum power factor. Moreover, by careful design of suitable molecular structures of organic semiconductors, highly intrinsic $\mu$ is expected to be achieved. Namely, an optimal doping level, as well as the suitable molecular structures could collectively give a large improvement of the power factor. On the other side, the thermal conductivity in organic TE materials is generally recognized to be dominated by $\kappa_L$. When constructing suitable nanostructures or fabricating nanocomposites of conducting polymers, thermal vibrations would be confined due to the interfacial phonon scattering, leading to largely decrease in $\kappa_L$. Simultaneously, the carrier mobility could also be benefited owing to anisotropic charge transport. Together, it can be seen that TE property parameters are able to be decoupled in organic TE materials, in stark contrast to those of conventional inorganic analogues, therefore showing great promise of organic TEs. Moreover, what makes organic TE materials stand out is the easy processing of flexible TE materials, which is indeed difficult to realize in inorganic TE materials. On the basis, here, we studied on some typical organic TE materials such as polyaniline and PEDOT, and then developed their thermoelectric performance for a promising TE material. The details for this thesis are as follow:

Chapter 1 is "General introduction". In this part, we introduce the development process

and working mechanism of thermoelectric materials. Influencing factors for the thermoelectric properties are also discussed. Finally, several effective methods to improve the thermoelectric performance for organic semiconductors have been summarized detailedly.

Chapter 2 is "Thermoelectric properties of PEDOT films prepared by electrochemical polymerization". Thermoelectric (TE) properties of flexible and free-standing poly(3,4-ethylenedioxythiophene) (PEDOT) films synthesized via galvanostatic polymerization of 3,4-ethylenedioxythiophene in propylene carbonate containing sulfated poly($\beta$-hydroxyethers) (S-PHE) as polymer electrolyte were elaborately studied. Both electrical conductivities ($\sigma$) and Seebeck coefficients ($S$) of the PEDOT:S-PHE films were increased by decreasing the temperature ($T$) or by increasing the current density ($J$) during electrosynthesis. Possible reasons for the lack of a trade-off relation commonly observed between $\sigma$ and $S$ are discussed on the basis of SEM and oxidation-level measurements. Preparation of the PEDOT:S-PHE films was optimized with respect to $T$ and $J$. In addition, the oxidation level of the PEDOT:S-PHE films was controlled by potential and the change of their TE performances was discussed in conjunction with the change of chemical species involved. The power factor ($PF = \sigma S^2$) of the PEDOT:S-PHE films reached 7.9 $\mu$W m$^{-1}$ K$^{-2}$, leading to a dimensionless TE figure-of-merit ($ZT$) of 0.013.

Chapter 3 is "Thermoelectric performances of graphene/polyaniline composites prepared by one-step electrosynthesis". Composite films comprising graphene and polyaniline were prepared in one step by a facile electrochemical technique with graphene oxide (GO) and aniline monomer as raw materials, and their thermoelectric properties were investigated. Electrical conductivities of the composite films generated on the fluorine-doped tin oxide (FTO) electrode were dependent on the weight ratio of GO and aniline, and they exhibited a peak value of 30 S cm$^{-1}$ at the GO/aniline ratio between 5:1 and 10:1, while Seebeck coefficients were less dependent on the weight ratio. The maximum power factor ($PF$) for the composite films was *ca.* 1 $\mu$W m$^{-1}$ K$^{-2}$. When the FTO electrode was replaced by the stainless steel electrode, conductivities of the

composite films with the GO/aniline ratio of 8:1 were increased up to *ca.* 130 S cm$^{-1}$. As a result, the *PF* and the dimensionless thermoelectric figure-of-merit (*ZT*) at room temperature reached 3.6 μW m$^{-1}$ K$^{-2}$ and 0.008, respectively. The *ZT* value is the highest among those reported so far for graphene/PANI composites. Possible reasons for the conductivity enhancement on the stainless steel electrode are also discussed on the basis of electrochemical measurements and X-ray photoelectron spectroscopy.

Chapter 4 is "Electrosynthesis of multilayer film stacked alternately by poly(3,4-ethylenedioxythiophene) and reduced graphene oxide from aqueous solution". Multilayer films stacked alternately by poly(3,4-ethylenedioxythiophene) and reduced graphene oxide layers were electrochemically synthesized from a single aqueous solution containing 3,4-ethylenedioxythiophene (EDOT) and graphene oxide (GO) by oxidizing EDOT and reducing GO repeatedly on the conductive substrate. In the proposed technique, film thicknesses of the respective layers were easily tuned by the electrolysis time, and the number of layers was increased just by repeating the potential-step sequence.

Chapter 5 is "Highly improved thermoelectric performances of PEDOT:PSS/SWCNT composites by solvent treatment". Composites of poly(3,4-ethylenedioxythiophene): poly(styrenesulfonate) (PEDOT:PSS) and single-wall carbon nanotube (SWCNT) were prepared by mixing aqueous dispersions of PEDOT:PSS and SWCNT at different weight ratios. By being soaked with DMSO for two minutes at room temperature, the PEDOT:PSS/SWCNT composite with an optimized SWCNT weight ratio of 74 wt% exhibited a high electric conductivity of 3,800 S cm$^{-1}$ and a reasonable Seebeck coefficient of 28 μV K$^{-1}$, leading to a promising power factor of 300 μW m$^{-1}$ K$^{-2}$.

Chapter 6 is "Conclusions". Several important conclusions of this study are given in detail and suggestions are provided for further study.

# Reference (1)

1. E. Kolasińska and P. Kolasiński, A Review on Electroactive Polymers for Waste Heat Recovery. Materials, 2016, *9*, 485.

2. J. Yang and T. Caillat, Thermoelectric Materials for Space and Automotive Power Generation. MRS Bulletin, 2006, *31*, 224.

3. M. Culebras, C. M. Gomez, and A. Cantarero, Review on Polymers for Thermoelectric Applications. Materials, 2014, *7*, 6701.

4. C. Han, Z. Li, and S. X. Dou, Recent progress in thermoelectric materials. Chin. Sci. Bull., 2014, *59*, 2073.

5. C. Gayner and K. K. Kar, Recent advances in thermoelectric materials. Prog. Mater. Sci., 2016, *83*, 330.

6. J. Yang, H. L. Yip, and A. K. Y. Jen, Rational Design of Advanced Thermoelectric Materials. Adv. Energy Mater., 2013, *3*, 549.

7. X. Zhang and L. D. Zhao, Thermoelectric materials: Energy conversion between heat and electricity. J. Materiomics, 2015, *1*, 92.

8. J. P. Fleurial, Thermoelectric Power generation materials: Technology and application opportunities. JOM, 2009, *61*, 79.

9. B. Zhong, Y. Zhang, W. Li, Z. Chen, J. Cui, W. Li, Y. Xie, Q. Hao, and Q. He, High superionic conduction arising from aligned large lamellae and large figure of merit in bulk Cu1.94Al0.02Se. Appl. Phys. Lett., 2014, *105*, 123902.

10. K. Biswas, J. He, I. D. Blum, C. I. Wu, T. P. Hogan, D. N. Seidman, V. P. Dravid, and M. G. Kanatzidis, High-performance bulk thermoelectrics with all-scale hierarchical architectures. Nature, 2012, *489*, 414.

11. L. D. Zhao, S. H. Lo, Y. Zhang, H. Sun, G. Tan, C. Uher, C. Wolverton, V. P. Dravid, and M. G. Kanatzidis, Ultralow thermal conductivity and high thermoelectric figure of merit in SnSe crystals. Nature, 2014, *508*, 373.

12. Z. Chen, Z. Jian, W. Li, Y. Chang, B. Ge, R. Hanus, J. Yang, Y. Chen, M. Huang, G. J. Snyder, and Y. Pei, Lattice Dislocations Enhancing Thermoelectric PbTe in Addition to Band Convergence. Adv. Mater., 2017.

13. R. Al Rahal Al Orabi, N. A. Mecholsky, J. Hwang, W. Kim, J. S. Rhyee, D. Wee, and M. Fornari, Band Degeneracy, Low Thermal Conductivity, and High Thermoelectric Figure of Merit in SnTe–CaTe Alloys. Chem. Mater., 2016, *28*, 376.

14. D. Yang, X. Su, Y. Yan, T. Hu, H. Xie, J. He, C. Uher, M. G. Kanatzidis, and X. Tang, Manipulating the Combustion Wave during Self-Propagating Synthesis for High Thermoelectric Performance of Layered Oxychalcogenide Bi1–xPbxCuSeO. Chem. Mater., 2016, *28*, 4628.

15. Q. Zhang, Y. M. Sun, W. Xu, and D. B. Zhu, Organic Thermoelectric Materials: Emerging Green Energy Materials Converting Heat to Electricity Directly and Efficiently. Adv. Mater., 2014, *26*,

6829.

16. H. Shirakawa, E. J. Louis, A. G. Macdiarmid, C. K. Chiang, and A. J. Heeger, Synthesis of Electrically Conducting Organic Polymers :Halogen Derivatives of Polyacetylene, (CH),. J. Chem. Soc. Chem. Commun., 1977, *16*, 578.

17. C. K. Chiang, C. R. Fincher, Y. W. Park, A. J. Heeger, H. Shirakawa, E. J. Louis, S. C. Gau, and A. G. MacDiarmid, Electrical Conductivity in Doped Polyacetylene. Phys. Rev. Lett., 1977, *39*, 1098.

18. L. Ghasemi-Mobarakeh, M. P. Prabhakaran, M. Morshed, M. H. Nasr-Esfahani, H. Baharvand, S. Kiani, S. S. Al-Deyab, and S. Ramakrishna, Application of conductive polymers, scaffolds and electrical stimulation for nerve tissue engineering. J. Tissue Eng. Regen Med., 2011, *5*, 17.

19. R. Balint, N. J. Cassidy, and S. H. Cartmell, Conductive polymers: towards a smart biomaterial for tissue engineering. Acta Biomater, 2014, *10*, 2341.

20. A. Pron and P. Rannou, Processible conjugated polymers: from organic semiconductors to organic metals and superconductors. Prog. Polym. Sci., 2002 *27*, 135.

21. C. S. Wang, J. Burkett, C. Y. C. Lee, and F. E. Arnold, Structure and Electrical Conductivity of Ion-Implanted Rigid-Rod and Ladder Polymers. J. Polym. Sci. Polym. Phys., 1993, *31*, 1799.

22. B. Ratier, J. Massengo, B. Guille, B. Lucas, and A. Moliton, Ion implanted poly(paraphenylene) electrical property modiRcations induced by cobalt 60 g ray irradiation. Synth. Met., 2000, *115*, 103.

23. R. A. Basheer and S. Jodeh, Electrically conducting thin films obtained by ion implantation in pyrolyzed polyacrylonitrile. Mat. Res. Innovat., 2001, *4*, 131.

24. W. Wang, S. Lin, J. Bao, T. Rang, H. Wan, and J. Sun, The n-type doping of polyaniline films by ion implantation. Nucl. Instrum. Methods Phys. Res., 1993, *74*, 514.

25. S. A. Jenekhe and S. J. Tibbetts, Ion Implantation Doping and Electrical Properties of High-temperature Ladder Polymers. J. Polym. Sci. Polym. Phys., 1988, *26*, 201.

26. W. C. Germs, K. Guo, R. A. Janssen, and M. Kemerink, Unusual thermoelectric behavior indicating a hopping to bandlike transport transition in pentacene. Phys. Rev. Lett., 2012, *109*, 016601.

27. Y. Wang, J. Zhou, and R. Yang, Thermoelectric Properties of Molecular Nanowires. J. Phys. Chem. C, 2011, *115*, 24418.

28. Y. Chen, Y. Zhao, and Z. Liang, Solution processed organic thermoelectrics: towards flexible thermoelectric modules. Energy Environ. Sci., 2015, *8*, 401.

29. Y. Harima, T. Eguchi, and K. Yamashita, Enhancement of carrier mobilities in poly(3-methylthiophene) electrochemical doping. Synth. Met., 1998, *95*, 69.

30. Y. Harima, T. Eguchi, K. Yamashita, K. Kojima, and M. Shiotani, An in situ ESR study on poly(3-methylthiophene) :charge transport due to polarons and bipolarons before the evolution of metallic conduction. Synth. Met., 1999, *105*, 121.

31. O. Bubnova, Z. U. Khan, A. Malti, S. Braun, M. Fahlman, M. Berggren, and X. Crispin, 36-

Optimization of the thermoelectric figure of merit in the conducting polymer poly(3,4-ethylenedioxythiophene). Nat. Mater., 2011, *10*, 429.

32. R. Kroon, D. A. Mengistie, D. Kiefer, J. Hynynen, J. D. Ryan, L. Yu, and C. Muller, Thermoelectric plastics: from design to synthesis, processing and structure-property relationships. Chem. Soc. Rev., 2016, *45*, 6147.

33. W. Shi, T. Zhao, J. Xi, D. Wang, and Z. Shuai, Unravelling Doping Effects on PEDOT at the Molecular Level: From Geometry to Thermoelectric Transport Properties. J. Am. Chem. Soc., 2015, *137*, 12929.

34. L. B. Groenendaal, F. Jonas, D. Freitag, H. Pielartzik, and J. R. Reynolds, Poly(3,4-ethylenedioxythiophene) and Its Derivatives: Past, Present, and Future. Adv. Mater., 2000, *12*, 481.

35. J. Liang, Y. Ma, F. Wang, and W. Yang, Flexible, Highly Transparent, and Conductive Poly(3,4-ethylenedioxythiophene)-Polypropylene Composite Films of Nanofibrillar Morphology. Chem. Mater., 2010, *22*, 4254.

36. Y. Tan and K. Ghandi, Kinetics and mechanism of pyrrole chemical polymerization. Synth. Met., 2013, *175*, 183.

37. F. Wang, Y. Lai, and M. Han, Stimuli-Responsive Conjugated Copolymers Having Electro-Active Azulene and Bithiophene Units in the Polymer Skeleton: Effect of Protonation and p-Doping on Conducting Properties. Macromolecules, 2004, *37*, 3222.

38. H. Farrokhi, O. Khani, F. Nemati, and M. Jazirehpour, Synthesis and investigation of microwave characteristics of polypyrrole nanostructures prepared via self-reactive flower-like $MnO_2$ template. Synth. Met., 2016, *215*, 142.

39. T. Song, T. Liu, X. Yang, and F. Bai, Raspberry-like particles via the heterocoagulated reaction between reactive epoxy and amino groups. Colloids Surf. A: Physicochem. Eng. Aspects, 2015, *469*, 60.

40. C. K. Chiang, M. A. Druy, S. C. Gau, A. J. Heeger, E. J. Louis, A. G. MacDiarmid, Y. W. Park, and H. Shirakawa, Synthesis of highly conducting films of derivatives of polyacetylene, (CH)x. J. Am. Chem. Soc., 1978, *100*, 1013.

41. J. Li, X. Tang, H. Li, Y. Yan, and Q. Zhang, Synthesis and thermoelectric properties of hydrochloric acid-doped polyaniline. Synth. Met., 2010, *160*, 1153.

42. P. A. Calvo, J. Rodríguez, H. Grande, D. Mecerreyes, and J. A. Pomposo, Chemical oxidative polymerization of pyrrole in the presence of m-hydroxybenzoic acid- and m-hydroxycinnamic acid-related compounds. Synth. Met., 2002, *126*, 111.

43. H. Yamato, K. I. Kai, M. Ohwa, T. Asakura, T. Koshiba, and W. Wernet, Synthesis of free-standing poly ( 3,4-ethylenedioxythiophene) conducting polymer films on a pilot scale. Synth. Met., 1996, *83*, 125.

44. Y. Sun and G. Shi, Graphene/polymer composites for energy applications. J. Polym. Sci. Part B: Polym. Phys., 2013, *51*, 231.

45. Y. Harima, S. Fukumoto, L. Zhang, X. Jiang, J. Yano, K. Inumaru, and I. Imae, Thermoelectric performances of graphene/polyaniline composites prepared by one-step electrosynthesis. RSC Adv., 2015, *5*, 86855.

46. F. Jiang, Z. Yao, R. Yue, Y. Du, J. Xu, P. Yang, and C. Wang, Electrochemical fabrication of long-term stable Pt-loaded PEDOT/graphene composites for ethanol electrooxidation. Int. J. Hydrogen Energy, 2012, *37*, 14085.

47. L. Zhang, T. Goto, I. Imae, Y. Sakurai, and Y. Harima, Thermoelectric properties of PEDOT films prepared by electrochemical polymerization. J. Polym. Sci. Part B: Polym. Phys., 2017, *55*, 524.

48. N. K. Guimard, N. Gomez, and C. E. Schmidt, Conducting polymers in biomedical engineering. Prog. Polym. Sci., 2007, *32*, 876.

49. M. Culebras, C. M. Gómez, and A. Cantarero, Enhanced thermoelectric performance of PEDOT with different counter-ions optimized by chemical reduction. J. Mate. Chem. A, 2014, *2*, 10109.

50. J. F. Rabek, J. Lucki, M. Zuber, B. J. Qu, and W. F. Shi, Polymerization of pyrrole by cationic photoinitiators. Polymer, 1992, *33*, 4838.

51. B. Aydogan, A. S. Gundogan, T. Ozturk, and Y. Yagci, Polythiophene derivatives by step-growth polymerization via photoinduced electron transfer reactions. Chem. Commun., 2009, 6300.

52. A. L. Gomes, M. B. Pinto Zakia, J. G. Filho, E. Armelin, C. Alemán, and J. Sinezio de Carvalho Campos, Preparation and characterization of semiconducting polymeric blends. Photochemical synthesis of poly(3-alkylthiophenes) using host microporous matrices of poly(vinylidene fluoride). Polym. Chem., 2012, *3*, 1334.

53. R. Zuzok, A. B. Kaiser, W. Pukacki, and S. Roth, Thermoelectric power and conductivity of iodine-doped ''new'' polyacetylene. J. Chem. Phys., 1991, *95*, 1270.

54. O. Bubnova, M. Berggren, and X. Crispin, Tuning the thermoelectric properties of conducting polymers in an electrochemical transistor. J. Am. Chem. Soc., 2012, *134*, 16456.

55. T. Park, C. Park, B. Kim, H. Shin, and E. Kim, Flexible PEDOT electrodes with large thermoelectric power factors to generate electricity by the touch of fingertips. Energy Environ. Sci., 2013, *6*, 788.

56. A. G. MacDiarmid and A. J. Epstein, The concept of secondary doping as applied to polyaniline. Synth. Met., 1994, *65*, 103.

57. N. Kim, S. Kee, S. H. Lee, B. H. Lee, Y. H. Kahng, Y. R. Jo, B. J. Kim, and K. Lee, Highly conductive PEDOT:PSS nanofibrils induced by solution-processed crystallization. Adv. Mater., 2014, *26*, 2268.

58. Q. Wei, M. Mukaida, K. Kirihara, Y. Naitoh, and T. Ishida, Recent Progress on PEDOT-Based Thermoelectric Materials. Materials, 2015, *8*, 732.

59. H. Shi, C. C. Liu, Q. L. Jiang, and J. K. Xu, Effective Approaches to Improve the Electrical Conductivity of PEDOT:PSS: A Review. Adv. Electron. Mater., 2015, *1*, 1500017.

60. G.-H. Kim, L. Shao, K. Zhang, and K. P. Pipe, Engineered doping of organic semiconductors for enhanced thermoelectric efficiency. Nat. Mater., 2013, *12*, 719.

61. Y. Hiroshige, M. Ookawa, and N. Toshima, Thermoelectric figure-of-merit of iodine-doped copolymer of phenylenevinylene with dialkoxyphenylenevinylene. Synth. Met., 2007, *157*, 467.

62. Y. Du, S. Z. Shen, K. Cai, and P. S. Casey, Research progress on polymer–inorganic thermoelectric nanocomposite materials. Prog. Polym. Sci., 2012, *37*, 820.

63. J. Briers, W. Eevers, P. Cos, H. J. Geiset, R. Mertens, P. Nagels, X. B. Zhang, G. V. Tendeloo, W. Herrebout, and B. V. d. Veken, Molecular orientation and conductivity in highly oriented poly(p-phenylene vinylene). Polymer, 1994, *35*, 4569.

64. Q. Yao, Q. Wang, L. Wang, and L. Chen, Abnormally enhanced thermoelectric transport properties of SWNT/PANI hybrid films by the strengthened PANI molecular ordering. Energy Environ. Sci., 2014, *7*, 3801.

65. C. T. Hong, Y. H. Kang, J. Ryu, S. Y. Cho, and K. S. Jang, Spray-printed CNT/P3HT organic thermoelectric films and power generators. J. Mater. Chem. A, 2015, *3*, 21428.

66. C. Yu, K. Choi, L. Yin, and J. C. Grunlan, Light-Weight Flexible Carbon Nanotube Based Organic Composites with Large Thermoelectric Power Factors. ACS Nano, 2011, *10*, 7885.

67. X. Hu, L. Chen, Y. Zhang, Q. Hu, J. Yang, and Y. Chen, Large-Scale Flexible and Highly Conductive Carbon Transparent Electrodes via Roll-to-Roll Process and Its High Performance Lab-Scale Indium Tin Oxide-Free Polymer Solar Cells. Chem. Mater., 2014, *26*, 6293.

68. D. Kim, Y. Kim, K. Choi, J. C. Grunlan, and C. Yu, Improved Thermoelectric Behavior of Nanotube-Filled Polymer Composites with Poly(3,4-ethylenedioxythiophene) Poly(styrenesulfonate). ACS Nano, 2010, *4*, 513.

69. G. P. Moriarty, S. De, P. J. King, U. Khan, M. Via, J. A. King, J. N. Coleman, and J. C. Grunlan, Thermoelectric behavior of organic thin film nanocomposites. J. Polym. Sci. Part B: Polym. Phys., 2013, *51*, 119.

70. G. P. Moriarty, K. Briggs, B. Stevens, C. Yu, and J. C. Grunlan, Fully Organic Nanocomposites with High Thermoelectric Power Factors by using a Dual-Stabilizer Preparation. Energy Technol., 2013, *1*, 265.

71. C. Bounioux, P. Díaz-Chao, M. Campoy-Quiles, M. S. Martín-González, A. R. Goñi, R. Yerushalmi-Rozen, and C. Müller, Thermoelectric composites of poly(3-hexylthiophene) and carbon nanotubes with a large power factor. Energy Environ. Sci., 2013, *6*, 918.

72. J. R. F. Foronda, S. M. R. Cabrera, D. L. Cumpas, P. G. A. Villar, J. L. Tan, and B. J. V. Tongol, Enhanced Electrocatalytic Activity of Pt Particles Supported on Reduced Graphene Oxide/Poly(3,4-ethylenedioxythiophene) RGO/PEDOT Composite towards Ethanol Oxidation. J. Chem., 2013, *2013*, 1.

73. L. Wang, Q. Yao, H. Bi, F. Huang, Q. Wang, and L. Chen, Large thermoelectric power factor in polyaniline/graphene nanocomposite films prepared by solution-assistant dispersing method. J. Mater. Chem. A, 2014, *2*, 11107.

74. H. Shi, C. Liu, J. Xu, H. Song, B. Lu, F. Jiang, W. Zhou, G. Zhang, and Q. Jiang, Facile Fabrication of PEDOT:PSS/Polythiophenes Bilayered Nanofilms on Pure Organic Electrodes and Their

Thermoelectric Performance. ACS Appl. Mater. Interf., 2013, *5*, 12811.

75. K. C. See, J. P. Feser, C. E. Chen, A. Majumdar, J. J. Urban, and R. A. Segalman, Water-Processable Polymer−Nanocrystal Hybrids for Thermoelectrics. Nano Lett., 2010, *10*, 4664.

76. Y. W. Park, Structure and morphology: relation to thermopower properties of conductive polymers. Synth. Met., 1991, *45*, 173.

77. B. Kim, H. Shin, T. Park, H. Lim, and E. Kim, NIR-sensitive poly(3,4-ethylenedioxyselenophene) derivatives for transparent photo-thermo-electric converters. Adv. Mater., 2013, *25*, 5483.

78. S. H. Lee, H. Park, S. Kim, W. Son, I. W. Cheong, and J. H. Kim, Transparent and flexible organic semiconductor nanofilms with enhanced thermoelectric efficiency. J. Mater. Chem. A, 2014, *2*, 7288.

79. C. Cho, K. L. Wallace, P. Tzeng, J. H. Hsu, C. Yu, and J. C. Grunlan, Outstanding Low Temperature Thermoelectric Power Factor from Completely Organic Thin Films Enabled by Multidimensional Conjugated Nanomaterials. Adv. Energy Mater., 2016, *6*, 1502168.

80. K. Suemori, Y. Watanabe, and S. Hoshino, Carbon nanotube bundles/polystyrene composites as high-performance flexible thermoelectric materials. Appl. Phys. Lett., 2015, *106*, 113902.

81. W. Lee, Y. H. Kang, J. Y. Lee, K. S. Jang, and S. Y. Cho, Improving the thermoelectric power factor of CNT/PEDOT:PSS nanocomposite films by ethylene glycol treatment. RSC Adv., 2016, *6*, 53339.

82. K. Kato, H. Hagino, and K. Miyazaki, Fabrication of Bismuth Telluride Thermoelectric Films Containing Conductive Polymers Using a Printing Method. J. Electron. Mater., 2013, *42*, 1313.

83. B. Zhang, J. Sun, H. E. Katz, F. Fang, and R. L. Opila, Promising thermoelectric properties of commercial PEDOT:PSS materials and their bi2Te3 powder composites. ACS Appl. Mater. Interfaces, 2010, *2*, 3170.

84. S. K. Yee, N. E. Coates, A. Majumdar, J. J. Urban, and R. A. Segalman, Thermoelectric power factor optimization in PEDOT:PSS tellurium nanowire hybrid composites. Phys. Chem. Chem. Phys., 2013, *15*, 4024.

85. A. Yoshida and N. Toshima, Gold Nanoparticle and Gold Nanorod Embedded PEDOT:PSS Thin Films as Organic Thermoelectric Materials. J. Electron. Mater., 2013, *43*, 1492.

# Chapter 2　Thermoelectric properties of PEDOT films prepared by electrochemical polymerization

## 2.1 Introduction

Thermoelectric (TE) devices based on the Seebeck effect are able to harvest electricity from waste heat generated from households, chemical plants, or even human bodies by utilizing the diffusion of charge carriers induced by the gradient of temperature. Up until quite recently, a number of studies have been devoted to the development of TE devices based on inorganic materials such as Bi-Te, Co-Sb, Bi-Pb, Sn-Te alloys, and transition metal oxides. [1-3] They provide fairly high TE performances at elevated temperatures, in particular. These inorganic TE materials, however, are expensive, rare, heavy, and relatively difficult to process, and thus impeding their widespread use. The performance of a TE material is judged by a dimensionless TE figure-of-merit (*ZT*) and a power factor (*PF*) defined, respectively, by $ZT= \sigma S^2 T/\kappa$ and $PF=\sigma S^2$, where $\sigma$, $S$, $\kappa$, and $T$ are electric conductivity, Seebeck coefficient, thermal conductivity, and absolute temperature, respectively. A typical inorganic TE material, $Bi_2Te_3$, gives *ZT* values greater than unity, which is a numerical target for a practical use of the materials in the TE devices. In recent years, organic TE materials have received a growing interest because of their advantages of low cost, abundance of raw materials, flexibility, and relatively simple manufacturing processes over traditional inorganic TE materials. [4-8] They are aimed at harvesting low-temperature exhaust heat below 200 $^{\circ}$C which occupies a large part of waste heat. Conducting polymers that exhibit high conductivities at oxidized (doped) states are a promising class of organic TE materials and among a variety of conducting polymers, poly(3,4-ethylenedioxythiophene): poly (styrenesulfonate) (PEDOT:PSS) that is commercially available has been intensively studied so far due to its stability in ambient atmosphere and extremely high conductivities exceeding $10^3$ S cm$^{-1}$. [9] A high *ZT* value of 0.42 at room temperature is reported for PEDOT:PSS films treated with dimethyl sulfoxide (DMSO) and ethylene glycol (EG). [10] The commercially obtained PEDOT:PSS has also been mixed with $Bi_2Te_3$ [11], Te [12], carbon nanotubes [13],

graphene [14], and Au nanoparticles [15] at different compositions to seek for PEDOT:PSS composites with higher TE performances.

In the present study, PEDOT films were prepared via a constant-current (galvanostatic) polymerization of 3,4-ethylenedioxythiophene (EDOT) in propylene carbonate (PC) containing a polymer electrolyte (S-PHE in Scheme 2-1) as dopant. In general, conducting polymers prepared electrochemically are fragile and need substrates for fixing them on. [16-18] In contrast, it has been reported that the electrosynthesized PEDOT:S-PHE films are flexible, free-standing, and mechanically strong. [19] These excellent film features allow us to use them in vertical TE devices as well as in in-plane TE devices. The former devices are favorable compared with the latter in a sense that flexible and compact TE devices can be realized by utilizing a soft nature of organic materials. It was found that both $\sigma$ and $S$ values of the PEDOT:S-PHE films were simultaneously increased by decreasing the polymerization temperature or by increasing the current density during polymerization. The observed simultaneous increase of $\sigma$ and $S$ were discussed on the basis of the SEM observations of the PEDOT:S-PHE films and oxidation-level measurements. The polymerization temperature, current density and oxidation level were optimized to yield higher TE performances for the PEDOT:S-PHE films. Furthermore, the oxidation level of the PEDOT:S-PHE films was controlled by potential and the change of their TE performances was discussed in conjunction with the change of chemical species involved. To the best of our knowledge, this may be the first to report an electrochemical control of oxidation states for tuning TE performances of conducting polymers.

## 2.2 Experimental

2.2.1 Materials

Poly($\beta$-hydroxyethers) (PHE) ($M_w$ = 50000, $M_w/M_n$ = 2.7) and propylene carbonate (PC) were purchased from Sigma-Aldrich, while 3,4-ethylenedioxythiophene (EDOT), tetraethylammonium perchlorate (TEAP), sulfur trioxide pyridine, and tetrabutylammonium hydroxide (40% in water) were obtained from TCI. PC and EDOT

were distilled under reduced pressure and stocked in a Schenk tube filled with Ar gas. S-PHE was synthesized according to Scheme 2-1 as described previously. [19, 20] The degree of sulfonation ratio of the synthesized S-PHE were almost 100%. All the other reagents were used as received without further purification.
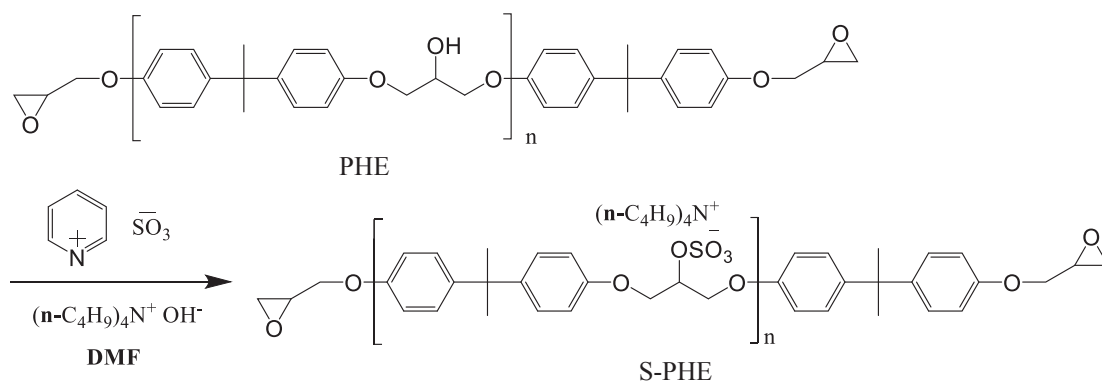


Scheme 2-1. Synthesis of sulfated poly($\beta$-hydroxyethers) (S-PHE) from poly($\beta$-hydroxyethers) (PHE).

## 2.2.2 Preparation of PEDOT:S-PHE films and their characterizations

PEDOT:S-PHE films were prepared in the two-electrode system with thin stainless steel (SUS 304) sheets used as working and counter electrodes, unless otherwise stated. The surface area of the working electrode was defined to be 1 cm$^2$. Galvanostatic polymerization of PEDOT:S-PHE films was carried out in PC containing S-PHE (50 mM), EDOT (0.5 M), and H$_2$O (0.5 M) at different current densities and at temperatures varying from -30 to 10 $^o$C. After polymerization, the PEDOT:S-PHE films were peeled off from the SUS electrodes and rinsed in neat PC and ethanol, and then dried under vacuum at 50 $^o$C for 12 hours. Thus obtained free-standing polymer films were subjected to the measurements of $\sigma$, $S$, and other properties. Conductivities of the PEDOT:S-PHE films were measured using the four-probe method with a resistivity meter (Loresta-GP MCP-T610, Mitsubishi Chemical Corp.). A custom-made setup composed of thermocouples and Peltier devices (Figure 2-1) was used to evaluate Seebeck coefficients, where it was calibrated in advance with the Seebeck coefficients of -18 and +22 $\mu$V K$^{-1}$ reported, respectively, for alumel and chromel alloys at room temperature. (Figure 2-2) [21]

Thermal conductivities ($\kappa$) can be defined as $\kappa = \rho \alpha C_p$, where $\rho$, $\alpha$, and $C_p$ denote density, thermal diffusion coefficient, and heat capacity of the film, respectively. The $\alpha$ values of the PEDOT:S-PHE films were measured with an apparatus (Mobile 2, ai-Phase Co., Ltd.) and the $C_p$ values were obtained with a differential scanning calorimeter (DSC-60, Shimadzu). All these TE properties of the PEDOT:S-PHE films were measured at room temperature. Film morphologies were observed with a field-emission scanning electron microscope (SEM, JSM-6320F, JEOL) and ultraviolet-visible-near-infrared (UV-Vis-NIR) spectra were taken on a spectrophotometer (UV-3150, Shimadzu). Electrochemical measurements were made with an automatic polarization system (HSV-100, Hokuto-Denko).
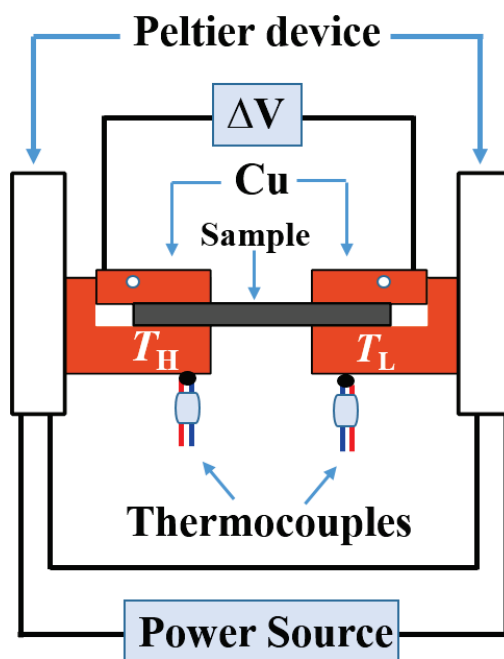


Figure 2-1 Schematic illustration of a setup for measuring Seebeck coefficients.
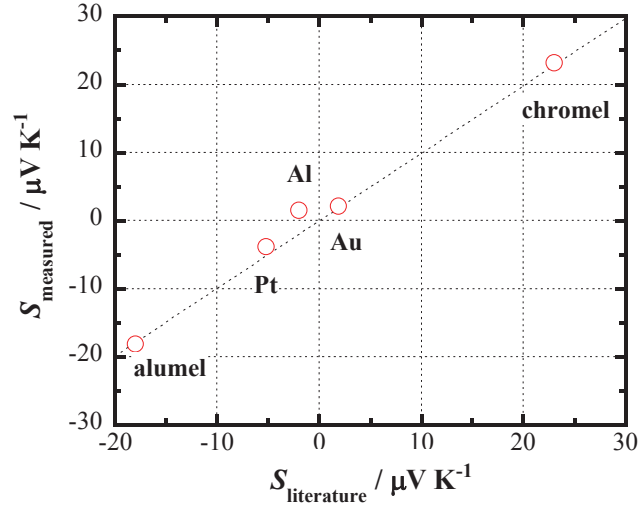
Figure 2-2 Seebeck coefficients of metals measured with our setup and reported in the literature.

2.2.3 Spectroelectrochemisty

UV-vis-NIR absorption measurements of the PEDOT:S-PHE films were made at room temperature with an air-tight thin layer cell (5 mm optical pathlength) with a polymer-coated ITO as the working electrode, ITO as the counter electrode, and the Ag/Ag$^+$ (0.01 M) reference electrode in a separate compartment. [22] Absorption spectra of the polymer film biased at different potentials were subtracted by that of the ITO electrode. PC was used as solvent with S-PHE (50 mM) as supporting electrolyte.

2.2.4 Control of oxidation states of PEDOT:S-PHE films

Oxidation states of the PEDOT:S-PHE films were controlled by applying a given potential to the PEDOT:S-PHE film on SUS using the three-electrode electrochemical cell with the Ag/Ag$^+$ (0.01 M) reference and Pt wire counter electrodes in PC containing TEAP (0.1 M). The PEDOT:S-PHE films at various oxidation states were washed in ethanol, dried, and then subjected to the measurements of the TE characteristics. Oxidation levels [23] of the polymer films were calculated by using the following equation:

$$\text{Oxidation level (\%)} = \frac{QM}{FW}*100 \qquad (2\text{-}1)$$

where $M$, $F$, and $W$ denote the sum of molecular weights of the monomer units of PEDOT and S-PHE, Faraday constant, and the weight of the PEDOT:S-PHE film, respectively. $Q$

43

in eqn. 2-1 is the amount of electricity passing through the electrode when the potential is stepped from a sufficiently negative potential, where the film can be completely reduced, to the more positive potential for oxidation of the films. Details of the measurements are described earlier. [24]

## 2.3 Results and discussion
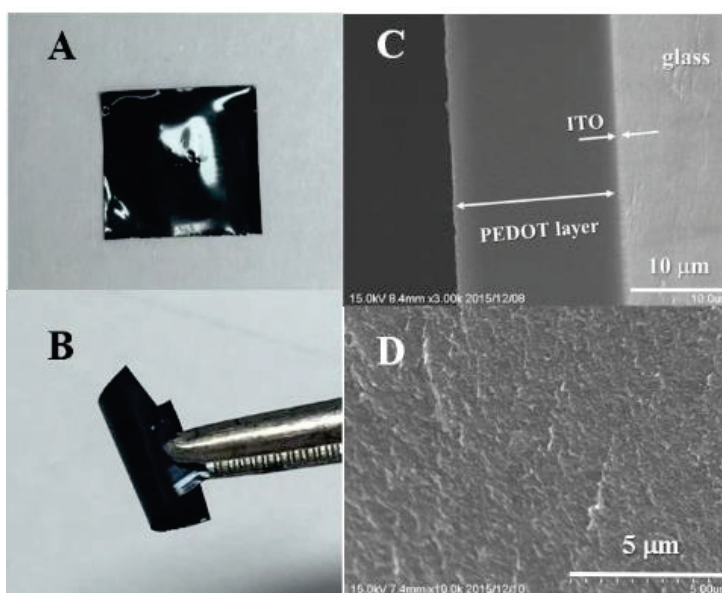
2.3.1 Characterization of PEDOT:S-PHE film



Figure 2-3 (A) and (B) Photos of PEDOT:S-PHE film, and (C) and (D) SEM images of cross-sectional view of PEDOT:S-PHE film of 17 μm in thickness grown at $J = 4.0$ mA cm$^{-2}$ on ITO substrate.

Figure 2-3A and 2-3B depict photos of a PEDOT:S-PHE film, showing a smooth and shiny surface with soft and flexible features. The cross-sectional SEM image of the PEDOT:S-PHE film grafted on indium-tin-oxide (ITO) substrate is shown in Figure 2-3C and 2-3D, which illustrate that the film is uniform and dense. Free-standing PEDOT:S-PHE films with shiny surfaces were always obtained under the polymerization conditions applied in the present study, unless otherwise stated. As is usual in the electropolymerization of conducting polymers, film thicknesses of the PEDOT films were controlled by changing the amount of electricity ($Q$) passing through the electrode during galvanostatic polymerization. Figure 2-4 shows a plot of film thickness of PEDOT:S-

PHE vs. $Q$ obtained at current densities ($J$) of 1.0, 2.0, and 3.0 mA cm$^{-2}$ at room temperature. The plot fits a single straight line irrespective of the difference in $J$.
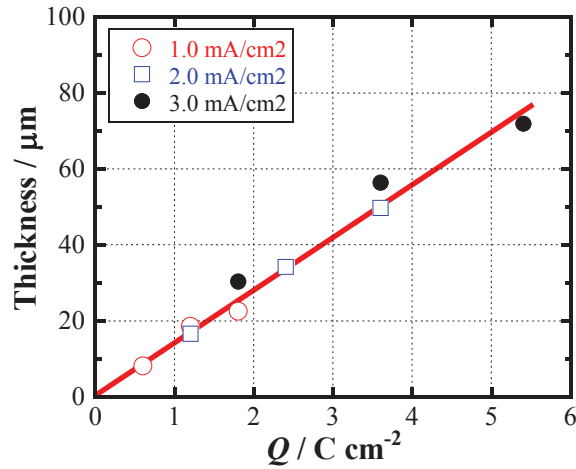


Figure 2-4 Thicknesses of PEDOT:S-PHE films plotted against $Q$ for galvanostatic polymerization at different $J$ values at room temperature.

2.3.2 Optimization of preparation conditions for PEDOT:S-PHE films

Influences of $J$ during polymerization on $\sigma$, $S$, and $PF$ of the PEDOT films were studied. Figure 2-5A depicts changes of $\sigma$ and $S$ with $J$ observed with the PEDOT:S-PHE films ($Q$ = 1.8 C cm$^{-2}$ corresponding to 25 μm in thickness) prepared at 10 $^{o}$C. The figure shows that when the $J$ is increased from 0.5 to 4 mA cm$^{-2}$, the $\sigma$ increases remarkably from 50 to 170 S cm$^{-1}$. The increase of $\sigma$ with $J$ has been reported earlier for the PEDOT:S-PHE films. [19] Similarly to the increase of $\sigma$, the $S$ value was also increased with the increase in $J$, although the change is much smaller than that of $\sigma$. By the simultaneous increase of $\sigma$ and $S$ with the increase in $J$, the $PF$ was drastically increased from 0.5 to 4.0 μW m$^{-1}$ K$^{-2}$, as shown in Figure 2-5B. We attempted to apply higher current densities to obtain PEDOT:S-PHE films with much greater $PF$ values. Because of the high solution resistance at 10 $^{o}$C, however, it was difficult to apply current densities higher than 4.0 mA cm$^{-2}$ so far as the galvanostat is employed. We used a constant resistance and a high voltage of 100 V to generate constant currents such as leading to $J$ values much greater than 5 mA cm$^{-2}$. When the $J$ is higher than 5 mA cm$^{-2}$, however, the resulting films became fragile and difficult to be used for the $\sigma$ and $S$ measurements.
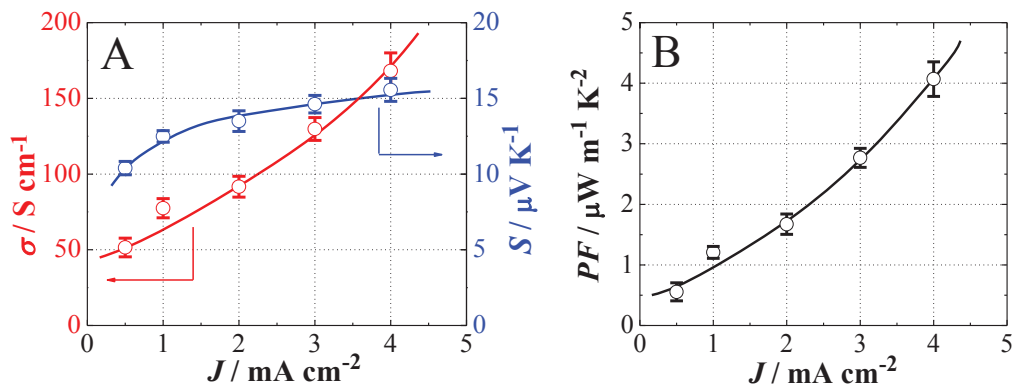
Figure 2-5 (A) $\sigma$ and $S$, and (B) $PF$ of PEDOT:S-PHE films ($Q = 1.8$ C cm$^{-2}$; $T = 10$ °C) prepared at $J$ = 0.50 to 4.0 mA cm$^{-2}$.

PEDOT:S-PHE films were grown by changing the polymerization temperature ($T$) from 10 to -30 °C at a constant $J$ of 0.50 mA cm$^{-2}$. Figure 2-6A illustrates $\sigma$ and $S$ for the PEDOT:S-PHE films as a function of $T$. As is clearly seen in the figure, the $\sigma$ is increased from 50 to 160 S cm$^{-1}$ corresponding to the decrease of $T$ from 10 to -30 °C. Likewise, the $S$ was also increased from 12 to 16 $\mu$V K$^{-1}$ for the same temperature change. Consequently, the $PF$ was greatly increased from 0.7 to 4.0 $\mu$W m$^{-1}$ K$^{-2}$ as shown in Figure 2-6B. The polymerization temperature was not lowered further below -30 °C due to the enhanced resistance of the solution. In order to optimize $PF$ of the PEDOT:S-PHE films with respect to $J$ and $T$, PEDOT:S-PHE films were prepared by changing $J$ at a constant $T$ of -30 °C, which gives the highest $PF$ at $J$ = 0.50 mA cm$^{-2}$. Figure 2-7A depicts dependences of $J$ on $\sigma$ and $S$ for the PEDOT:S-PHE films. The change of $S$ is small for the change of $J$ ranging from 0.40 to 2.1 mA cm$^{-2}$. In contrast, the $\sigma$ was increased with the increase of $J$ and exhibited a maximum of 200 S cm$^{-1}$ when the $J$ is around 1.2 mA cm$^{-2}$. By increasing $J$ further, the $\sigma$ was decreased. Consequently, the $PF$ had a peak value of 5.2 $\mu$W m$^{-1}$ K$^{-2}$ for the PEDOT:S-PHE films grown at $T$ = -30 °C and $J$ = 1.2 mA cm$^{-2}$, as shown in Figure 2-7B. It is likely that the degradation of the PEDOT:S-PHE films due to over-oxidation is responsible for the decrease of $\sigma$ at higher current densities.
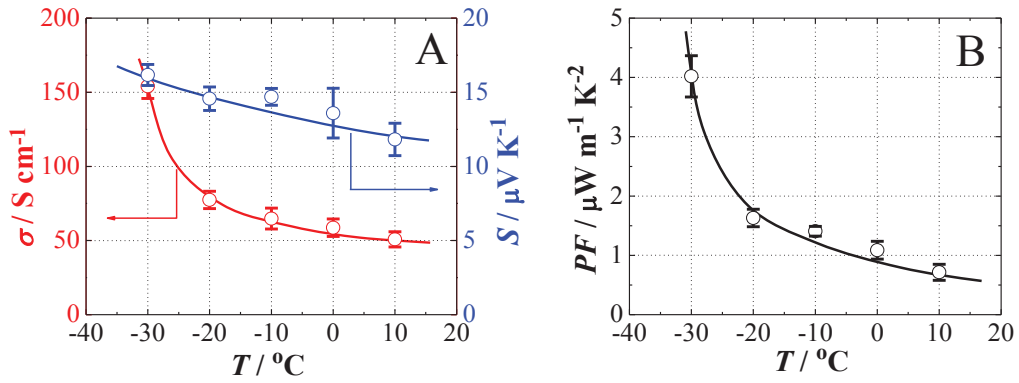
Figure 2-6 (A) $\sigma$ and $S$, and (B) $PF$ of PEDOT:S-PHE films ($Q$ = 1.8 C cm$^{-2}$; $J$ = 0.50 mA cm$^{-2}$) prepared at $T$ = -30 to 10 °C.
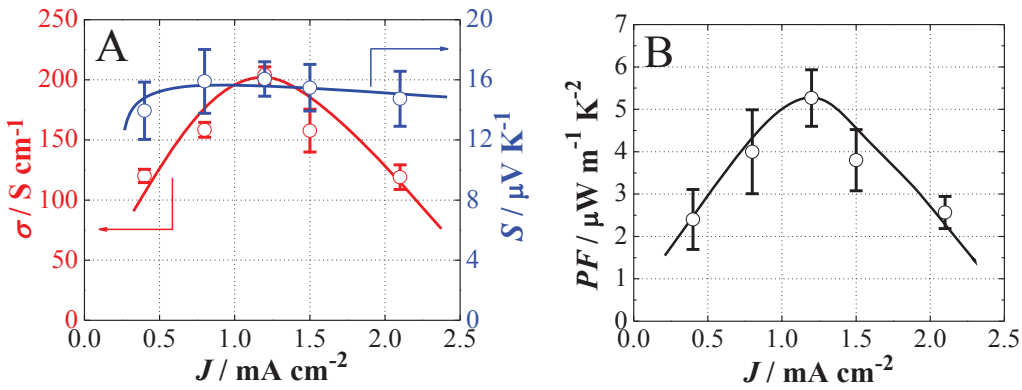


Figure 2-7 (A) $\sigma$ and $S$, and (B) $PF$ of PEDOT:S-PHE films ($Q$ = 1.8 C cm$^{-2}$; $T$ = -30 °C) prepared at $J$ = 0.40 to 2.1 mA cm$^{-2}$.

2.3.3 Theoretical analysis for the simultaneously increase of $\sigma$ and $S$

A salient feature to be noted in Figure 2-5A and 2-6A is a simultaneous increase of $\sigma$ and S with the increase in $J$ or with the decrease in $T$, in contrast to a trade-off relation between $\sigma$ and S commonly observed for a number of inorganic TE materials. [1] Up to the present time, a couple of studies with conducting polymers and their composites have reported a simultaneous increase of the two TE quantities by changing chemical compositions or preparation conditions, although no detailed explanation for this has not been attempted. [25-29] We will discuss below a possible reason for the lack of a trade-off relation observed for PEDOT:S-PHE films.

The trade-off relation between $\sigma$ and S can simply be expected by assuming the following equations: [30]

$$\sigma = en\mu \qquad (2\text{-}2)$$

47

$$S = \frac{\pi^2 k_B{}^2 m^* T}{(3\pi^2)^{\frac{2}{3}}\hbar e n^{\frac{2}{3}}} \qquad (2\text{-}3)$$

where $\mu$ denotes the carrier mobility, $n$ the concentration of charge carriers, $m^*$ the effective mass of charge carriers, and $k_B$, $\hbar$, $T$, and $e$ have their usual significances. Eqn. 2-3 derived for metals and degenerate inorganic semiconductors predicts an increase of $S$ with a decrease of $n$ and such a trend has been frequently observed for organic TE materials as well. [31-33] At first, oxidation levels of as-synthesized PEDOT:S-PHE films were measured with $J$ and $T$ as parameter. Figure 2-8A for the change of $J$ represents that the oxidation level, which is proportional to $n$, is decreased with the increase of $J$, while as shown in Figure 2-8B, the oxidation level tends to increase with the increase of $T$. In both figures, the directions of the change of $S$ are opposite to those for the oxidation level as expected from eqn. 2-3. According to eqn. 2-2, the increase of $n$ (oxidation level) may lead to the increase of $\sigma$ if $\mu$ does not change much with a change of $n$ as in the case of most inorganic solids, and thus a well-known trade-off relation can be expected between $\sigma$ and $S$.
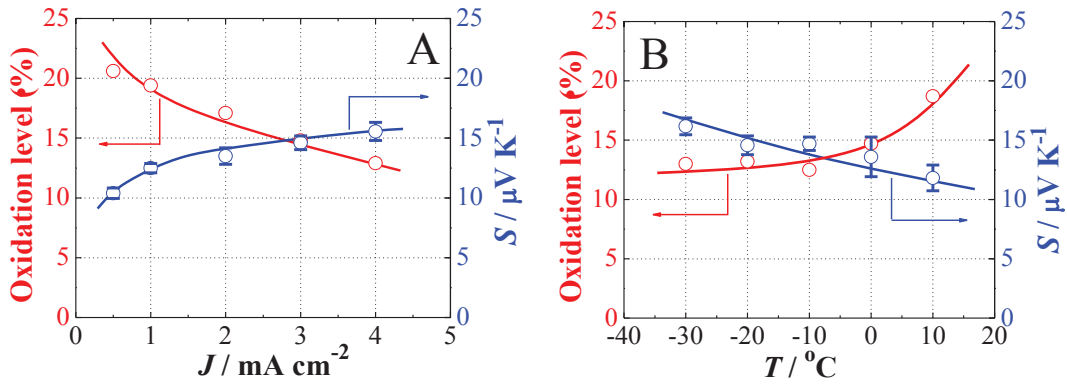


Figure 2-8 Oxidation levels of PEDOT:S-PHE films prepared under the same polymerization conditions (A) as in Figure 2-5 and (B) as in Figure 2-6. The $S$ values are reproduced from those in Figure 2-5 and 2-6.

As for conducting polymers, however, the charge-transport is mainly governed by the interchain and intrachain hopping of charge carriers from one localized state to another within a lattice of molecular sites. Generally, an ordered chain arrangement would result in reduced barriers of both interchain and intrachain hopping, and therefore enhance $\mu$. [7, 31] Figure 2-9 and 2-10 compare the surface morphologies of PEDOT:S-PHE films

prepared under the same polymerization conditions as in Figure 2-5 ($J = 0.50$ to 4.0 mA cm$^{-2}$ at $T = 10$ °C) and in Figure 2-6 ($T = 10$ to -30 °C at $J = 0.50$ mA cm$^{-2}$), respectively. As seen from the SEM images, with the increase in $J$ or the decrease in $T$, the surface morphology of the PEDOT:S-PHE film becomes smoother, implying more intimate interactions of adjacent polymer chains by π-π stacking. Such ordered chain arrangement may facilitate the hopping transport or metallic conduction between the polymer chains and further enhance $\mu$ in the PEDOT:S-PHE films. The highly improved carrier mobility should be beneficial to the improvement of $\sigma$, because the changes of $n$ (oxidation level) accompanied by the changes of $J$ or $T$ are small as shown in Figure 2-8.
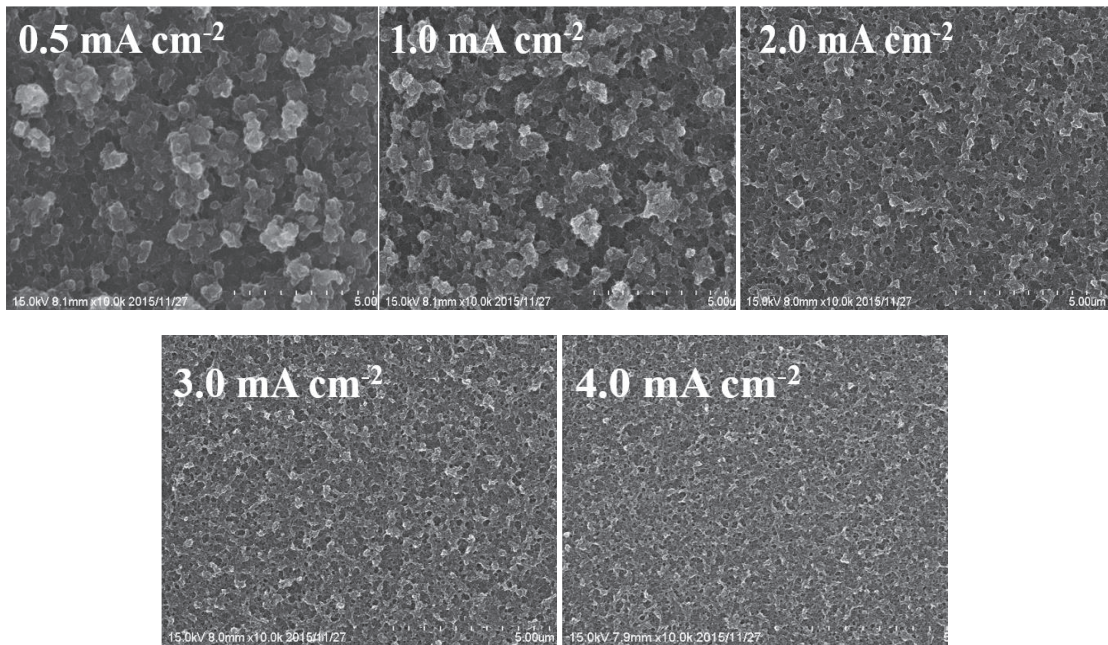


Figure 2-9. SEM images of PEDOT:S-PHE films ($Q = 0.36$ C cm$^{-2}$; $T = 10$ °C) prepared at $E = 0.50$ to 4.0 mA cm$^{-2}$.

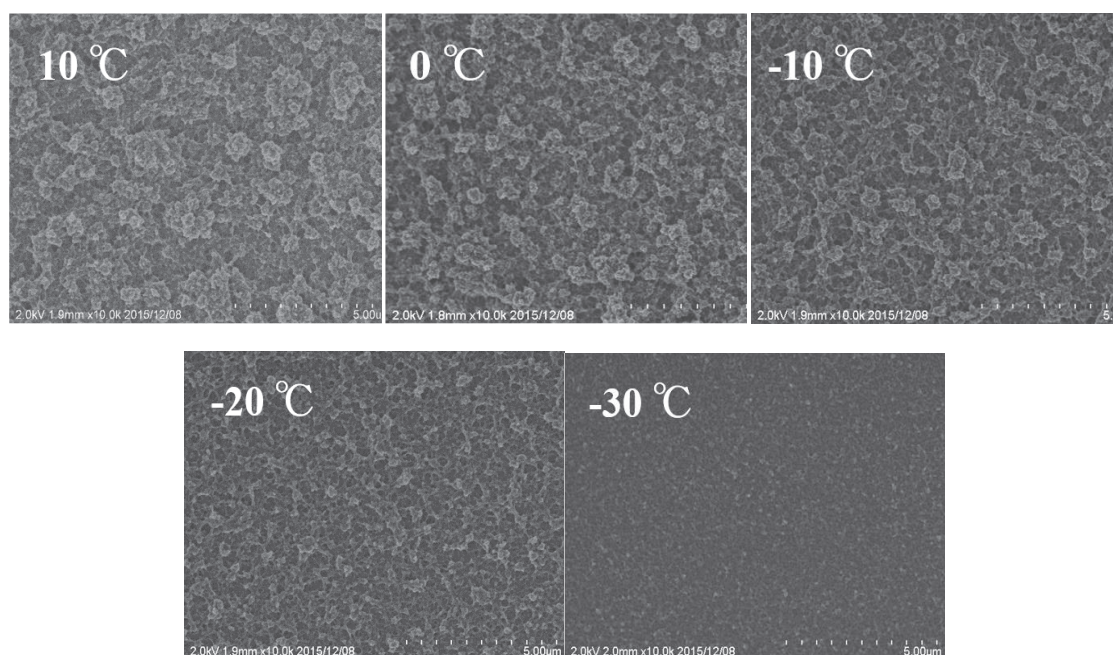Figure 2-10 SEM images of PEDOT:S-PHE films ($Q$ = 0.36 C cm$^{-2}$; $J$ = 0.50 mA cm$^{-2}$) prepared at $T$ = 10 to -30 $^{o}$C.

In summary, a simultaneous increase of $\sigma$ and $S$ for the PEDOT:S-PHE films can be explained as follows: the increase in $J$ or the decrease in $T$ leads to the decrease of the oxidation level responsible for the increase of $S$, while such a change in $J$ or $T$ induces denser morphologies leading to the enhanced $\mu$ or $\sigma$. Thus both $S$ and $\sigma$ are increased by increasing $J$ or decreasing $T$.

2.3.4 Optimization of the oxidation level of PEDOT:S-PHE film via electrochemistry

Crispin and his research group have revealed that the oxidation state of conducting polymers is a crucial factor for determining the TE performances. [31, 34] Theoretical considerations are also made on influences of the oxidation state on the TE performances. [35, 36] In ref. 34 with regioregular poly(3-hexylthiophene) (rrPHT) films, the oxidation state of the films was changed by chemically oxidizing the rrPHT films with nitrosyl hexafluorophosphate (NOPF$_6$) and the oxidation level was evaluated with X-ray photoelectron spectroscopy (XPS) from the ratio of the intensities of the P($2p$) signal from PF$_6^-$ counter ions and the S($2p$) signal from rrPHT. In ref. 31, the oxidation level of the PEDOT films prepared by chemical oxidation of EDOT monomers was evaluated also by use of XPS. In the present study with PEDOT:S-PHE films, the oxidation state was

50

controlled by potential and the oxidation level was precisely determined by potential-step chronocoulometry as has been performed previously. [24]

Figure 2-11A depicts a cyclic voltammogram of the PEDOT:S-PHE film, where the potential of as-synthesized PEDOT:S-PHE film was initially set at -1.6 V until the polymer film may be reduced completely and then scanned to the anodic direction. The oxidation level of the PEDOT:S-PHE film is plotted against potential in Figure 2-11B. As has been reported earlier for poly(3-metylthiophene) [24] and other conducting polymers [37-39], the logarithm of oxidation level increases linearly with potential and tends to saturate at more positive potentials. The maximum oxidation level for the PEDOT:S-PHE film was around 16%, slightly smaller than 20-30% reported for conducting polymers doped with small anions such as $ClO_4^-$ and $PF_6^-$. Absorption spectra of the PEDOT:S-PHE film were taken at different potentials in order to identify chemical species that may be generated at various oxidation states of the polymer film (Figure 2-12). At a sufficiently negative potential of -1.2 V, the polymer film exhibits a main absorption band at 610 nm, ascribable to $\pi$-$\pi$* transition of a neutral PEDOT film. By increasing the potential, the intensity of the 610-nm band decreases, and a new broad band appears at 900 nm and gains its intensity, suggesting the increased fraction of polarons and/or $\pi$-dimers in the PEDOT:S-PHE film. When the applied potential was increased further, both the 610- and 900-nm bands disappeared and only absorption band in the NIR due to bipolarons was observed. [40]
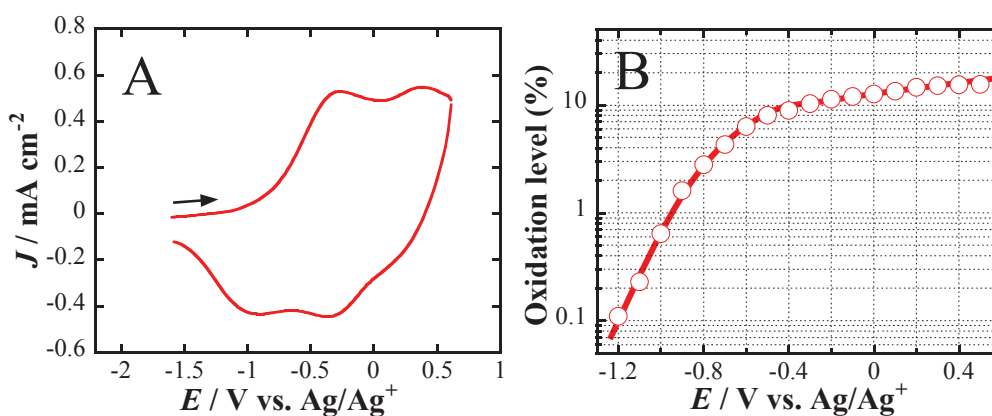


Figure 2-11 (A) Cyclic voltammogram and (B) plot of oxidation level vs. potential (*E*) for PEDOT:S-PHE film ($Q$ = 0.18 C cm$^{-2}$; $J$ = 1.2 mA cm$^{-2}$; $T$ = -30 °C) measured in PC/TEAP (0.1 M) at room
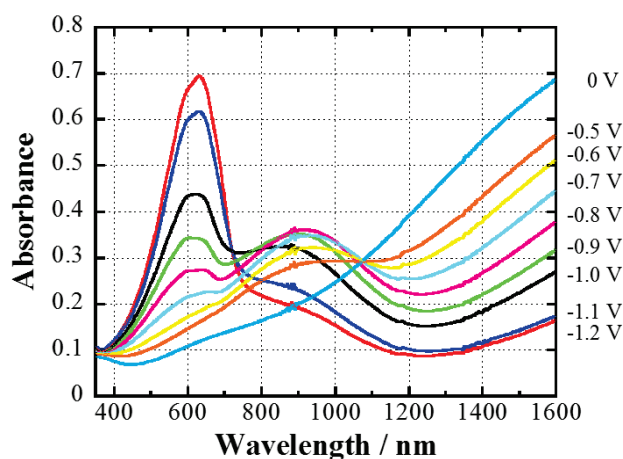
temperature. Potential-scan rate in Figure 2-11A is 50 mV s$^{-1}$.



Figure 2-12. In-situ absorption spectra of PEDOT:S-PHE film ($Q$ = 0.02 C cm$^{-2}$; $J$ = 1.0 mA cm$^{-2}$) prepared on ITO electrode at room temperature. The applied potential was changed from -1.2 to 0.5 V vs. Ag/Ag$^+$, although absorption spectra at 0.1-0.5 V were not shown here because no appreciable changes of spectra were seen.

The PEDOT:S-PHE films were prepared under the optimized polymerization conditions ($J$ = 1.2 mA cm$^{-2}$; $T$ = -30 °C) and the films were biased at respective potentials in PC/TEAP (0.1 M) to control their oxidation states. After the potentiostatic control of the oxidation state, the PEDOT:S-PHE films were peeled off from the SUS substrate and were subjected to the $\sigma$ and $S$ measurements. The obtained $\sigma$ and $S$ values are plotted in Figure 2-13A against the oxidation level in place of potential. As the oxidation level was decreased from 10 to 0.1%, the $\sigma$ was decreased greatly from 150 to 0.2 S cm$^{-1}$ while the $S$ was increased monotonously from 19 to 123 $\mu$V K$^{-1}$. The $PF$ values calculated from $\sigma$ and $S$ in Figure 2-13A are plotted against the oxidation level in Figure 2-13B. The plot demonstrates a significant influence of the oxidation state of the polymer film on $PF$. The maximum $PF$ value of 7.9 $\mu$W m$^{-1}$ K$^{-2}$ was obtained at the oxidation level of 6%, where predominant chemical species on PEDOT chains are $\pi$-dimers and bipolarons. The $\kappa$ value of the PEDOT:S-PHE film was evaluated as 0.186 W m$^{-1}$ K$^{-1}$, comparable to the literature value of 0.18 W m$^{-1}$ K$^{-1}$ for PEDOT:PSS [41], by using the equation $\kappa = \rho\alpha C_p$ with the data of $\rho$ = 1.02 g cm$^{-3}$, $C_p$ = 1.38 J g$^{-1}$ K$^{-1}$, and $\alpha$ = 1.32 x 10$^{-7}$ m$^2$ s$^{-1}$ measured in this study. The combination of the maximum $PF$ of 7.9 $\mu$W m$^{-1}$ K$^{-2}$ with the $k$ of 0.186

W m$^{-1}$ K$^{-1}$ yielded a *ZT* value of 0.013 at 300 K.
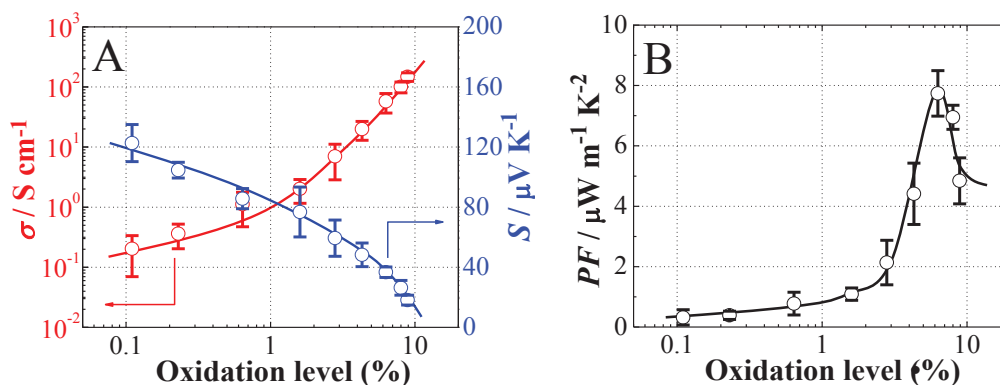


Figure 2-13 (A) $\sigma$ and *S*, and (B) *PF* of PEDOT:S-PHE films (*Q* = 0.90 C cm$^{-2}$; *J* = 1.2 mA cm$^{-2}$; *T* = -30 °C) plotted against oxidation level.

## 2.4 Conclusions

Flexible and free-standing PEDOT:S-PHE films were prepared by galvanostatic polymerization and their thermoelectric performances were investigated. In contrast to a trade-off relation between $\sigma$ and *S* observed for inorganic TE materials, $\sigma$ and *S* values were simultaneously increased by decreasing the polymerization temperature or by increasing the current density during polymerization. The reason for this unique feature characteristic of conducting polymers was explained reasonably on the basis of SEM and oxidation-level measurements. The influence of oxidation state of the PEDOT:S-PHE films on their TE performances was also studied by changing the oxidation level by controlling the applied potential. Under the optimized polymerization conditions (*T* = -30 °C, *J* = 1.2 mA cm$^{-2}$, oxidation level = 6%), the *PF* and *ZT* values of the PEDOT:S-PHE films were 7.9 µW m$^{-1}$ K$^{-2}$ and 0.013, respectively.

# Reference (2)

1. Recent progress on inorganic thermoelectric materials is reviewed in, Thermoelectric Nanomaterials: Materials Design and Applications, ed. K. Koumoto and T. Mori, Springer, Dordrecht, **2013**.

2. R. Al Rahal Al Orabi, N. A. Mecholsky, J. Hwang, W. Kim, J. S. Rhyee, D. Wee, and M. Fornari, Band Degeneracy, Low Thermal Conductivity, and High Thermoelectric Figure of Merit in SnTe–CaTe Alloys. Chem. Mater., 2016, *28*, 376.

3. D. Yang, X. Su, Y. Yan, T. Hu, H. Xie, J. He, C. Uher, M. G. Kanatzidis, and X. Tang, Manipulating the Combustion Wave during Self-Propagating Synthesis for High Thermoelectric Performance of Layered Oxychalcogenide Bi1–xPbxCuSeO. Chem. Mater., 2016, *28*, 4628.

4. L. B. Groenendaal, F. Jonas, D. Freitag, H. Pielartzik, and J. R. Reynolds, Poly(3,4-ethylenedioxythiophene) and Its Derivatives: Past, Present, and Future. Adv. Mater., 2000, *12*, 481.

5. R. B. Aïch, N. Blouin, A. Bouchard, and M. Leclerc, Electrical and Thermoelectric Properties of Poly(2,7-Carbazole) Derivatives. Chem. Mater., 2009, *21*, 751.

6. C. K. Mai, R. A. Schlitz, G. M. Su, D. Spitzer, X. Wang, S. L. Fronk, D. G. Cahill, M. L. Chabinyc, and G. C. Bazan, Side-chain effects on the conductivity, morphology, and thermoelectric properties of self-doped narrow-band-gap conjugated polyelectrolytes. J. Am. Chem. Soc., 2014, *136*, 13478.

7. W. Ma, K. Shi, Y. Wu, Z. Y. Lu, H. Y. Liu, J. Y. Wang, and J. Pei, Enhanced Molecular Packing of a Conjugated Polymer with High Organic Thermoelectric Power Factor. ACS Appl. Mater. Interfaces, 2016, *8*, 24737.

8. M. N. Gueye, A. Carella, N. Massonnet, E. Yvenou, S. Brenet, J. Faure-Vincent, S. Pouget, F. Rieutord, H. Okuno, A. Benayad, R. Demadrille, and J. P. Simonato, Structure and Dopant Engineering in PEDOT Thin Films: Practical Tools for a Dramatic Conductivity Enhancement. Chem. Mater., 2016, *28*, 3462.

9. K. Sun, S. Zhang, P. Li, Y. Xia, X. Zhang, D. Du, F. H. Isikgor, and J. Ouyang, Review on application of PEDOTs and PEDOT:PSS in energy conversion and storage devices. J. Mater. Sci.: Mater. Electron., 2015, *26*, 4438.

10. G.-H. Kim, L. Shao, K. Zhang, and K. P. Pipe, Engineered doping of organic semiconductors for enhanced thermoelectric efficiency. Nat. Mater., 2013, *12*, 719.

11. B. Zhang, J. Sun, H. E. Katz, F. Fang, and R. L. Opila, Promising thermoelectric properties of commercial PEDOT:PSS materials and their bi2Te3 powder composites. ACS Appl. Mater. Interfaces, 2010, *2*, 3170.

12. E. J. Bae, Y. H. Kang, K. S. Jang, and S. Y. Cho, Enhancement of Thermoelectric Properties of PEDOT:PSS and Tellurium-PEDOT:PSS Hybrid Composites by Simple Chemical Treatment. Sci. Rep., 2016, *6*, 18805.

13. C. Yu, K. Choi, L. Yin, and J. C. Grunlan, Light-Weight Flexible Carbon Nanotube Based Organic Composites with Large Thermoelectric Power Factors. ACS Nano, 2011, *10*, 7885.

14. G. H. Kim, D. H. Hwang, and S. I. Woo, Thermoelectric properties of nanocomposite thin films prepared with poly(3,4-ethylenedioxythiophene) poly(styrenesulfonate) and graphene. Phys. Chem. Chem. Phys., 2012, *14*, 3530.

15. N. Toshima, N. Jiravanichanun, and H. Marutani, Organic Thermoelectric Materials Composed of Conducting Polymers and Metal Nanoparticles. J. Electron. Mater., 2012, *41*, 1735.

16. S. H. Cho, H. J. Lee, Y. Ko, and S.-M. Park, Electrochemistry of Conductive Polymers 47: Effects of Solubilizers on 3,4-Ethylenedixoythiophene Oxidation in Aqueous Media and Properties of Resulting Films. J. Phys. Chem. C, 2011, *115*, 6545.

17. C. Kvarnström, H. Neugebauer, S. Blomquist, H. J. Ahonen, J. Kankare, and A. Ivaska, In situ spectroelectrochemical characterization of poly(3,4-ethylenedioxythiophene). Electrochim. Acta, 1999, *44*, 2739.

18. M. Culebras, C. M. Gómez, and A. Cantarero, Enhanced thermoelectric performance of PEDOT with different counter-ions optimized by chemical reduction. J. Mater. Chem. A, 2014, *2*, 10109.

19. H. Yamato, K.-i. Kai, M. Ohwa, T. Asakura, T. Koshiba, and W. Wernet, Synthesis of free-standing poly ( 3,4-ethylenedioxythiophene) conducting polymer films on a pilot scale. Synth. Met., 1996, *83*, 125.

20. W. Wernet and J. Stoffer, USPatent_5061401_1991. US Patent, 1991, *5061401*, 1.

21. Y. Harima, S. Fukumoto, L. Zhang, X. Jiang, J. Yano, K. Inumaru, and I. Imae, Thermoelectric performances of graphene/polyaniline composites prepared by one-step electrosynthesis. RSC Adv., 2015, *5*, 86855.

22. H. Tang, L. Zhu, Y. Harima, K. Yamashita, J. Ohshita, A. Kunai, and M. Ishikawa, Electrochemistry and spectroelectrochemistry of poly[(tetraethyldisilanylene)quinque(2,5-thienylene)]. Electrochim. Acta, 1999, *44*, 2579.

23. "Oxidation level" in place of doping level is used here because S-PHE is a polymer electrolyte which is hardly dedoped or removed by reduction of the PEDOT:S-PHE films..

24. Y. Harima, T. Eguchi, and K. Yamashita, Enhancement of carrier mobilities in poly(3-methylthiophene) electrochemical doping. Synth. Met., 1998, *95*, 69.

25. H. Yan, T. Ohta, and N. Toshima, Stretched Polyaniline Films Doped by (l)-10- Camphorsulfonic Acid: Anisotropy and Improvement of Thermoelectric Properties. Macromol. Mater. Eng. , 2001, *286*, 139.

26. Y. Sun, Z. Wei, W. Xu, and D. Zhu, A three-in-one improvement in thermoelectric properties of polyaniline brought by nanostructures. Synth. Met., 2010, *160*, 2371.

27. Y. Du, S. Z. Shen, W. Yang, R. Donelson, K. Cai, and P. S. Casey, Simultaneous increase in conductivity and Seebeck coefficient in a polyaniline/graphene nanosheets thermoelectric nanocomposite. Synth. Met., 2012, *161*, 2688.

28. C. Liu, J. Xu, B. Lu, R. Yue, and F. Kong, Simultaneous Increases in Electrical Conductivity and

Seebeck Coefficient of PEDOT:PSS Films by Adding Ionic Liquids into a Polymer Solution. J. Electron. Mater., 2012, *41*, 639.

29. Y. Du, K. F. Cai, S. Chen, P. Cizek, and T. Lin, Facile preparation and thermoelectric properties of Bi(2)Te(3) based alloy nanosheet/PEDOT:PSS composite films. ACS Appl. Mater. Interfaces, 2014, *6*, 5735.

30. G. J. Snyder and E. S. Toberer, Complex thermoelectric materials. Nat. Mater., 2008, *7*, 105.

31. O. Bubnova, Z. U. Khan, A. Malti, S. Braun, M. Fahlman, M. Berggren, and X. Crispin, Optimization of the thermoelectric figure of merit in the conducting polymer poly(3,4-ethylenedioxythiophene). Nat. Mater., 2011, *10*, 429.

32. N. Lu, L. Li, and M. Liu, A review of carrier thermoelectric-transport theory in organic semiconductors. Phys. Chem. Chem. Phys., 2016, *18*, 19503.

33. O. Bubnova, M. Berggren, and X. Crispin, Tuning the thermoelectric properties of conducting polymers in an electrochemical transistor. J. Am. Chem. Soc., 2012, *134*, 16456.

34. Y. Xuan, X. Liu, S. Desbief, P. Leclère, M. Fahlman, R. Lazzaroni, M. Berggren, J. Cornil, D. Emin, and X. Crispin, 35-Thermoelectric properties of conducting polymers: The case of poly(3-hexylthiophene). Phys. Rev. B, 2010, *82*, 115454.

35. W. Shi, T. Zhao, J. Xi, D. Wang, and Z. Shuai, Unravelling Doping Effects on PEDOT at the Molecular Level: From Geometry to Thermoelectric Transport Properties. J. Am. Chem. Soc., 2015, *137*, 12929.

36. B. Zhang, K. Wang, D. Li, and X. Cui, Doping effects on the thermoelectric properties of pristine poly(3,4-ethylenedioxythiophene). RSC Adv., 2015, *5*, 33885.

37. X. Jiang, Y. Harima, K. Yamashita, Y. Tada, J. Ohshita, and A. Kunai, Doping-induced change of carrier mobilities in poly(3-hexylthiophene) films with different stacking structures. Chem. Phys. Lett., 2002, *364*, 616.

38. R. Patil, X. Jiang, and Y. Harima, Mobilities of charge carriers in poly(o-methylaniline) and poly(o-methoxyaniline). Electrochim. Acta, 2004, *49*, 4687.

39. Y. Harima, X. Jiang, Y. Kunugi, K. Yamashita, A. Naka, K. Koo Lee, and M. Ishikawa, Influence of π-conjugation length on mobilities of charge carriers in conducting polymers. J. Mater. Chem., 2003, *13*, 1298.

40. E. G. Tolstopyatova, N. A. Pogulaichenko, S. N. Eliseeva, and V. V. Kondratiev, Spectroelectrochemical study of poly-3,4-ethylenedioxythiophene films in the presence of different supporting electrolytes. Russ. J. Electrochem., 2009, *45*, 252.

41. H. Song, F. Kong, C. Liu, J. Xu, Q. Jiang, and H. Shi, Improved thermoelectric performance of PEDOT:PSS film treated with camphorsulfonic acid. J. Polym. Res., 2013, *20*, 316.

# Chapter 3　Thermoelectric performances of graphene/polyaniline composites prepared by one-step electrosynthesis

## 3.1 Introduction

Thermoelectric (TE) materials have received much interest because they are capable of directly converting exhaust heat to electricity with no use of moving mechanisms responsible for noises and outages. Their performances are evaluated by a thermoelectric power factor (*PF*) and a dimensionless thermoelectric figure-of-merit (*ZT*) defined by $PF = S^2\sigma$ and $ZT = S^2\sigma T/\kappa$, where $S$, $\sigma$, $\kappa$, and $T$ are Seebeck coefficient, electric conductivity, thermal conductivity, and absolute temperature, respectively. $Bi_2Te_3$, which has been used in a Peltier element, is a typical inorganic TE material giving a *ZT* value close to unity, [1] which is believed to be a numerical target for a practical use of the TE materials. TE materials based on inorganic compounds have been intensively studied so far and those having *ZT* values greater than unity have already been developed. However, the high TE performances of them tend to be realized only at increased temperatures beyond 400 $^o$C, although a large part of exhaust heat from households as well as chemical plants, so-called low-temperature exhaust heat, is known to be below 200 $^o$C and thus TE materials efficient at low temperatures are needed for practical applications. In addition, most of efficient inorganic TE materials developed so far are composed of Bi, Sb, Te, Pb, Co, or Ge, that are expensive, brittle, unstable in air, and even toxic. Very recently, an increasing number of studies have been devoted to organic alternatives to inorganic TE materials. In general, organic compounds are weak against heat compared with inorganic ones, but they can be used for an effective recovery of a low-temperature exhaust heat occupying 70% of a total exhaust heat. Instead, organic TE materials are attractive candidates because of low cost of fabrication due to a plenty of resources and ease of synthesis, light weight, flexibility, and low thermal conductivities leading to high *ZT* values. Conducting polymers match the above conditions and polyaniline (PANI), one of conducting polymers, was an

57

organic TE material studied first by Toshima group in 1999. [2, 3] Conducting polymers such as polypyrrole [4, 5], polyphenylenevinylenes [6], polythiophene [7], and its derivatives including poly(3,4-ethylene-dioxythiophene):poly(styrenesulfonate) (PEDOT:PSS) have also been investigated as a class of possible organic TE materials. It has been reported that the commercially available PEDOT:PSS films after treatment with organic solvents and/or chemical or electrochemical control of their oxidation levels give the $ZT$ values of 0.25 [8], 0.31 [9], and 0.42 [10]. Another strategy to improve the TE performances is to fabricate composites by expecting a possible synergistic effect arising from a combination of materials with different properties. Indeed, composites of carbon nanotube (CNT) and conducting polymers were examined and a synergistic effect was found. [11-14] Composites consisting of PANI and graphene oxide (GO) or reduced GO have also been intensively studied. [15-22]

In the present study, graphene/PANI composites prepared by a simple electrochemical technique developed earlier for producing electrochemical capacitors are investigated from the viewpoint of their application to TE materials. [23] The composites with different weight ratios of graphene and PANI are prepared, and their conductivities and Seebeck coefficients are measured at room temperature to evaluate TE performances. It is found that the conductivities of the composite films are enhanced by four times when the fluorine-doped tin oxide (FTO) electrode is replaced by the stainless steel (SUS) electrode. The composite films prepared on the SUS electrodes with the GO/aniline weight ratio of 8:1 give the maximum $PF$ of 3.6 $\mu W\ m^{-1}\ K^{-2}$ and $ZT$ value of 0.008 at room temperature. The conductivity enhancement on the SUS electrode is also discussed on the basis of electrochemical measurements and X-ray photoelectron spectroscopy.

### 3.2 Experimental

3.2.1 Preparation of GO/aniline film

GO was synthesized from a natural graphite powder (SNO-10 from SEC Carbon Ltd.) by a modified Hummers method as described. [24] A desired concentration of GO-

dispersed solution was prepared by adding a given amount of GO powder into 10 mL of deionized water and ultrasonicated for one hour to enhance exfoliation. Mixtures of GO/aniline at different weight ratios ($W_{GO}/W_{ANI}$) were prepared by adding a controlled volume of purified aniline into 10 ml of 3 mg mL$^{-1}$ GO dispersion. The GO/aniline mixtures were well dispersed after being sonicated for 10 min. GO/aniline films (0.50 mg) with different GO/aniline weight ratios were prepared by casting a given volume of the above mixtures on an FTO electrode or a thin stainless steel (SUS 304) sheet fixed by a double-face adhesive tape on a glass plate. Surface areas of the GO/aniline films were controlled to be 0.785 cm$^2$ (diameter of the film: 1.0 cm) irrespective of the weight ratio. A photo of the composite film prepared as described below is shown in Figure 3-1B.
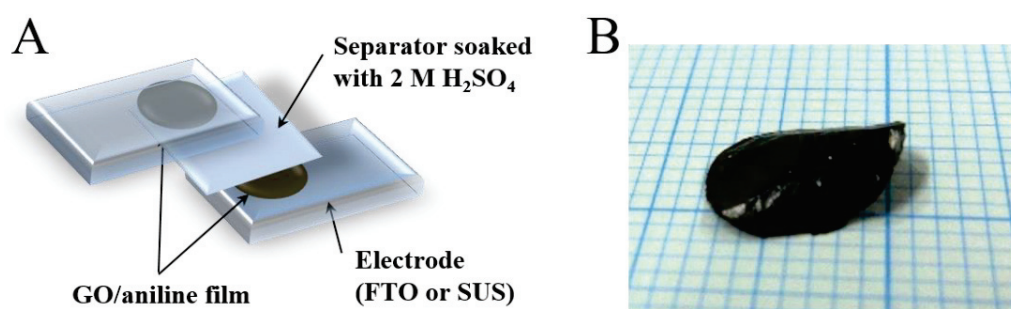


Figure 3-1 (A) Illustration of a two-electrode cell for electrochemical conversion of GO/aniline film to erGO/PANI composite and (B) photo of erGO/PANI film.

3.2.2 Preparation of erGO/PANI film

The structure of the two-electrode cell is shown in Figure 3-1A, where a filter paper soaked with acid (2 M H$_2$SO$_4$) is sandwiched between the two conductive substrates (FTO or SUS) on which GO/aniline films having the same GO/aniline ratios are deposited. The successive triangular-wave voltage between -1.4 and +1.4 V at a scan rate of 100 mV s$^{-1}$ was applied to the electrodes to convert GO to its reduced form (electrochemically reduced GO: erGO) and, concurrently, to oxidize aniline to PANI in the GO/aniline films deposited on the electrodes. Alternatively, the redox cycles were performed by stepping the applied voltage between +1.4 and -1.4 V with a rest time of 20 s at each stepped voltage. As is schematically shown in Figure 3-2, the top GO/aniline film will be oxidized

to give PANI and the bottom film will be reduced to give erGO. When the voltage is reversed, on the other hand, GO in the top film will be reduced and aniline in the bottom film will be oxidized. Thus, by cycling the voltage between +1.4 and -1.4 V in the voltage-sweep and –step methods, aniline and GO in both films can be simultaneously oxidized and reduced to PANI and erGO, respectively. The voltage of 1.4 V was decided according to our previous work. [23] After the experiment, the two-electrode cell was short-circuited and decomposed to pick up erGO/PANI composite films, and then the free-standing composite films (*ca.* 5 μm in thickness) were obtained.
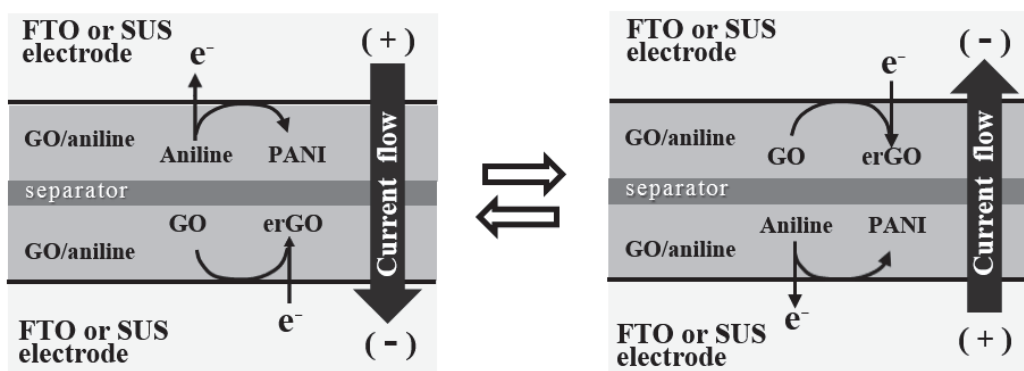


Figure 3-2 Illustration for mechanisms of electrochemical conversion of GO/aniline film to erGO/PANI composite in two-electrode cell.

### 3.2.3 Characterization of erGO/PANI film

The obtained erGO/PANI films were then subjected to the measurements of conductivity, Seebeck coefficient, and other properties. Conductivities of the composite films were determined by the four-probe method using a resistivity meter (Loresta-GP MCP-T610, Mitsubishi Chemical Corp.). Seebeck coefficients were measured using a custom made set-up composed of thermocouples and Peltier devices. This set-up was calibrated with the Seebeck coefficients of -18 and +22 $\mu V\ K^{-1}$ reported for alumel and chromel alloys at room temperature, respectively, which is consistent with that reported in the literature. XPS spectra of the composite films were taken on an X-ray photoelectron spectroscopy (XPS: ESCA-3400, Kratos Analytical). Film morphologies were observed with a field-emission scanning electron microscope (SEM, JEOL JSM-6320F).

Electrochemical measurements were made with an automatic polarization system (Hokuto Denko HSV-100).

## 3.3 Results and discussion

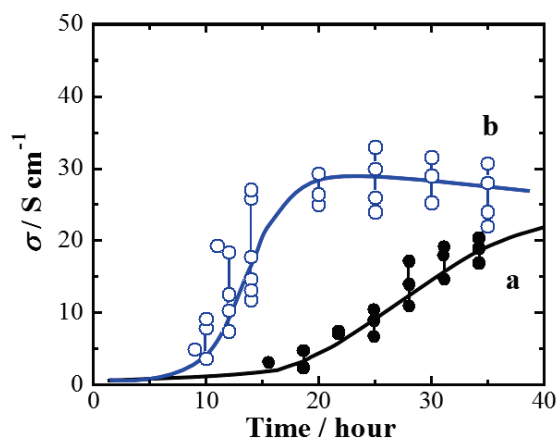3.3.1 Influence of electro-polymerization method on erGO/PANI film



Figure 3-3 Changes in conductivity ($\sigma$) of GO/aniline ($W_{GO}/W_{ANI}$=8) film with electrolysis time, prepared on FTO electrodes by a) voltage-sweep and b) voltage-step methods. In the former method, voltage of the two electrodes was cycled between -1.4 and +1.4 V at a sweep rate of 100 mV s$^{-1}$, while in the latter, voltage was stepped repeatedly between +1.4 and -1.4 V, and kept at respective voltages for 20 s. Weights of the respective GO/aniline films were ca. 0.50 mg. All the curves and the vertical segments in Figures 3-3 are drawn for guides of eyes.

In our previous study [23], GO/aniline films in the two-electrode cell were converted successfully to erGO/PANI composite films by cycling the voltage between -1.4 and +1.4 V at ±100 mV s$^{-1}$. The integral area of the current *vs.* voltage curve during the voltage cycling could be a measure of the extent of the reaction and also provided an integral capacitance of the composite film. In the present study, GO/aniline films was treated in a similar fashion and the voltage cycling was stopped at a given time to decompose the two-electrode cell and pick up thus treated films for the conductivity measurements. Black circles in Figure 3-3 depict conductivities of the films obtained in this way, where the $W_{GO}/W_{ANI}$ of GO/aniline film was 8:1 and the FTO electrode was used. The films were almost insulating when the time of the voltage cycling was shorter than 10 hours, whereas the conductivity increased slowly with time and was 20 S cm$^{-1}$ even 15 hours

after the start of voltage cycling. In order to shorten the time required for the conversion of GO/aniline to erGO/PANI, a square-wave voltage between +1.4 and -1.4 V was applied to the cell (20 s at each voltage). The conductivities of the composite films converted by the square-wave voltage are shown by blue circles in Figure 3-3. As expected, the conductivities increase in much shorter time and level off at ca. 30 S cm$^{-1}$ at 13 hours or later, although the conductivity values of the composite films prepared under the same condition are somewhat scattered. We have already noted that the almost complete conversion to the composite requires longer times when the $W_{GO}/W_{ANI}$ values of the GO/aniline films are larger. [23] In view of this, in the subsequent study, we electrolyzed the GO/aniline in the two-electrode cell for 20 hours irrespective of their composition ($W_{GO}/W_{ANI}$).

### 3.3.2 Influence of GO/aniline weight ratio ($W_{GO}/W_{ANI}$) on erGO/PANI film
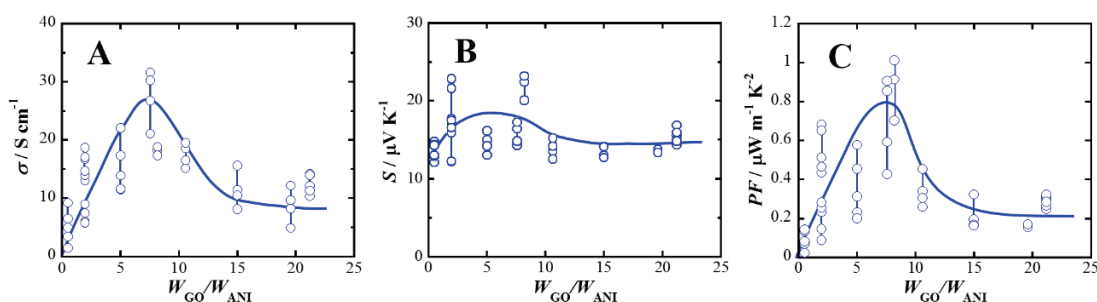


Figure 3-4 Changes in A) conductivity ($\sigma$), B) Seebeck coefficient ($S$), and C) power factor ($PF$) of erGO/PANI composite with GO/aniline weight ratio, $W_{GO}/W_{ANI}$, where GO/aniline films were treated by voltage-step method with FTO electrodes.

Figure 3-4 illustrates conductivities ($\sigma$), Seebeck coefficients ($S$), and power factors ($PF$s) of the erGO/PANI films obtained by electrosynthesis of GO/aniline films with different $W_{GO}/W_{ANI}$ values on the FTO electrodes for 20 hours by using the square-wave voltage. It is seen from Figure 3-4A that the conductivities increase with the increase of $W_{GO}/W_{ANI}$ and show a broad peak in the range of $W_{GO}/W_{ANI}$ between 5 and 10. By increasing the ratio of GO in the GO/aniline film further, the conductivities dropped to around 10 S cm$^{-1}$. Figure 3-4B depicts a plot of Seebeck coefficient against $W_{GO}/W_{ANI}$. The Seebeck coefficients are positive, demonstrating that main charge carriers in the

composites have a positive sign. As is the case of conductivities, Seebeck coefficients of the composite films are scattered, but we see that they are not dependent much on $W_{GO}/W_{ANI}$ compared with the conductivities. Figure 3-4C depicts power factors of the composite films calculated with the data shown in Figures 3-4A and 3-4B. The figure shows clearly that there is a $W_{GO}/W_{ANI}$ value which gives a maximum power factor of c*a.* 1 μW m$^{-1}$ K$^{-2}$. By referring to this result, the GO/aniline films of $W_{GO}/W_{ANI}$ = 8 were employed for examining an influence of an electrode material as described below.

3.3.3 Influence of working electrode (FTO or SUS) on erGO/PANI film

In Figure 3-5 are compared the TE properties of the GO/aniline films ($W_{GO}/W_{ANI}$ = 8) treated with the FTO and SUS electrodes using the voltage-step technique (±1.4 V). As shown in Figure 3-5A, conductivities of the composite films prepared with SUS (red) start to increase with a lapse of electrolysis time without delay like the case of FTO (blue) and reach c*a.* 130 S cm$^{-1}$ 10 hours after the start of electrolysis, being followed by the decrease of conductivities by further electrolysis. It is likely that the conductivity decrease is due to overoxidation of PANI on the SUS electrode. Seebeck coefficients were also measured for the composite films prepared on FTO and SUS electrodes and the results are depicted in Figure 3-5B. In contrast to the case of conductivities, the Seebeck coefficients were almost independent of the electrolysis time for both FTO and SUS electrodes, and were around 16 μV K$^{-1}$ irrespective of the difference of the electrode materials, although the Seebeck coefficients for the FTO electrode were small in the short electrolysis time. It is well-known in TE materials studies that there is a trade-off relation between conductivity ($\sigma$) and Seebeck coefficient ($S$). It is likely that such a relation does not hold for the erGO/PANI composites: a large change in $\sigma$ with a negligible change in $S$ with the electrolysis time. It is known that the Seebeck coefficient ($S$) is explained by the following equation: [25]

$$S = \frac{\pi^2 k_B{}^2 m^* T}{(3\pi^2)^{\frac{2}{3}} \hbar e n^{\frac{2}{3}}} \qquad (1)$$

where $m^*$ denotes the effective mass of charge carriers, $n$ the density of charge carriers, and $k_B$, $\hbar$, $T$, and $e$ have their usual significances. Thus, almost constant values of $S$ in Fig.

3-5B suggest that the density of charge carriers ($n$) does not change with the electrolysis time so far as the $m^*$ value is constant. On the other hand, the electrical conductivity ($\sigma$) is a product of $n$ and the charge carrier mobility ($\mu$) as expressed by $\sigma = en\mu$. Therefore, the $\sigma$ values should not change when the $n$ and $\mu$ values do not change. Nevertheless, the $\sigma$ values change with the electrolysis time as shown in Figure 3-5A. Consequently, the observed change of $\sigma$ is likely to be ascribed to the development of electrically conductive domains in the GO/aniline film with the increase in the electrolysis time.
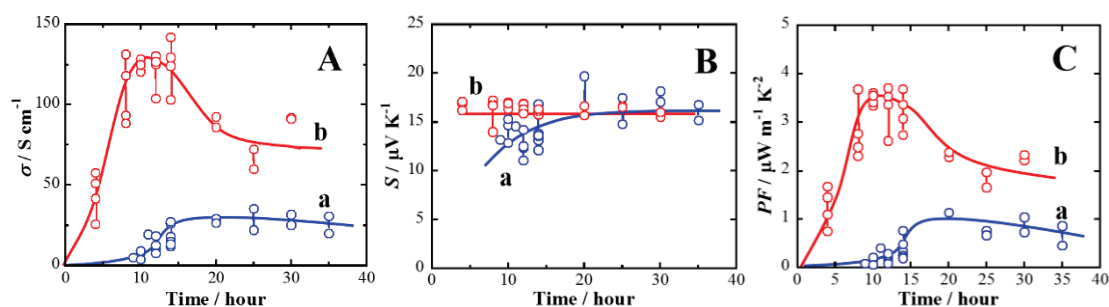


Figure 3-5 Changes in A) conductivity ($\sigma$), B) Seebeck coefficient ($S$), and C) power factor ($PF$) of GO/aniline ($W_{GO}/W_{ANI} = 8$) films with electrolysis time, where GO/aniline films were treated by voltage-step method with a) FTO and b) SUS electrodes.

Figure 3-5C depicts the power factors of the composite films prepared with the SUS electrode in comparison with those with the FTO electrode. The maximum power factor for the former films is close to 3.6 $\mu$W m$^{-1}$ K$^{-2}$ when the electrolysis time is 10 hours, while the power factor for the latter film is less than 1 $\mu$W m$^{-1}$ K$^{-2}$. Very recently, thermal conductivities of reduced graphene oxide-polyaniline composites have been reported to be 0.1078 to 0.1433 W m$^{-1}$ K$^{-1}$ for 0 to 80 wt% of reduced GO, less dependent on the composition ratio. [21] If we assume the thermal conductivity of the erGO/PANI film ($W_{GO}/W_{ANI} = 8$) as 0.13 W m$^{-1}$ K$^{-1}$, one can evaluate the maximum $ZT$ value for the composite films as 8x10$^{-3}$ at room temperature. This $ZT$ value is much smaller than those for the PEDOT:PSS films, [8-10] but is high compared with those reported so far for graphene/polyaniline composites: $1.37\times10^{-3}$ [15], 1.26 x $10^{-4}$ [17], 4.86 x10$^{-4}$ [18], 1.95x10$^{-3}$ [20], 4.23x10$^{-4}$ [21], and 4.6x10$^{-3}$ [22]. It is also much greater than those for PANI alone. [3]

64

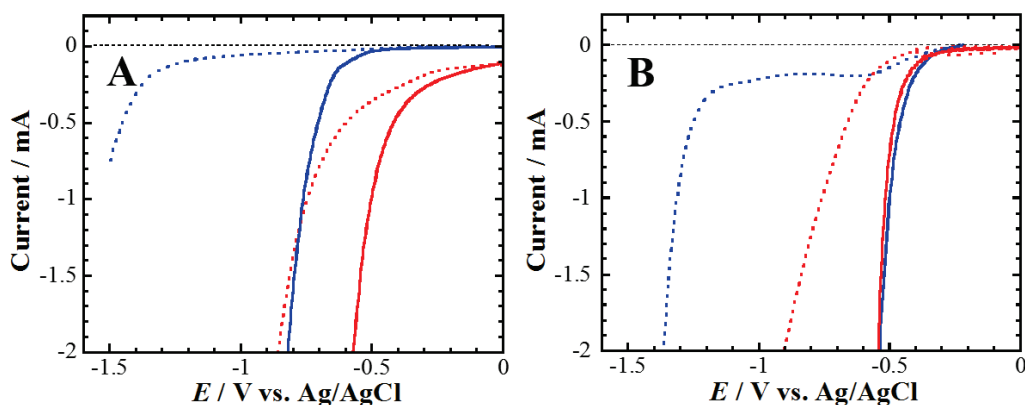### 3.3.4 Characterization and analysis of erGO/PANI film



Figure 3-6 Linear-sweep voltammograms (LSVs) of A) FTO and B) SUS electrodes in aqueous solutions of 0.1 M KCl (broken line) and 2 M $H_2SO_4$ (solid line) at 50 mV s$^{-1}$. LSVs on GO-deposited FTO and GO-deposited SUS electrodes are also included in the figure and expressed by red lines, while those on bare FTO and SUS electrodes are by black lines.

We will now discuss the reason for the conductivities of the erGO/PANI composites enhanced by the use of the SUS electrode. Figure 3-6A depicts linear-sweep voltammograms (LSVs) of FTO and GO-deposited FTO electrodes measured with a three-electrode system in aqueous solutions of 0.1 M KCl and 2 M $H_2SO_4$, while Figure 3-6B denote LSVs on SUS and GO-deposited SUS electrodes in the same solutions. On the bare FTO electrode in KCl solution (black broken curve), only small cathodic currents flow at potentials more positive than -1.4 V. In the $H_2SO_4$ solution, the cathodic current rise starts at 0.7 V, which is shifted to a positive direction (black solid curve) due to the reduction of protons on the FTO electrode. LSVs of GO-deposited FTO in KCl and $H_2SO_4$ solutions (red broken curve) suggest that the reduction of GO deposited on FTO takes place in KCl solution and the GO reduction is slightly enhanced in $H_2SO_4$. Here, by comparing LSVs of FTO and GO-deposited FTO electrodes in the $H_2SO_4$ solution, we see that in the two-electrode cell, GO on FTO will be reduced without appreciable evolution of hydrogen gas. As is shown in Figure 3-6B, on the other hand, protons are more easily reduced on SUS than FTO because of a low hydrogen overpotential of SUS and GO deposited on SUS is reduced at the same potentials as the reduction of protons. Therefore, one can presume that in the two-electrode cell experiments with SUS, the

65

electrochemical reduction of GO may take place concurrently with the evolution of hydrogen gas on the surface of SUS. On this basis, we presume that the relatively high conductivities of the erGO/PANI composites prepared with SUS are due to an efficient conversion of GO to erGO by the electrochemical reduction of GO in the presence of a highly reducing hydrogen gas.
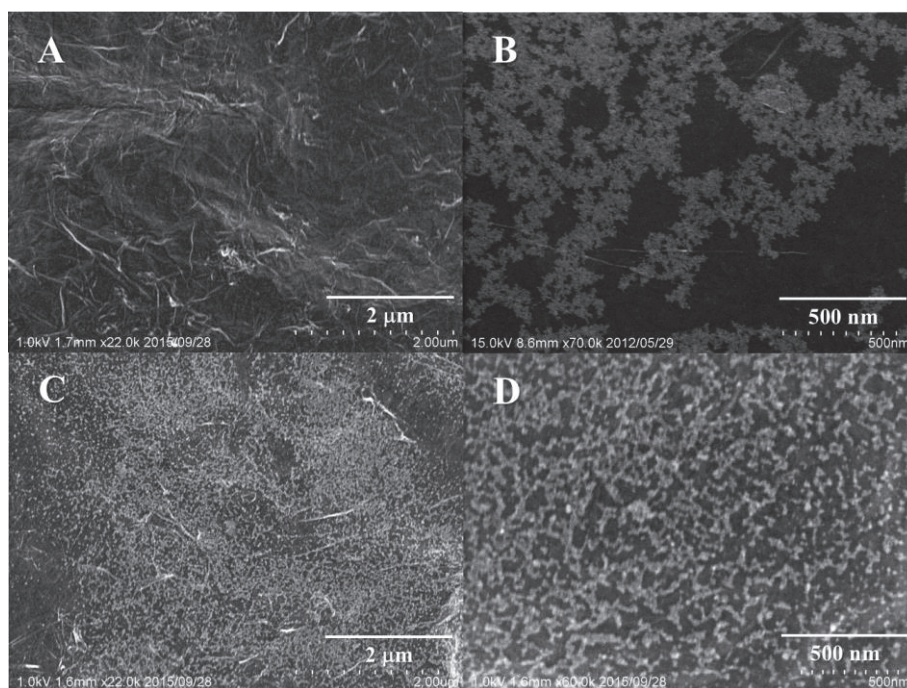


Figure 3-7 SEM images of erGO/PANI composites obtained by electrolysis of GO/aniline ($W_{GO}/W_{ANI}$=8) films on A) and B) FTO, and C) and D) SUS electrodes.

The erGO/PANI composites were prepared by using the voltage-step technique (±1.4 V, 10 hours) with the FTO and SUS electrodes and the SEM images of the obtained composite films are shown in Figure 3-7. At low magnification, both the surfaces of the composites prepared with FTO and SUS show a wrinkled structure characteristic of GO. A clear difference is seen in the SEM images taken at high magnification: PANI nanoparticles are dispersed better in the erGO/PANI composite prepared with SUS than in those obtained with FTO. The more uniformly-dense distribution of the PANI nanoparticles for the composites obtained with the SUS electrode may be related to the evolution of hydrogen gas during preparation of the composites.

Table 3-1 Fitted results (%) of C1s XPS spectra of erGO/PANI composites prepared on FTO and SUS

electrodes

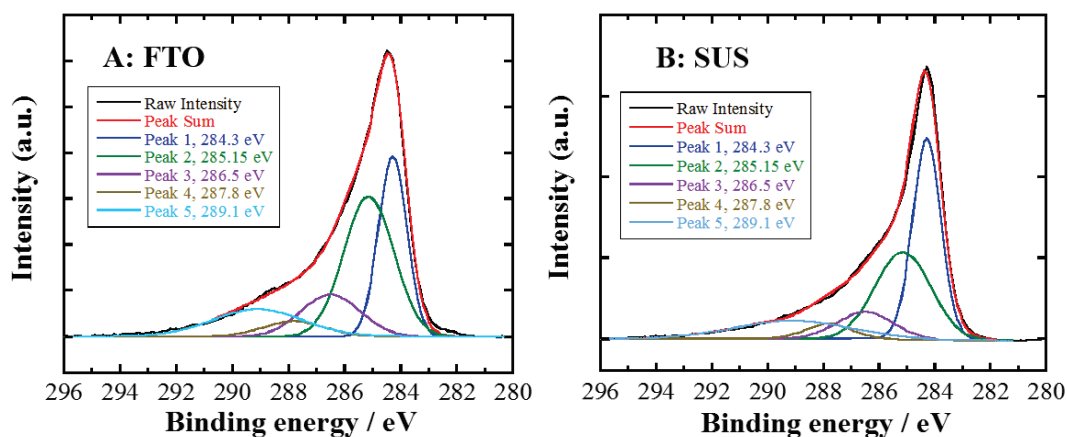| Electrode | Peak 1 C-C (sp$^2$) 284.3 eV | Peak 2 C-C (sp$^3$ defect) 285.15 eV | Peak 3 C-O(hydroxyl and epoxy) 286.5 eV | Peak 4 C=O (carbonyl) 287.8 eV | Peak 5 O-C=O (carboxyl) 289.1 eV |
|---|---|---|---|---|---|
| FTO | 28.3 | 38.5 | 13.7 | 5.3 | 14.2 |
| SUS | 38.9 | 32.2 | 10.1 | 4.7 | 14.1 |



Figure 3-8 XPS spectra for C1s of erGO/PANI ($W_{GO}/W_{ANI}$=8) composite films obtained by voltage-step method with A) FTO and B) SUS electrodes.

Figures 3-8A and 3-8B show the C1s XPS spectra of the erGO/PANI-8:1 films ($W_{GO}/W_{ANI}$ = 8) prepared with the FTO and SUS electrodes, respectively, and detailed information of each peak in the fitted results of the C1s XPS spectra is summarized in Table 3-1. The composite film (FTO) contains 33.2% oxygenated carbons including 13.7% C–O (hydroxyl and epoxy) centered at 286.5 eV, 5.3% C=O (carbonyl) at 287.8 eV, and 14.2% O-C=O (carboxyl) at 289.1 eV. [26, 27] Carbon atoms of 66.8% are nonoxygenated, including 28.3% sp$^2$ carbons at 284.3 eV and 38.5% sp$^3$ carbons (defect) at 285.15 eV. When the SUS electrode is used in the two-electrode cell, on the other hand, sp$^2$ carbons increase from 28.3% to 38.9% with a slight decrease of sp$^3$ carbons (38.5% to 32.2%). The nonoxygenated carbon groups in erGO/PANI (SUS) increase from 66.8% to 71.1%, suggesting that the oxygen-containing functional groups are removed effectively by using SUS in place of FTO. The effective removal of the oxygen species on the SUS electrode can be a reason for the formation of highly conductive erGO/PANI composites.

## 3.4 Conclusions

Composite films of graphene/polyaniline were prepared by a one-step electrochemical technique with GO and aniline monomer, and their thermoelectric performances were optimized with respect to the electrolysis time and the weight ratio of GO and aniline. It was found that the electrical conductivities of the composite films can be enhanced *ca.* four times by employing SUS in place of FTO, while no appreciable change was observed for the Seebeck coefficients. The composite films of the GO/aniline weight ratio of 8:1 prepared on the SUS electrodes gave the maximum power factor of 3.6 $\mu$W m$^{-1}$ K$^{-2}$ and *ZT* value of 0.008 at room temperature. In addition, the conductivity enhancement on the SUS electrode were accounted for in terms of the efficient removal of oxygen species of GO by the direct electrochemical reduction of GO on SUS concurrently with the reduction of GO by hydrogen gas generated by reduction of protons on SUS.

# Reference (3)

1. A recent progress on inorganic thermoelectric materials is reviewed in K. Kumoto and T. Mori (Eds.), Springer, Dordrecht, 2013.

2. H. Yan and N. Toshima, Thermoelectric Properties of Alternatively Layered Films of Polyaniline and (±)-10-Camphorsulfonic Acid-Doped Polyaniline. Chem. Lett., 1999, *28*, 1217.

3. N. Toshima, Conductive polymers as a new type of thermoelectric material. Macromol. Symp., 2002, *186*, 81.

4. D. S. Maddison and J. Unsworth, Electrical conductivity and thermoelectric power of polypyrrole with different doping levels. Synth. Met., 1988, *26*, 99.

5. N. Mateeva, H. Niculescu, J. Schlenoff, and L. R. Testardi, Correlation of Seebeck coefficient and electric conductivity in polyaniline and polypyrrole. J. Appl. Phys., 1998, *83*, 3111.

6. Y. Hiroshige, M. Ookawa, and N. Toshima, High thermoelectric performance of poly(2,5-dimethoxyphenylenevinylene) and its derivatives. Synth. Met., 2006, *156*, 1341.

7. K. Hiraishi, A. Masuhara, H. Nakanishi, H. Oikawa, and Y. Shinohara, Evaluation of Thermoelectric Properties of Polythiophene Films Synthesized by Electrolytic Polymerization. Jap. J. Appl. Phys., 2009, *48*, 071501.

8. O. Bubnova, Z. U. Khan, A. Malti, S. Braun, M. Fahlman, M. Berggren, and X. Crispin, Optimization of the thermoelectric figure of merit in the conducting polymer poly(3,4-ethylenedioxythiophene). Nat. Mater., 2011, *10*, 429.

9. S. H. Lee, H. Park, S. Kim, W. Son, I. W. Cheong, and J. H. Kim, Transparent and flexible organic semiconductor nanofilms with enhanced thermoelectric efficiency. J. Mater. Chem. A, 2014, *2*, 7288.

10. G. H. Kim, L. Shao, K. Zhang, and K. P. Pipe, Engineered doping of organic semiconductors for enhanced thermoelectric efficiency. Nat. Mater., 2013, *12*, 719.

11. C. Meng, C. Liu, and S. Fan, A promising approach to enhanced thermoelectric properties using carbon nanotube networks. Adv. Mater., 2010, *22*, 535.

12. Q. Yao, L. Chen, W. Zhang, S. Liufu, and X. Chen, Enhanced Thermoelectric Performance of Single-Walled Carbon Nanotubes/Polyaniline Hybrid Nanocomposites. ACS Nano, 2010, *4*, 2445.

13. D. Kim, Y. Kim, K. Choi, J. C. Grunlan, and C. Yu, Improved Thermoelectric Behavior of Nanotube-Filled Polymer Composites with Poly(3,4-ethylenedioxythiophene) Poly(styrenesulfonate). ACS Nano, 2010, *4*, 513.

14. C. Yu, K. Choi, L. Yin, and J. C. Grunlan, Light-Weight Flexible Carbon Nanotube Based Organic Composites with Large Thermoelectric Power Factors. ACS Nano, 2011, *10*, 7885.

15. L. Wang, D. Wang, G. Zhu, J. Li, and F. Pan, Thermoelectric properties of conducting polyaniline/graphite composites. Mater. Lett., 2011, *65*, 1086.

16. Y. Du, S. Z. Shen, W. Yang, R. Donelson, K. Cai, and P. S. Casey, Simultaneous increase in conductivity and Seebeck coefficient in a polyaniline/graphene nanosheets thermoelectric

nanocomposite. Synth. Met., 2012, *161*, 2688.

17. J. Xiang and L. T. Drzal, Templated growth of polyaniline on exfoliated graphene nanoplatelets (GNP) and its thermoelectric properties. Polymer, 2012, *53*, 4202.

18. Y. Zhao, G. S. Tang, Z. Z. Yu, and J. S. Qi, The effect of graphite oxide on the thermoelectric properties of polyaniline. Carbon, 2012, *50*, 3064.

19. B. Abad, I. Alda, P. Díaz-Chao, H. Kawakami, A. Almarza, D. Amantia, D. Gutierrez, L. Aubouy, and M. Martín-González, Improved power factor of polyaniline nanocomposites with exfoliated graphene nanoplatelets (GNPs). J. Mater. Chem. A, 2013, *1*, 10450.

20. Y. Lu, Y. Song, and F. Wang, Thermoelectric properties of graphene nanosheets-modified polyaniline hybrid nanocomposites by an in situ chemical polymerization. Mater. Chem. Phys., 2013, *138*, 238.

21. W. Wang, Q. Zhang, J. Li, X. Liu, L. Wang, J. Zhu, W. Luo, and W. Jiang, An efficient thermoelectric material: preparation of reduced graphene oxide/polyaniline hybrid composites by cryogenic grinding. RSC Adv., 2015, *5*, 8988.

22. M. Mitra, C. Kulsi, K. Chatterjee, K. Kargupta, S. Ganguly, D. Banerjee, and S. Goswamid, Reduced graphene oxide-polyaniline composites—synthesis, characterization and optimization for thermoelectric applications. RSC Adv., 2015, *5*, 31039.

23. X. Jiang, S. Setodoi, S. Fukumoto, I. Imae, K. Komaguchi, J. Yano, H. Mizota, and Y. Harima, An easy one-step electrosynthesis of graphene/polyaniline composites and electrochemical capacitor. Carbon, 2014, *67*, 662.

24. Y. Xu, H. Bai, G. Lu, C. Li, and G. Shi, Flexible Graphene Films via the Filtration of Water-Soluble Noncovalent Functionalized Graphene Sheets. J. Am. Chem. Soc., 2008, *130*, 5856.

25. Y. Chen, Y. Zhao, and Z. Liang, Solution processed organic thermoelectrics: towards flexible thermoelectric modules. Energy Environ. Sci., 2015, *8*, 401.

26. Y. Shao, J. Wang, M. Engelhard, C. Wang, and Y. Lin, Facile and controllable electrochemical reduction of graphene oxide and its applications. J. Mater. Chem., 2010, *20*, 743.

27. X. Y. Peng, X. X. Liu, D. Diamond, and K. T. Lau, Synthesis of electrochemically-reduced graphene oxide film with controllable size and thickness and its use in supercapacitor. Carbon, 2011, *49*, 3488.

# Chapter 4    Electrosynthesis of multilayer film stacked alternately by poly(3,4-ethylenedioxythiophene) and reduced graphene oxide from aqueous solution

## 4.1 Introduction

Since the late 1970's, electrically conducting polymers based on π-conjugated polymers have attracted a great deal of attention from many researchers, especially in the field of plastic electronics [1-5]. To further enhance their electrical performances by the synergistic effects, many types of composites of conducting polymers and carbon-based nanomaterials have been developed and applied to organic electronics such as capacitors [6], electrochromic displays [7], and thermoelectrics [8-12]. Among carbon-based materials, graphene has attracted a huge interest in recent years because of their excellent mechanical, thermal, and electrical properties [13].

In most reports, however, conducting polymers and graphene or graphene-like materials are mixed in the composites without any detailed control of their structures. It is interesting to obtain the multilayer films stacked alternately by two materials with different electronic properties, because such a multilayer structure may lead to manifestation of anisotropic properties in thermal and electrical conduction [14]. Actually, it has been reported that thermoelectric properties of inorganic materials are improved by the introduction of quantum-well superlattice structures using multilayer structure [15].

In this report, we describe a novel and facile technique to obtain the multilayer structure of conducting polymers and graphene by electrolysis of an aqueous solution of 3,4-ethylenedioxythiophene (EDOT) [16-18] and graphene oxide (GO) [19, 20]. EDOT is known as a monomer of poly(3,4-ethylenedioxythiophene) (PEDOT), which is one of the most famous conducting polymers due to its highly electrical conductivity [21, 22]. The electrolytic polymerization of EDOT in water can easily give PEDOT. On the other hand, GO can be obtained by oxidation of natural graphite, followed by exfoliation of graphite oxide. With a large amount of oxygen-containing functional groups such as hydroxyl, alkoxy, epoxy, carbonyl, and carboxyl groups, GO has a negative surface charge and is

well-dispersed in water. It is well-known that GO can be reduced to give a graphene-like material (reduced GO, rGO) by electrochemical means [23-26]. These facts hint us that the multilayer film stacked by PEDOT and rGO can be obtained by applying a suitable potential sequence on a conductive substrate in aqueous solutions containing only EDOT and GO (Scheme 4-1A). It is very useful from the viewpoint of industrial aspect to utilize the electrolysis method because this method can develop to prepare the film with large area. The resulting multilayer composite films (PEDOT/rGO) were characterized by X-ray photoemission spectroscopy (XPS), X-ray diffraction (XRD) and field-emission scanning electron microscopy (FE-SEM) analysis, and electrical conductivity measurements. The multilayer structures of PEDOT and rGO were controlled by the electrode potentials and the electrolysis times.
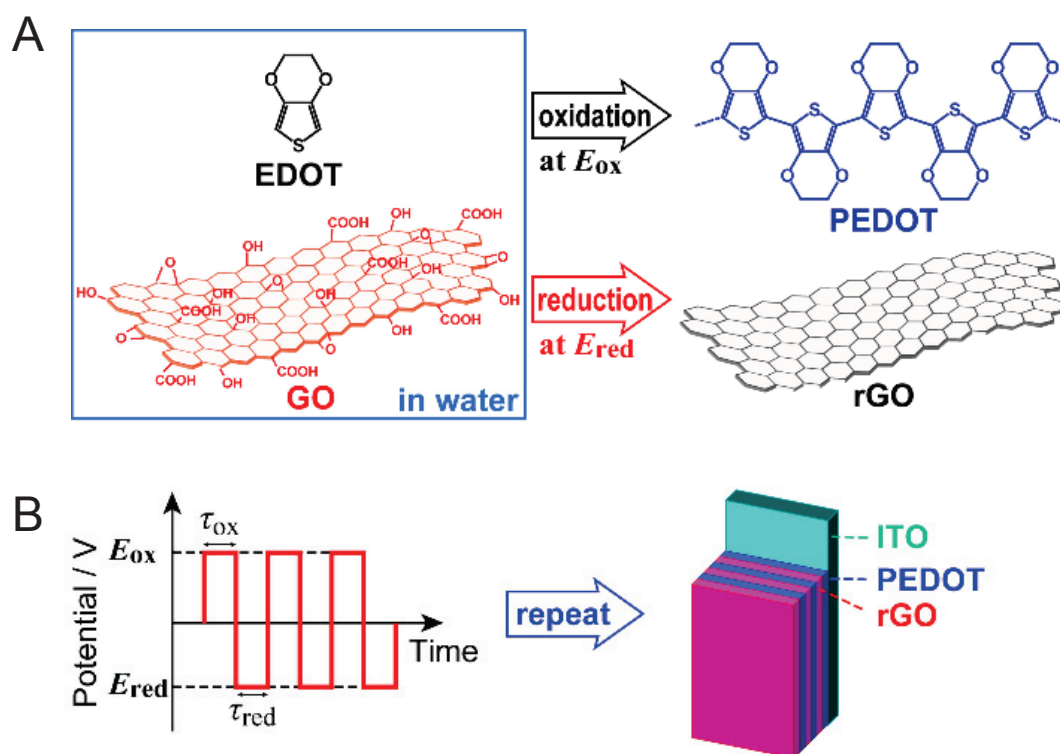


Scheme 4-1 (A)Electrochemical oxidation of EDOT at anodic potential ($E_{ox}$) and reduction of GO at cathodic potential ($E_{red}$) in aqueous solution of EDOT and GO to generate PEDOT and rGO films, respectively; (B) Potential-sequence to produce multilayer film composed of PEDOT and rGO.

## 4.2 Experimental

4.2.1 Preparation of multilayered PEDOT/rGO film

GO was synthesized from a natural graphite powder (SNO-10, SEC Carbon Ltd.) by a modified Hummers method as described [27]. The multilayered PEDOT/rGO films were electro-synthesized via alternate potential-sequence in an aqueous solution consisted of 3 mg mL$^{-1}$ GO and 20 mM EDOT. Then PEDOT layer was formed at anodic potential, while rGO layer at cathodic potential. (Illustration is given in Scheme 4-1B) The multilayer structures and thicknesses of PEDOT and rGO could be controlled by the electrode potentials and the electrolysis times.

4.2.2 Characterization of multilayered PEDOT/rGO film

The obtained films were then characterized by XPS (ESCA-3400, Kratos Analytica), XRD (Bruker AXS), and FE-SEM (JEOL JSM-6320F). Film thicknesses were evaluated by a 3D laser microscope (Keyence, VK-9700). Electrical conductivities were measured by the four-probe method using a low resistivity meter (Mitsubishi Chemical, Loresta-GP, MCP-T610).

## 4.3 Results and discussion

4.3.1 Potential-sweep voltammograms

Figure 4-1 depicts potential-sweep voltammograms of an ITO electrode in an aqueous solution containing EDOT and GO with Pt wire and Ag/AgCl as counter and reference electrodes, respectively. As a reference, a potential-sweep voltammetry was carried out in an aqueous KCl solution. In the KCl solution, cathodic currents due to the reduction of water were observed at around -1.3 V vs. Ag/AgCl, while the voltammogram in the solution containing both EDOT and GO showed an anodic current at around 1.0 V vs. Ag/AgCl ascribable to the oxidation of EDOT and a cathodic current at more positive potentials than in the KCl solution, which can be ascribed to the reduction of GO.
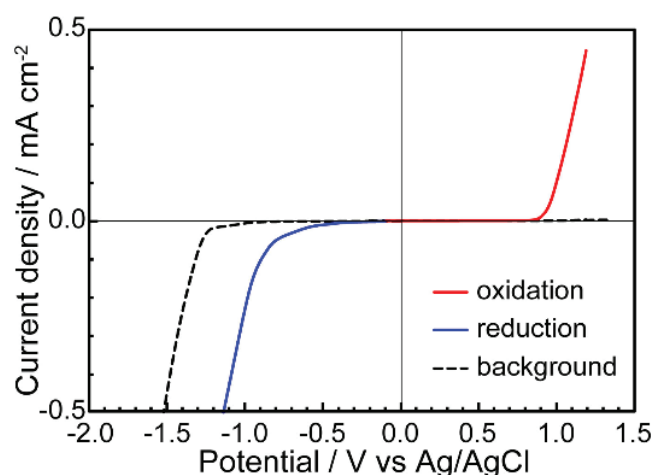
Figure 4-1 Potential-sweep voltammograms of ITO electrode at 50 mV sec^{-1} in aqueous solution containing EDOT (20 mM) and GO (3.0 mg mL^{-1}) (red: positive scan, blue: negative scan) and only KCl (3.0 M) (dashed black: background), respectively.

## 4.3.2 Characterization and analysis

The PEDOT film obtained at 1.1 V was subjected to the XPS analysis. The C1s signals of the film were observed at 285 eV as a broad peak and at 287 eV as a shoulder (Figure 4-2A). The signal at 285 eV can be ascribed to $sp^2$ and $sp^3$ carbons of PEDOT and GO, while the signal at 287 eV is due to oxygenated carbons such as ester, ether, and hydroxyl groups in GO [28, 29]. For reference, the XPS spectrum of a PEDOT:PSS film prepared by electrolytic polymerization of EDOT in the presence of poly(styrenesulfonic acid) (PSS) is shown in Figure 4-2B, where no shoulder is seen at 287 eV. These results demonstrate that GO is incorporated in the PEDOT film as a counter anion. When the film was reduced at -1.0 V in an aqueous solution containing only KCl as an electrolyte, the intensity of the shoulder at 287 eV decreased (Figure 4-2C). The decreased intensity of the shoulder upon electrochemical reduction implies that oxygen groups of GO doped in PEDOT film are eliminated to give a reduced GO (rGO), consistent with the previous results [28].

The films were further characterized by XRD analysis. The electrochemically oxidized film showed a broad peak at around 8°, due to the (001) diffraction corresponding to a distance of 1.1 nm between stacked GO sheets (Figure 4-2D). This is consistent with the thickness of a GO single layer, which was observed to be around 1 nm [30]. After the

74

electrochemical reduction of the film, the intensity of this peak became weak, and instead, the intensity of another peak at 26° increased. The latter peak is at a slightly lower angle than the peak for bulk graphite, suggesting that the rGO sheets stayed exfoliated and disorderly packed in the film [31, 32]. PEDOT films as thick as 4-6 μm were prepared by a prolonged electrolysis of an aqueous solution of EDOT and GO. The resulting films were peeled off from the ITO substrate and subjected to the measurements of electrical conductivities using the four-probe method. The free-standing PEDOT films exhibited low conductivities of the order of $10^{-5}$ S $cm^{-1}$. The low conductivities may be ascribed to the incorporation of the insulating GO layers into the PEDOT films as a dopant. When the as-prepared PEDOT film was electrochemically reduced in KCl solution, the conductivity of the film was increased drastically to a few S $cm^{-1}$ due to the reduction of GO in the film to the electrically conductive rGO.
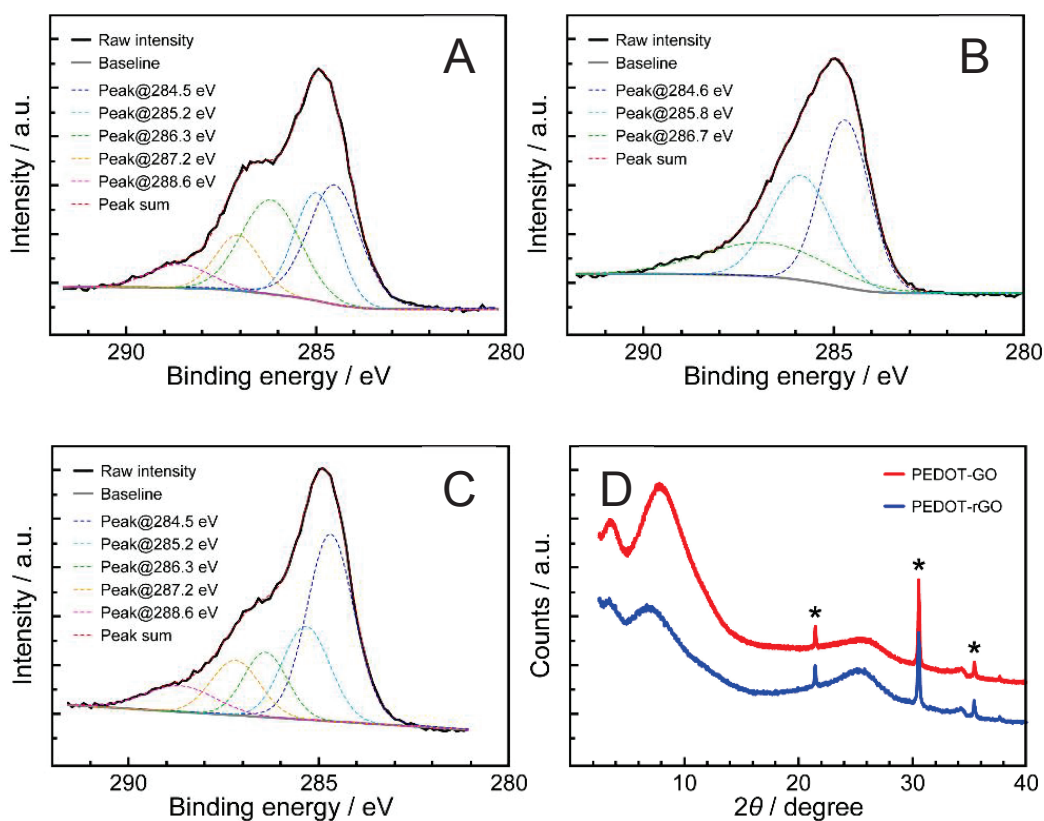


Figure 4-2 C1s XPS spectra of (a) PEDOT film obtained by oxidizing solution with EDOT and GO, (b) PEDOT:PSS film, and (c) PEDOT film reduced in KCl solution. (284.5 eV: C-C ($sp^2$); 285.2 eV: C-C ($sp^3$ defect); 286.3 eV: C-O (hydroxyl and epoxy); 287.2 eV: C=O (carbonyl); 288.6 eV: O-C=O (carboxyl)); (d) XRD patterns of PEDOT film (red line) and PEDOT film reduced in KCl solution

(black line). (* signal from ITO substrate)

The thicknesses of the PEDOT and rGO films obtained by various electrolysis times were monitored by 3D-laser microscope. In both oxidation and reduction reactions, the thicknesses were linearly increased with the electrolysis time (Figure 4-3A and 3B), although the film growth rates estimated by the least-squares method were greatly different: 120 and 8.0 nm min$^{-1}$ for oxidation and reduction, respectively. The film morphology was further analyzed by FE-SEM. The PEDOT layer showed a slightly wrinkled surface, suggesting the incorporation of GO (Figure 4-3C). The wrinkle was more notable on rGO layer (Figure 4-3D). These wrinkle surfaces are typical of GO and rGO.
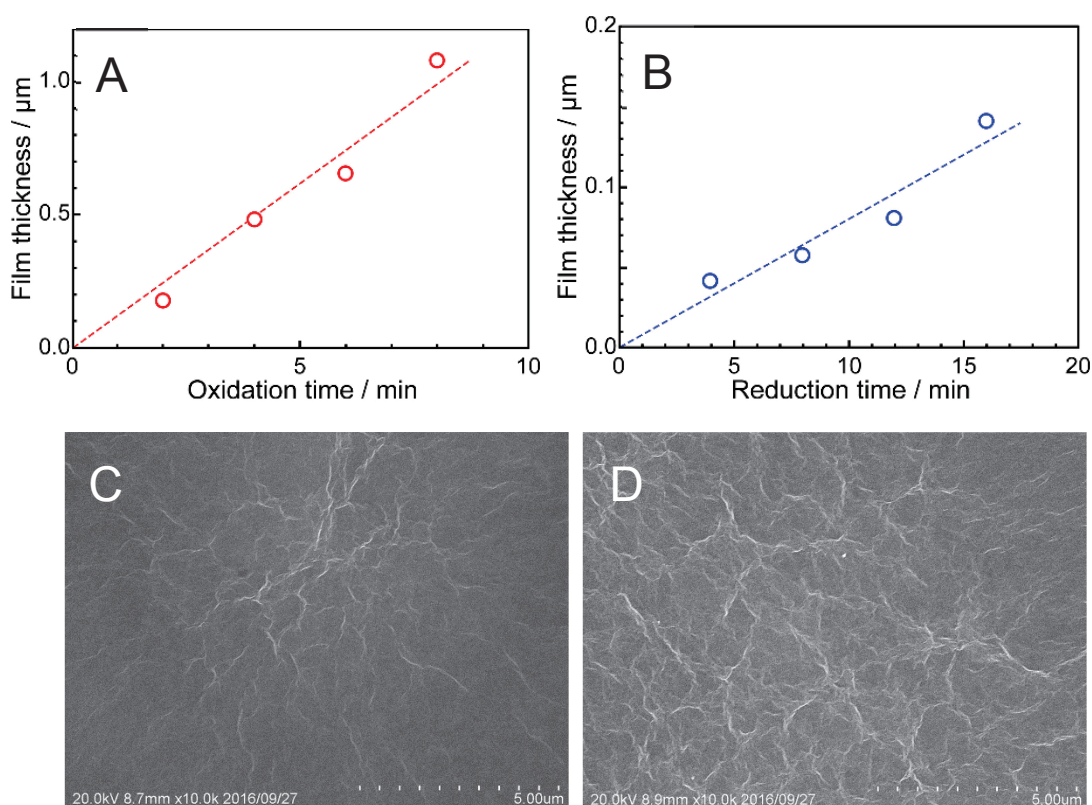


Figure 4-3 Thicknesses (A: PEDOT, B: rGO) and FE-SEM images (C: PEDOT, D: rGO) of PEDOT films obtained by oxidation at 1.0 V and rGO films by reduction at -1.1 V in the same solution as in Figure 4-1 at various electrolysis times.

### 4.3.3 Formation of multilayers composed of PEDOT and rGO

The above results suggest a possible formation of multilayers composed of PEDOT and rGO. To confirm this, the following experiment was performed (Figure 4-4A): the

ITO electrode was raised by 2.5 mm after each electrolysis while the potential was stepped to 1.1 V for 30 sec and then to -1.0 V for 2 min, and this potential-step sequence was repeated four times (Figure 4-4B). A photograph of the resulting film is shown in Figure 4-4C. Surfaces of the bands 1, 3, 5, and 7 on the film showed a dark-blue color, whereas those of the bands 2, 4, 6, and 8 were dark-gray, typical of the oxidized PEDOT and the rGO, respectively. When the water was dropped on the film, it was located only on the PEDOT surface (Figure 4-4D), reflecting that PEDOT is hydrophilic due to ionic oxidized PEDOT and oxygen groups in GO and rGO is hydrophobic due to the lack of oxygen groups by the reduction of GO. The difference of wettability is responsible for the fact that the vertical length of each band is not uniform though the electrode was raised by the same distance of 2.5 mm. The thicknesses of the eight layers measured by a 3-D laser microscope are shown in Figure 4-4E. It shows that the thickness of each layer increases almost linearly under the potential-step sequence employed in this experiment (Figure 4-4B). Although the film thickness increased linearly until 30 cycles, but the grow rate of the thickness is reduced and did not show linearity at 200 cycles. These results strongly demonstrate the formation of multilayer structure stacked alternately by PEDOT and rGO.
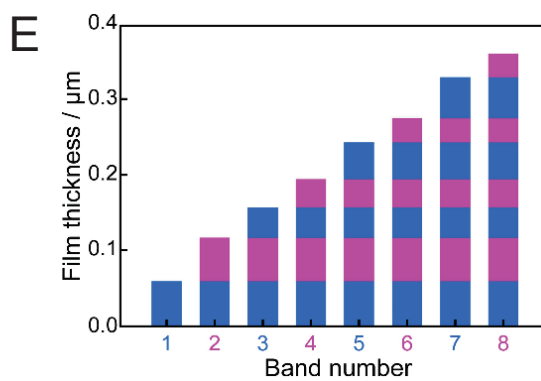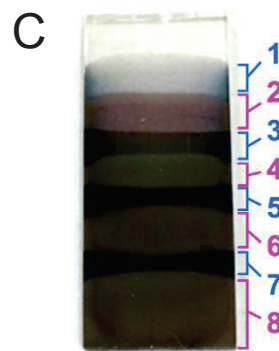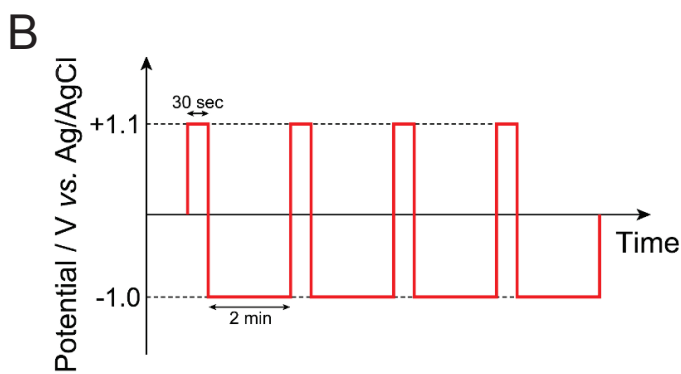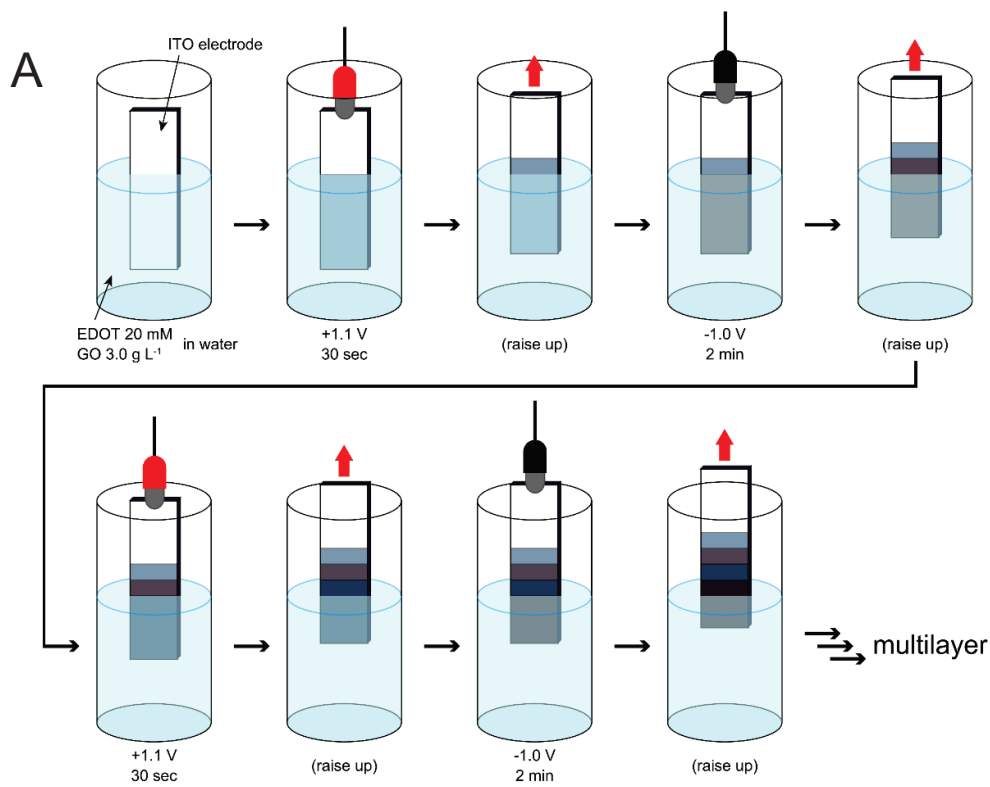
Figure 4-4 (A) Schematic illustration of experiment to demonstrate formation of PEDOT/rGO multilayer structure. (B) Potential-step sequence applied to ITO working electrode for the fabrication

of PEDOT/rGO multilayer composite film. Photographs of (C) PEDOT/rGO multilayer film and (D) the same film on which water was dropped. (E) Change of film thickness of the composite film.

PEDOT [33, 34] and its composites with graphene [11, 12] are well-known as good candidates for the high-performance thermoelectric materials. As above-mentioned, it is known that the introduction of multilayer structure can improve the thermoelectric properties in the case of inorganic materials due to their quantum-well effects [15]. Thus, the introduction of multilayer structure into the composite of PEDOT and rGO will be expected to show some unique thermoelectric performances as well. The application of this multi-layered composite film to thermoelectric materials is under progress.

## 4.4 Conclusions

We have succeeded in the synthesis of multilayer composite films stacked alternately by PEDOT and rGO by a repetitive potential application for reducing and oxidizing an aqueous solution containing only EDOT and GO. In the proposed technique, GO acts as a supporting electrolyte and a dopant. On the other hand, when the electrochemical reduction was carried out, not only GO doped in PEDOT but also GO in solution were reduced to give rGO, so that a single rGO layer was deposited on the PEDOT layer. Thus, multilayer structure stacked alternately by PEDOT and rGO can be easily obtained just by applying the repetitive potential of 1.0 and -1.1 V. It was revealed further that the thickness of each layer can be easily controlled by the electrolysis time. The preparation of PEDOT/rGO multilayer composite films thick enough to enable us to measure physical properties such as electrical and thermal conductivities, and Seebeck coefficients for their thermoelectric application with a special attention on the anisotropic natures is currently under investigation.

# Reference (4)

1. T. A. Skotheim and J. R. Reynolds, Handbook of Conducting Polymers. 3rd ed, CRC Press: Boca Raton, 2007.

2. M. Leclerc and J. F. Morin, Design and Synthesis of Conjugated Polymers. Wiley-VCH, Weinheim, 2010.

3. G. Inzelt, Conducting Polymers: A New Era in Electrochemistry. Springer: Heidelberg, 2012.

4. H. Shi, C. C. Liu, Q. L. Jiang, and J. K. Xu, Effective Approaches to Improve the Electrical Conductivity of PEDOT:PSS: A Review. Adv. Electron. Mater., 2015, *1*, 1500017.

5. W. T. Neo, Q. Ye, S. J. Chua, and J. Xu, Conjugated polymer-based electrochromics: materials, device fabrication and application prospects. J. Mater. Chem. C, 2016, *4*, 7364.

6. Y. K. Zhou, B. L. He, W. J. Zhou, J. Huang, X. H. Li, B. Wu, and H. L. Li, Electrochemical capacitance of well-coated single-walled carbon nanotube with polyaniline composites. Electrochim. Acta, 2004, *49*, 257.

7. S. Bhandari, M. Deepa, A. K. Srivastava, C. Lal and R. Kant, Poly(3,4-ethylenedioxythiophene) (PEDOT)-Coated MWCNTs Tethered to Conducting Substrates: Facile Electrochemistry and Enhanced Coloring Efficiency. Macromol. Rapid Commun., 2008, *29*, 1959.

8. Y. Y. Wang, K. F. Cai, S. Shen, and X. Yao, In-situ fabrication and enhanced thermoelectric properties of carbon nanotubes filled poly(3,4-ethylenedioxythiophene) composites. Synth. Met., 2015, *209*, 480.

9. H. Wang, S. I. Yi, and C. Yu, Engineering electrical transport at the interface of conjugated carbon structures to improve thermoelectric properties of their composites. Polymer, 2016, *97*, 487.

10. L. Liang, C. Gao, G. Chen, and C. Y. Guo, Large-area, stretchable, super flexible and mechanically stable thermoelectric films of polymer/carbon nanotube composites. J. Mater. Chem. C, 2016, *4*, 526.

11. F. Li, K. Cai, S. Shen, and S. Chen, Preparation and thermoelectric properties of reduced graphene oxide/PEDOT:PSS composite films. Synth. Met., 2014, *197*, 58.

12. Y. Harima, S. Fukumoto, L. Zhang, X. Jiang, J. Yano, K. Inumaru, and I. Imae, Thermoelectric performances of graphene/polyaniline composites prepared by one-step electrosynthesis. RSC Adv., 2015, *5*, 86855.

13. M. Wang, X. Duan, Y. Xu, and X. Duan, Functional Three-Dimensional Graphene/Polymer Composites. Acs NANO, 2016, *10*, 7231.

14. Kittel, C. Introduction to Solid State Physics. 8th ed, Wiley, New York, 2005.

15. L. D. Hicks, T. C. Harman, and M. S. Dresselhaus, Use of quantum-well superlattices to obtain a high figure of merit from nonconventional thermoelectric materials. Appl. Phys. Lett., 1993, *63*, 3230.

16. M. Turbiez, P. Frère, M. Allain, C. Videlot, J. Ackermann, and J. Roncali, Design of Organic Semiconductors: Tuning the Electronic Properties of π-Conjugated Oligothiophenes with the 3,4-

Ethylenedioxythiophene (EDOT) Building Block. Chem. Eur. J., 2005, *11*, 3742.

17. I. Imae, S. Imabayashi, K. Korai, T. Mashima, Y. Ooyama, K. Komaguchi, and Y. Harima, Electrosynthesis and charge-transport properties of poly(3′,4′-ethylenedioxy-2,2′:5′,2″-terthiophene). Mater. Chem. Phys., 2012, *131*, 752.

18. I. Imae, S. Imabayashi, K. Komaguchi, Z. Tan, Y. Ooyama, and Y. Harima, Synthesis and electrical properties of novel oligothiophenes partially containing 3,4-ethylenedioxythiophenes. RSC Adv., 2014, *4*, 2501.

19. D. R. Dreyer, S. Park, C. W. Bielawski, and R. S. Ruoff, The chemistry of graphene oxide. Chem. Soc. Rev., 2010, *39*, 228.

20. R. K. Joshi, S. Alwarappan, M. Yoshimura, V. Sahajwalla, and Y. Nishina, Review Graphene Oxide: The New Membrane Material. Appl. Mater. Today, 2015, *1*, 1.

21. S. Kirchmeyer and K. Reuter, Scientific Importance, Properties and Growing Applications of Poly(3,4-ethylenedioxythiophene). J. Mater. Chem., 2005, *15*, 2077.

22. A. Elschner, S. Kirchmeyer, W. Lövenich, U. Merker and K. Reuter, PEDOT: Principles and Applications of an Intrinsically Conductive Polymer. CRC Press: Boca Raton, 2011.

23. N. A. Kotov, I. DPkriny, and J. H. Fendler, Ultrathin Graphite Oxide-Polyelectrolyte Composites Prepared by Self-Assembly: Transition Between Conductive and Non-Conductive States. Adv. Mater., 1996, *8*, 637.

24. H. L. Guo, X. F. Wang, Q. Y. Qian, F. B. Wang, and X. H. Xia, A Green Approach to the Synthesis of Graphene Nanosheets. ACS Nano, 2009, *3*, 2653.

25. C. L. Scott, G. Zhao, and M. Pumera, Stacked graphene nanofibers doped polypyrrole nanocomposites for electrochemical sensing. Electrochem. Commun., 2010, *12*, 1788.

26. L. Chen, Y. Tang, K. Wang, C. Liu, and S. Luo, Direct electrodeposition of reduced graphene oxide on glassy carbon electrode and its electrochemical application. Electrochem. Commun., 2011, *13*, 133.

27. I. Imae, T. Oonishi, I. S. Isaak, S. Yamamoto, and Y. Harima, Facile fabrication of transparent conductive graphene/silica composite films with high mechanical strength. Synth. Met., 2017, *224*, 33.

28. X. Jiang, S. Setodoi, S. Fukumoto, I. Imae, K. Komaguchi, J. Yano, H. Mizota, and Y. Harima, An easy one-step electrosynthesis of graphene/polyaniline composites and electrochemical capacitor. Carbon, 2014, *67*, 662.

29. G. H. Kim, D. H. Hwang, and S. I. Woo, Thermoelectric properties of nanocomposite thin films prepared with poly(3,4-ethylenedioxythiophene) poly(styrenesulfonate) and graphene. Phys Chem Chem Phys, 2012, *14*, 3530.

30. T. N. Blanton and D. Majumdar, X-ray diffraction characterization of polymer intercalated graphite oxide. Powder Diffraction, 2012, *27*, 104.

31. L. J. Cote, R. Cruz-Silva, and J. Huang, Flash Reduction and Patterning of Graphite Oxide and Its Polymer Composite. J. Am. Chem. Soc., 2009, *131*, 11027.

32. T. N. Blanton and D. Majumdar, Characterization of X-ray Irradiated Graphene Oxide Coatings Using X-ray Diffraction, X-ray Photoelectron Spectroscopy, and Atomic Force Microscopy. Powder Diffraction, 2013, *28*, 68.

33. B. Russ, A. Glaudell, J. J. Urban, M. L. Chabinyc and R. A. Segalman, Organic Thermoelectric Materials for Energy Harvesting and Temperature Control. Nature Rev. Mater., 2016, *1*, 16050.

34. Z. Zhu, C. Liu, F. Jiang, J. Xu, and E. Liu, Effective treatment methods on PEDOT:PSS to enhance its thermoelectric performance. Synth. Met., 2017, *225*, 31.

# Chapter 5   Highly improved thermoelectric performances of PEDOT:PSS/SWCNT composites by solvent treatment

## 5.1 Introduction

Thermoelectric (TE) devices based on the Seebeck effect now have aroused increasing attention as clean energy-conversion systems which can harvest electricity from waste heat. [1, 2] Performance of TE material is described by a dimensionless TE figure-of-merit ($ZT$) and a power factor ($PF$) defined by $ZT= S^2\sigma T/\kappa$ and $PF= S^2\sigma$, respectively, where $S$, $\sigma$, $\kappa$, and $T$ are Seebeck coefficient, electrical conductivity, thermal conductivity, and absolute temperature, respectively. [3] Traditional inorganic TE materials are usually expensive, rare, heavy, and relatively difficult to process, and thus impeding their widespread use. In this regard, with advantages of low cost, abundance of raw materials, flexibility, and relatively simple manufacturing processes, organic TE materials have received a growing interest.

Among the organic TE materials, conducting polymers such as poly(3,4-ethylenedioxythiophene): poly (styrenesulfonate) (PEDOT:PSS), polyaniline (PANI) and poly(3-hexylthiophene) (P3HT) have been intensively studied so far. [4-6] However, these pristine polymers always exhibit relatively low electrical conductivity which largely suppressed their applications. [7] To satisfy the requirement for promising TE materials, further improvement of the performance is deserved. One effective way is to combine polymers simply with highly conductive carbon nanotubes (CNTs). [6, 8] Due to the π−π interaction between CNT and polymers, the nanotubes establish intermolecular connections which facilitates electrical conduction. Additionally, the highly oriented CNT can also enhance the degree of ordering of the polymer chains around the aligned CNT, thereby enhancing the $\sigma$. [9] On the other hand, the thermal conductivity in organic TE materials is probably dominated by phonons. [10] Although the junctions between CNT and polymer chains could promote electron conduction, it is known that the junctions can reversely act as the barrier for phonon transport between carbon nanotubes, making the CNT/polymer composites to exhibit a polymer-like thermal conductivity,

ranging from 0.2 to 0.7 W m$^{-1}$ K$^{-1}$, which is much smaller than that of pure CNT (~1000 W m$^{-1}$ K$^{-1}$). [8, 11, 12] Accordingly, we could expect relatively low thermal conductivity as well as the high electrical conductivity by the combination of CNT and polymer, which may lead to an expectable $ZT$ value.

Till now, several works on high performance conjugated polymers with CNT have been published. Quite recently, Cho et al. reported a large $PF$ of 151 μW m$^{-1}$ K$^{-2}$ for PEDOT:PSS/CNT composites by treating them in ethylene glycol (EG) for one hour followed by annealing at 140 °C for ten minutes.[6] Similar $PF$ values of 140 and 160 μW m$^{-1}$ K$^{-2}$ have also been reported earlier for the PEDOT:PSS/ single-wall carbon nanotube (SWCNT) composites. [11, 13] However, such obtained composites often requires complicated fabrication process. Here, a more facile technique to produce PEDOT:PSS/SWCNT composites with a larger $PF$ of 300 μW m$^{-1}$ K$^{-2}$ is demonstrated. To best of our knowledge, such PF value is the highest among the PEDOT:PSS/CNT composites reported before. [6, 8]

## 5.2 Experimental

5.2.1 Materials

SWCNT ink (EC-DH, 0.2 wt%) was purchased from Meijo Nano Carbon Co. Ltd, while PEDOT:PSS (Clevios PH1000, 1.1 wt%) from Heraeus. Before use, SWCNT ink was diluted to 0.1 wt% with distilled water in order to reduce the viscosity. All the other reagents were obtained from TCI and used as received without further purification.

5.2.2 Preparation of PEDOT:PSS/SWCNT and their characterizations

PEDOT:PSS/SWCNT composites with various SWCNT weight ratios ($W_{SWCNT}$) were prepared by simply mixing two aqueous dispersions of PEDOT:PSS and SWCNT at different feeding weight ratio and then stirring overnight. Then, 60 μL of the mixed solution was doctor bladed on the precleaned glass substrates and dried at 60 $^O$C, unless otherwise stated. The precleaning of the glass substrates was performed by immersed in the piranha (H$_2$SO$_4$/H$_2$O$_2$ 3/1 v/v) solution for 3 h, then rinsed with detergent, deionized

water and ethanol subsequently. [14] The thickness of the as-obtained composite films was around 1 μm. All the solvent treatment were implemented at room temperature and then dried at 60 $^\text{O}$C.

Thickness of the PEDOT:PSS/SWCNT composites was obtained by 3D Laser Scanning Microscope (VK-9700, KEYENCE), while conductivities were measured using the four-probe method with a resistivity meter (Loresta-GP MCP-T610, Mitsubishi Chemical Corp.). A custom-made setup composed of thermocouples and Peltier devices was used to evaluate Seebeck coefficients, where it was calibrated in advance with the Seebeck coefficients of -18 and +22 μV K$^{-1}$, respectively, for alumel and chromel alloys at room temperature. [3] All these TE properties of the PEDOT:PSS/SWCNT composites were measured at room temperature. Film morphologies were observed with a field-emission scanning electron microscope (SEM, JSM-6320F, JEOL) and a transmission electron microscopy (TEM, JEM 2010, JEOL) attached with energy dispersive X-ray spectrometer (EDX, JED2300-T, JEOL). Element amount was analyzed on element analysis (EA, CHNS/0 2400II).

## 5.3 Results and discussion

5.3.1 TE performance of as-prepared PEDOT:PSS/SWCNT composites

The TE performances of as-prepared composite films with different CNT contents are shown in Figure 5-1. $\sigma$ and $S$ values of the pristine PEDOT:PSS film are 0.2 S cm$^{-1}$ and 19 μV K$^{-1}$ ($PF$ = 0.007 μW m$^{-1}$ K$^{-2}$), while those for the SWCNT film are 303 S cm$^{-1}$ and 24 μV K$^{-1}$ ($PF$ = 17 μW m$^{-1}$ K$^{-2}$). By increasing $W_\text{SWCNT}$, the $PF$ values were increased and the maximum $PF$ was attained at $W_\text{SWCNT}$ = 74 wt%. However, the $PF$ value was still as small as 29 μW m$^{-1}$ K$^{-2}$. It is quite likely that these low TE performances of as-prepared composites are ascribed to the surfactant, sodium dodecylbenzenesulfonate (SDBS), used to disperse SWCNTs in water, which can prevent a charge transport in the composites because of its insulating property. Indeed, when the as-prepared SWCNT films were soaked in water, the weights of the SWCNT films were decreased to ca. one fourth of those for the original films, demonstrating that a lot amount of surfactant is included in
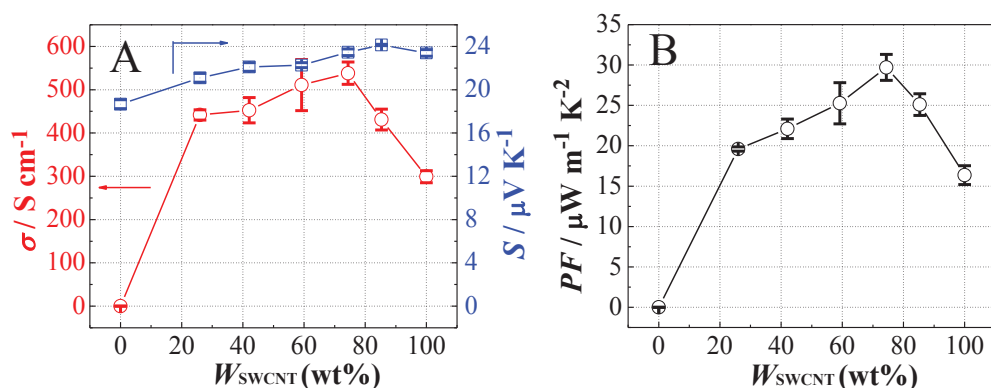
the SWCNT ink.



Figure 5-1 Changes of (A) $\sigma$ and $S$, and (B) $PF$ of PEDOT:PSS/SWCNT composites with $W_{SWCNT}$.

## 5.3.2 PEDOT:PSS/SWCNT composites with solvent treatment

Five polar solvents such as acetonitrile (AN), water ($H_2O$), ethanol (EtOH), ethylene glycol (EG), and DMSO were examined as a soaking medium for removing the surfactant from the as-prepared composites to improve their TE performances. The values of $\sigma$, $S$, and $PF$ for the PEDOT:PSS/SWCNT composites ($W_{SWCNT}$ = 74 wt%) treated with the five polar solvents for one hour are compared in Figure 5-2. As expected, the composites soaked in all these solvents exhibited a distinct enhancement in conductivity. Furthermore, a slight increase in Seebeck coefficient was observed. Among all the polar solvents examined, DMSO was found to exhibit the most effective capability for improving the TE performances. The $PF$ of the DMSO-treated composite reached 210 $\mu W\ m^{-1}\ K^{-2}$, much greater than 29 $\mu W\ m^{-1}\ K^{-2}$ for the as-prepared PEDOT:PSS/SWCNT composite.
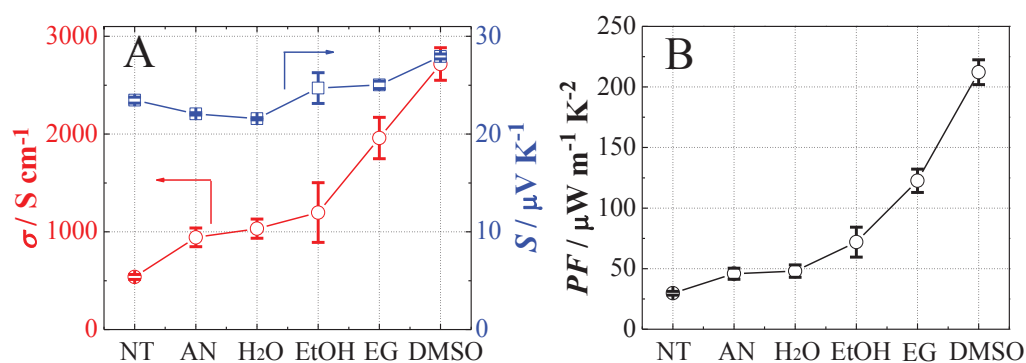


Figure 5-2 (A) $\sigma$ and $S$, and (B) $PF$ of PEDOT:PSS/SWCNT composites ($W_{SWCNT}$ = 74 wt%) soaked in different polar solvents for one hour at room temperature. (NT denotes no treatment with polar solvent)
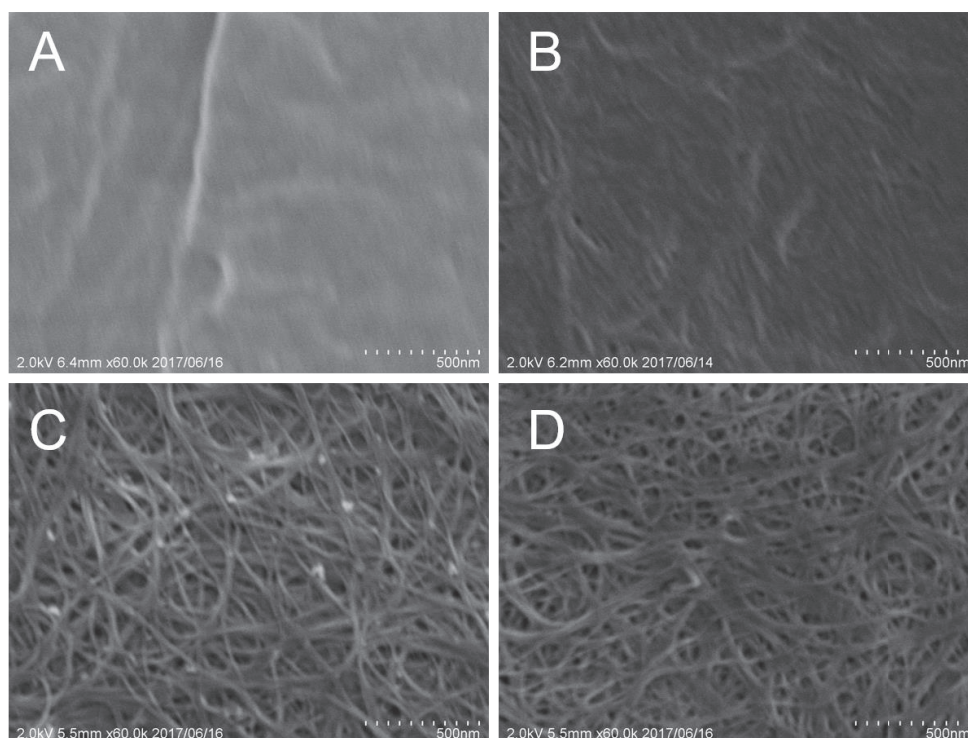
Figure 5-3 SEM images of (A) non-solvent treated SWCNT, (B) non-solvent treated PEDOT:PSS/SWCNT composites, (C) DMSO-treated SWCNT and (D) DMSO-treated PEDOT:PSS/SWCNT composites.

Figure 5-3 shows the SEM images of SWCNT and PEDOT:PSS/SWCNT composite films before and after solvent treatment. As to the composites before DMSO treatment, no CNT bundles are seen by being covered with a lot amount of SDBS (Figure 5-3A and 3B). When the films were washed with DMSO, the bundle structures were observed. (Figure 5-3C and 3D) These SEM observations suggest that an effective removal of electrically insulating SDBS is responsible for a drastic increase in $\sigma$ of the composites by DMSO treatment shown in Figure 5-2A. Indeed, an obvious decrease of film weight of SWCNT and PEDOT:PSS/SWCNT composites via DMSO treatment in Figure 5-4 is observed. The figure shows that the weight of a SWCNT film is decreased from 300 to 70 μg by soaking the film in DMSO. Similar changes of film weights were observed also for PEDOT:PSS/SWCNT composites. To confirm the reason for the weight change, the elemental analysis of the SWCNT films before and after DMSO treatment was carried out (shown in Table 5-1). It was found that the weight ratio of sulfur originating from SDBS (348 g mol$^{-1}$) was decreased from 8 % to 3 % by DMSO treatment. This implies

that an original SWCNT film (300 μg) contains 261 μg of SDBS, while the DMSO-treated SWCNT film (70 μg) does only 24 μg of SDBS, showing that more than 90% SDBS is removed from the SWCNT film by DMSO treatment and the weight loss of SWCNT film observed in Figure 5-4 arises mainly from removal of SDBS. It is known well that the treatment with DMSO can effectively remove excess PSS molecular which gives rise to insulating properties on surfaces of PEDOT grains. Indeed, as is shown in Figure 5-4, the weight loss was observed also for the PEDOT:PSS film soaked in DMSO, although the degree of the weight change is much smaller than those for PEDOT:PSS/SWCNT composites.

Table 5-1 Weight percent of C, H, S in SWCNT and DMSO treated SWCNT by element analysis..

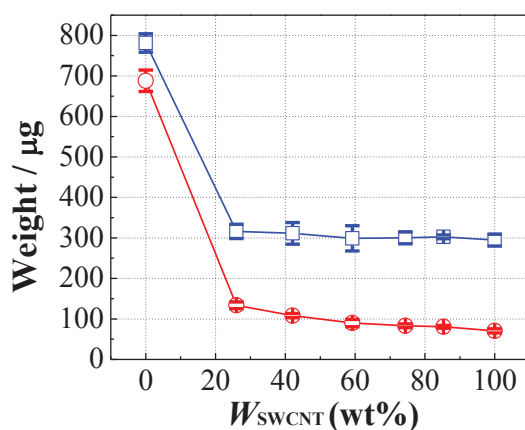|  | SWCNT | | | DMSO treated SWCNT | | |
|---|---|---|---|---|---|---|
|  | Sample 1 | Sample 2 | Average | Sample 1 | Sample 2 | Average |
| C (wt%) | 63.24 | 63.93 | 63.58 | 78.20 | 77.30 | 77.75 |
| S (wt%) | 8.26 | 7.57 | 7.92 | 2.90 | 3.24 | 3.07 |



Figure 5-4 Weights of 60 μL of mixed solutions as a function of $W_{SWCNT}$ before (blue cubic) and after (red circle) DMSO treatment.

Additionally, in contrast to DMSO-treated SWCNT, it was observed that additional materials are attached on some junctions between CNTs in the composite film (Figure 5-3D). To confirm this, high resolution transmission electron microscopies of these thin films were measured (Figure 5-5A and 5B). While DMSO-treated SWCNT showed only bundle structures, some particles were observed at the junctions between CNTs of the composite film. These particles were characterized to be PEDOT:PSS by the elemental

analysis using the energy dispersive X-ray spectrometer attached with TEM. As explained, the presence of the junctions is believed to promote the electron conduction which gives rise to exceptional thermoelectric properties. [13, 15] Consequently, the enhancement of the conductivities for the PEDOT:PSS/SWCNT composite film can be ascribed to the improvement of charge-transport by the introduction of PEDOT:PSS located at the junctions between CNTs.
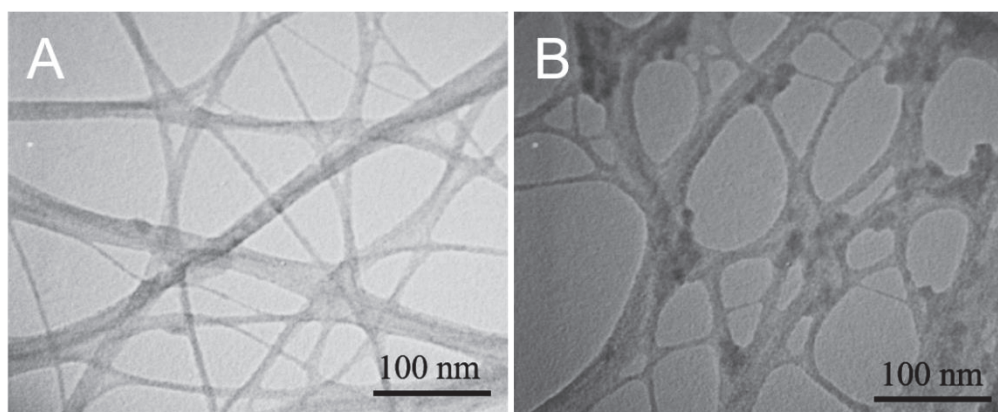


Figure 5-5 TEM images of (A) SWCNT and (B) PEDOT:PSS/SWCNT composites.

### 5.3.3 Optimization of the TE performance of PEDOT:PSS/SWCNT composites

Figure 5-6 depicts an influence of the soaking time on $\sigma$ and $S$ for PEDOT:PSS/SWCNT composites treated with DMSO. The figure shows that by soaking the composite just for two minutes at room temperature, $\sigma$ was increased dramatically from 500 to 3,800 S cm$^{-1}$ while the $S$ was increased slightly from 24 to 28 $\mu$V K$^{-1}$. When the treatment time was longer than two minutes, the $\sigma$ of the composite started to decrease, in agreement with the dedoping studies of PEDOT:PSS with EG and DMSO previously published. [16] PSS is known to be involved in the PEDOT:PSS as non-ionized and ionized molecules. The ionized PSS could act as the effective dopant for PEDOT:PSS, while the non-ionized one as barriers for electric conduction. By the DMSO treatment, the insulating PSS can be effectively removed from PEDOT:PSS chains which are responsible for electric conduction. [17] When the treatment time is longer than two minutes, however, not only the insulating non-ionized PSS layer, but also the dopant PSS could be removed. Namely, PEDOT:PSS could be dedoped when the DMSO treating

time is longer, which may decrease the conductivity. As we mentioned before, PEDOT:PSS here is acted as the junctions to promote the carrier transport. However, when the conductivity of the PEDOT:PSS is decreased, the resistivity in the junctions for carrier transport would increase, decreasing the electrical conductivity.
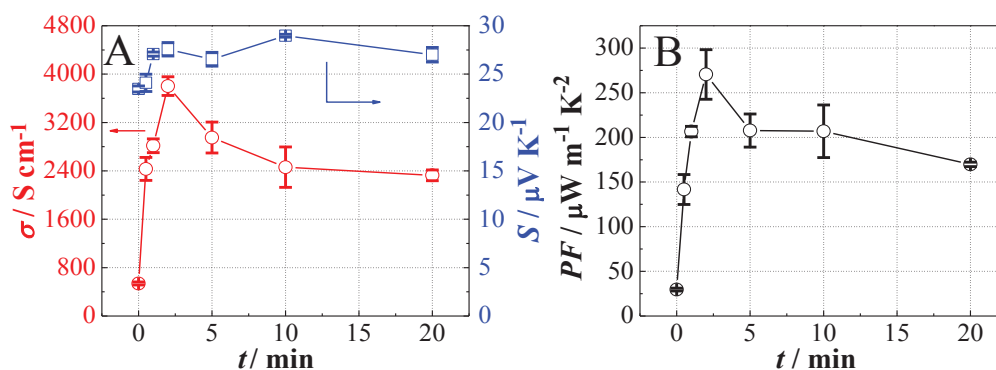


Figure 5-6 Influence of DMSO-treatment time ($t$) on (A) $\sigma$ and $S$, and (B) $PF$ for PEDOT:PSS/SWCNT composites ($W_{SWCNT}$ = 74 wt%) at room temperature.

In view of the above findings, TE performances of the PEDOT:PSS/SWCNT composites soaked with DMSO for two minutes at room temperature were studied as a function of $W_{SWCNT}$. The changes of $\sigma$, $S$, and $PF$ for thus treated PEDOT:PSS/SWCNT composites with a change of $W_{SWCNT}$ are depicted in Figure 5-7. It is seen from the figure that both $\sigma$ and $S$ values of the DMSO-treated composites exhibited maxima of 3,800 S cm$^{-1}$ and $S$ = 28 $\mu$V K$^{-1}$, respectively, at $W_{SWCNT}$ = 74 wt% and, consequently, the $PF$ of the composite reached a peak value of 300 $\mu$W m$^{-1}$ K$^{-2}$. It is quite striking that such a facile treatment (two-min soaking in DMSO at room temperature) is successful in improving the $PF$ value of the as-prepared PEDOT:PSS/SWCNT composite ($W_{SWCNT}$ = 74 wt%) almost ten times from 29 to 300 $\mu$W m$^{-1}$ K$^{-2}$. The change of $\sigma$ with $W_{SWCNT}$ in Figure 5-7 may be explained in the following way. As we described before, the junctions between the SWCNT and PEDOT:PSS promotes the charge transport, thus enhancing their electrical conductivity. However, when the ratio of SWCNT in the composite is increased further, the number of the junctions originated from the connection of PEDOT:PSS and SWCNT would reduce. Consequently, the electrical conductivity decreased, which, on the other hand, explained the reason of a relatively small $\sigma$ value of

the SWCNT film compared with that of the composites. We presume that the best balanced condition is attained at $W_{SWCNT}$ = 74 wt% in our experiments with aqueous dispersions of PEDOT:PSS and SWCNT.
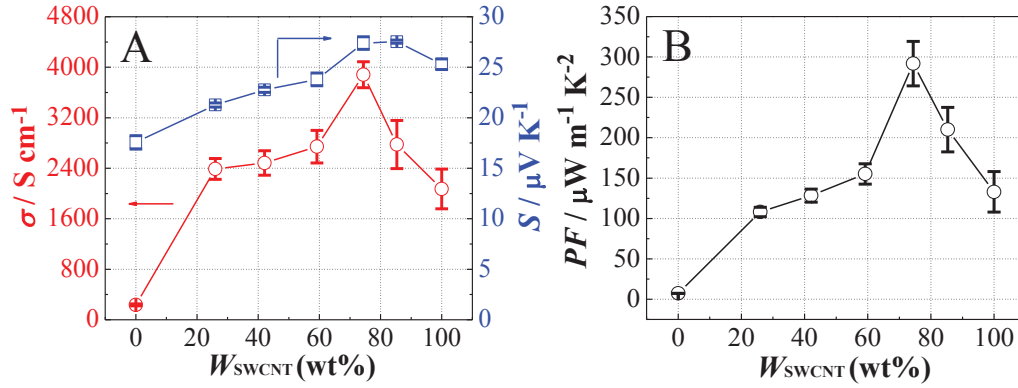


Figure 5-7 Changes of (A) $\sigma$ and $S$, and (B) $PF$ of PEDOT:PSS/SWCNT composites treated with DMSO for two minutes at room temperature with $W_{SWCNT}$.

## 5.4 Conclusion

By simply mixing the aqueous dispersions of SWCNT and PEDOT:PSS at different weight ratios, PEDOT:PSS/SWCNT composites were prepared. With an optimization of the feeding weight ratio of PEDOT:PSS and SWCNT, a peak value of $PF$ at 29 $\mu$W m$^{-1}$ K$^{-2}$ was achieved. Furthermore, when being soaked in DMSO for two minutes at room temperature, these composites yielded a highly improved TE performance at $W_{SWCNT}$ = 74 wt%: $\sigma$ = 3,800 S cm$^{-1}$, $S$ = 28 $\mu$V K$^{-1}$, and $PF$ = 300 $\mu$W m$^{-1}$ K$^{-2}$. The $PF$ is the largest among those reported so far for composites based on PEDOT:PSS and CNT.

# Reference (5)

1. E. J. Bae, Y. H. Kang, K. S. Jang, and S. Y. Cho, Enhancement of Thermoelectric Properties of PEDOT:PSS and Tellurium-PEDOT:PSS Hybrid Composites by Simple Chemical Treatment. Sci. Rep., 2016, *6*, 18805.

2. D. Yang, X. Su, Y. Yan, T. Hu, H. Xie, J. He, C. Uher, M. G. Kanatzidis, and X. Tang, Manipulating the Combustion Wave during Self-Propagating Synthesis for High Thermoelectric Performance of Layered Oxychalcogenide Bi1–xPbxCuSeO. Chem. Mater., 2016, *28*, 4628.

3. L. Zhang, T. Goto, I. Imae, Y. Sakurai, and Y. Harima, Thermoelectric properties of PEDOT films prepared by electrochemical polymerization. J. Polym. Sci. Part B: Polym. Phys., 2017, *55*, 524.

4. C. T. Hong, Y. H. Kang, J. Ryu, S. Y. Cho, and K.-S. Jang, Spray-printed CNT/P3HT organic thermoelectric films and power generators. J. Mater. Chem. A, 2015, *3*, 21428.

5. Q. Yao, Q. Wang, L. Wang, and L. Chen, Abnormally enhanced thermoelectric transport properties of SWNT/PANI hybrid films by the strengthened PANI molecular ordering. Energy Environ. Sci., 2014, *7*, 3801.

6. W. Lee, Y. H. Kang, J. Y. Lee, K.-S. Jang, and S. Y. Cho, Improving the thermoelectric power factor of CNT/PEDOT:PSS nanocomposite films by ethylene glycol treatment. RSC Adv., 2016, *6*, 53339.

7. F. X. Jiang, J. K. Xu, B. Y. Lu, Y. Xie, R. J. Huang, and L. F. Li, Thermoelectric Performance of Poly(3,4-ethylenedioxythiophene):Poly(styrenesulfonate). Chin. Phys. Lett., 2008, *25*, 2202.

8. D. Kim, Y. Kim, K. Choi, J. C. Grunlan, and C. Yu, Improved Thermoelectric Behavior of Nanotube-Filled Polymer Composites with Poly(3,4-ethylenedioxythiophene) Poly(styrenesulfonate). ACS Nano, 2010, *4*, 513.

9. X. Hu, L. Chen, Y. Zhang, Q. Hu, J. Yang, and Y. Chen, Large-Scale Flexible and Highly Conductive Carbon Transparent Electrodes via Roll-to-Roll Process and Its High Performance Lab-Scale Indium Tin Oxide-Free Polymer Solar Cells. Chem. Mater., 2014, *26*, 6293.

10. Y. Chen, Y. Zhao, and Z. Liang, Solution processed organic thermoelectrics: towards flexible thermoelectric modules. Energy Environ. Sci., 2015, *8*, 401.

11. G. P. Moriarty, S. De, P. J. King, U. Khan, M. Via, J. A. King, J. N. Coleman, and J. C. Grunlan, Thermoelectric behavior of organic thin film nanocomposites. J. Polym. Sci. Part B: Polym. Phys., 2013, *51*, 119.

12. M. Culebras, C. M. Gomez, and A. Cantarero, Review on Polymers for Thermoelectric Applications. Materials, 2014, *7*, 6701.

13. C. Yu, K. Choi, L. Yin, and J. C. Grunlan, Light-Weight Flexible Carbon Nanotube Based Organic Composites with Large Thermoelectric Power Factors. ACS Nano, 2011, *10*, 7885.

14. Q. Jiang, C. Liu, H. Song, H. Shi, Y. Yao, J. Xu, G. Zhang, and B. Lu, Improved thermoelectric performance of PEDOT:PSS films prepared by polar-solvent vapor annealing method. J. Mater. Sci.: Mater. Electron., 2013, *24*, 4240.

15. M. He, F. Qiu, and Z. Lin, Towards high-performance polymer-based thermoelectric materials. Energy Environ. Sci., 2013, *6*, 1352.

16. G. H. Kim, L. Shao, K. Zhang, and K. P. Pipe, Engineered doping of organic semiconductors for enhanced thermoelectric efficiency. Nat. Mater., 2013, *12*, 719.

17. S. H. Lee, J. S. Sohn, S. B. Kulkarni, U. M. Patil, S. C. Jun, and J. H. Kim, Modified physico–chemical properties and supercapacitive performance via DMSO inducement to PEDOT:PSS active layer. Org. Electron., 2014, *15*, 3423.

# Chapter 6　Conclusion

## 6.1 Summary of the study

The research presented in this dissertation focus on the fabrication and development of PEDOT and polyaniline based organic TE materials. It is important to control the structure and surface morphology of organic materials, and optimize the doping level, thereby collectively leading to the balanced TE properties while simultaneously engineering an electronic structure. On such basis, the fabrication conditions were carefully investigated and the morphology and characterizations were described for innovative organic materials. In addition, further treatment such as secondary doping, electrochemical dedoping were also deeply studied to enhance their thermoelectric performance for a promising TE material. The main conclusions in this thesis were summarized as follows:

1. Flexible and free-standing PEDOT:S-PHE films were prepared by galvanostatic polymerization and their thermoelectric performances were investigated. In contrast to a trade-off relation between $\sigma$ and $S$ observed for inorganic TE materials, $\sigma$ and $S$ values were simultaneously increased by decreasing the polymerization temperature or by increasing the current density during polymerization. The reason for this unique feature characteristic of conducting polymers was explained reasonably on the basis of SEM and oxidation-level measurements. The influence of oxidation state of the PEDOT:S-PHE films on their TE performances was also studied by changing the oxidation level by controlling the applied potential. Under the optimized polymerization conditions ($T$ = -30 $^{\circ}$C, $J$ = 1.2 mA cm$^{-2}$, oxidation level = 6%), the $PF$ and $ZT$ values of the PEDOT:S-PHE films were 7.9 $\mu$W m$^{-1}$ K$^{-2}$ and 0.013, respectively.

2. Composite films of graphene/polyaniline were prepared by a one-step electrochemical technique with GO and aniline monomer, and their thermoelectric performances were optimized with respect to the electrolysis time and the weight ratio of GO and aniline. It was found that the electrical

conductivities of the composite films can be enhanced *ca.* four times by employing SUS in place of FTO, while no appreciable change was observed for the Seebeck coefficients. The composite films of the GO/aniline weight ratio of 8:1 prepared on the SUS electrodes gave the maximum power factor of 3.6 $\mu$W m$^{-1}$ K$^{-2}$ and *ZT* value of 0.008 at room temperature. In addition, the conductivity enhancement on the SUS electrode were accounted for in terms of the efficient removal of oxygen species of GO by the direct electrochemical reduction of GO on SUS concurrently with the reduction of GO by hydrogen gas generated by reduction of protons on SUS.

3. Multilayer composite films stacked alternately by PEDOT and rGO were successfully synthesized via a repetitive potential application for reducing and oxidizing an aqueous solution containing only EDOT and GO. In the proposed technique, GO acts as a supporting electrolyte and a dopant. On the other hand, when the electrochemical reduction was carried out, not only GO doped in PEDOT but also GO in solution were reduced to give rGO, so that a single rGO layer was deposited on the PEDOT layer. Thus, multilayer structure stacked alternately by PEDOT and rGO can be easily obtained just by applying the repetitive potential of 1.0 and -1.1 V. It was revealed further that the thickness of each layer can be easily controlled by the electrolysis time. The preparation of PEDOT/rGO multilayer composite films thick enough to enable us to measure physical properties such as electrical and thermal conductivities, and Seebeck coefficients for their thermoelectric application with a special attention on the anisotropic natures is currently under investigation.

4. PEDOT:PSS/SWCNT composites could be successfully prepared by simply mixing the aqueous dispersions of SWCNT and PEDOT:PSS at different weight ratios,. With an optimization of the feeding weight ratio of PEDOT:PSS and SWCNT, a peak value of *PF* at 29 $\mu$W m$^{-1}$ K$^{-2}$ was achieved. Furthermore, when being soaked in DMSO for two minutes at room temperature, these composites yielded a highly improved TE performance at $W_{SWCNT}$ = 74 wt%: $\sigma$ = 3,800 S cm$^{-1}$, *S* = 28 $\mu$V K$^{-1}$, and *PF* = 300

$\mu W\ m^{-1}\ K^{-2}$. The *PF* is the largest among those reported so far for composites based on PEDOT:PSS and CNT.

## 6.2 Outlook

We have demonstrated some novel methods to fabricate and develop the typical organic TE materials expectably. Still, the pursuit of new organic materials with more desirable TE properties should move forward. In stark contrast to those of conventional inorganic analogues, TE property parameters are able to be decoupled in organic TE materials, therefore showing great promise of organic TEs. On the other hand, owing to the advantages of mechanical flexibility, cost-effectiveness, light-weight, and scalable production methods, organic TE materials hold great promise in a range of applications such as flexed or curved TE devices and wearable electronic devices operated just by body heat. More importantly, manufacturing methods such as screen-printing, ink-jet printing and roll-to-roll printing have been shown to be scalable methods for production of organic TE generators. With all these exciting advances in organic TE materials, the development of personal, portable, and flexible thermal modules will no longer be just a possibility.

# Acknowledgements

First and foremost, I would like to take this opportunity to express my heartfelt gratitude to Prof. Yutaka Harima, for his careful guidance, great support and encouragement during my doctoral academic years. He has offered me valuable suggestions in the academic studies, spent much time reading drafts and provided me with inspiring advice. His profound knowledge and perseverance in the pursuit of scientific challenges have provided me with lifetime benefits. Moreover, I would like to give my special thanks to Prof. Harima's wife, Mrs. Harima for her kindness. When I first came to Hiroshima, it's Prof. Harima and his wife who drove me out for the basic living items. I still remember the scene that Mrs. Harima helped me to measure the length of the curtains in my house, which made me feel warm in the unfamiliar country.

I would like to express my heartfelt gratitude to my supervisor Prof. Ichiro Imae, for his kind guidance in my experiments and insightful discussion on my research work. He helped me a lot in the graduation dissertation and gave constant concern about my life.

Not forgetting my tutor Mr. Goto, for his warm-hearted assistance in my research work and daily life, after I came to Hiroshima University. I would also like to thank all other group members in the Materials Physical Chemistry Laboratory, for their sustained help and all the good moments we spent together.

I am also grateful to Japan Government for granting me generous financial support under Monbukagakusho Scholarship, enabling me to study without any economic pressure.

Last, my thanks would go to my beloved family for their loving considerations and great confidence in me all through these years. I also gratitude to my friends and my fellow classmates who gave me endless encouragements and support to help me work out my problems during the difficult.